(aSiGe/ncSi) Superlattice thin film silicon solar cell

By

Nayan Chakravarty

A dissertation submitted to the graduate faculty
in partial fulfillment of the requirements for the degree of
DOCTOR OF PHILOSOPHY

Major: Electrical Engineering

Program of Study Graduate Committee:
Vikram Dalal, Major Professor
Rana Biswas
Joseph Shinar
Ruth Shinar
Mani Mina

Iowa State University

Ames, Iowa

2011

TABLE OF CONTENTS

LIST OF FIGURES

ACKNOWLEDGMENT

ABSTRACT

Nanocrystalline silicon solar cell has come up as a potential material in the photovoltaic industry [1-3]. There are various benefits of nanocrystalline silicon which makes it superior to its counterparts such as amorphous silicon and amorphous silicon germanium. Narrow band gap of 1.12eV helps to generate more current by utilizing the red and infrared region of the solar spectrum. High current producing ability makes it suitable material for the bottom cell of a tandem solar cell [4]. The growth of nanocrystalline silicon is not as simple as the growth of amorphous silicon. The material grows in a conical fashion which results to large grain boundary formation if not controlled properly. The large grain boundaries hamper the electronic properties of the material. To prevent the formation of the large grain boundaries several design of nanocrystalline silicon solar cell has been used. Hydrogen profile, Power profile and Superlattice structures help to control the crystallinity of the material as it grows. There are other deposition parameters such as deposition temperature, pressure and frequency if changed may alter the morphology of the material by changing the grain size of crystals [5-10]. For high mobility and more absorption of photons we need large grains sizes of <220> which can be achieved by high temperature and high pressure deposition conditions. We are going to discuss about the superlattice structure and ways to improve the quality of the solar cell. Amorphous silicon germanium has superior absorption coefficient as compared to amorphous silicon therefore in this report we would discuss how we can incorporate amorphous silicon germanium with nanocrystalline silicon to enhance the current of the solar cell. The grain structure and superior electronic property of nanocrystalline silicon will be utilized to collect the carriers from the thin amorphous silicon germanium tissue. We will also show the increase in current can be achieved by incorporating a back-reflector in a solar cell.

CHAPTER 1. INTRODUCTION

Nanocrystalline silicon (ncSi:H) was first fabricated by Veprek and Maracek in the year 1968 [11]. It is an important material used in photovoltaic devices and thin film transistors. After an extensive preliminary work by Lucovsky et al. and Faraji et. al, were able to fabricate successful photovoltaic device made from ncSi:H intrinsic layer [12,13]. In the initial years of the fabrication, material had 'n' type character and high defect density which restricted its use into limited areas. IMT Neuchatel played a crucial role to modify the quality of ncSi:H material which later on used for photo-generation layer in a solar cell [14]. Nanocrystalline silicon is made up of small grains of crystalline silicon of the order 10-100nm, embedded inside an amorphous silicon tissue of few nanometers. The grain boundaries are passivated with hydrogen and amorphous silicon tissue. Nanocrystalline silicon material has an indirect band-gap which requires thicker material to absorb sufficient amount of photons. The absorption coefficient of ncSi:H closely follows crystalline silicon as shown in fig 1.1. The increase in absorption coefficient beyond 1.8eV can be explained from its composition which also contains amorphous silicon tissue [15].
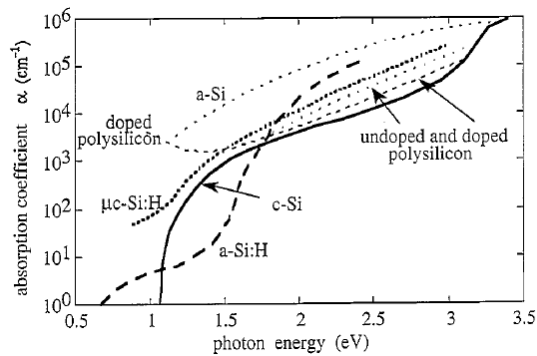
Fig 1: Absorption Coefficient of different silicon materials [15]

CHAPTER 2. GROWTH & PROPERTIES OF NANOCRYSTALLINE SILICON

Nanocrystalline silicon growth is a complex phenomenon and still a topic of research. Unlike amorphous silicon the growth of the film results to change morphology of the growing layers. Material becomes more crystalline on increasing thickness. On increasing the crystallinity, surface of ncSi becomes rough. The name nanocrystalline silicon suggests that it has nanometer sized crystalline silicon embedded inside thin amorphous silicon tissue. To understand the growth process of the film we have to first look at various stages of the growth. Nucleation process is the very first step of the growth which literally decides the sites for the crystal growth. Collins et. al have shown the nucleating sites with the help of a TEM image in fig 2.1 where the conical fashion growth of ncSi:H is visible [16]. Bailat et. al has also argued that the initial nucleation site is primarily decided by the dilution of the gas. More nucleation sites are formed as the dilution increases. Nevertheless heterophase of aSi:H and ncSi:H also decreases on increasing dilution which suggest that aSi:H seed layer effective thickness decreases as the film grows [17]
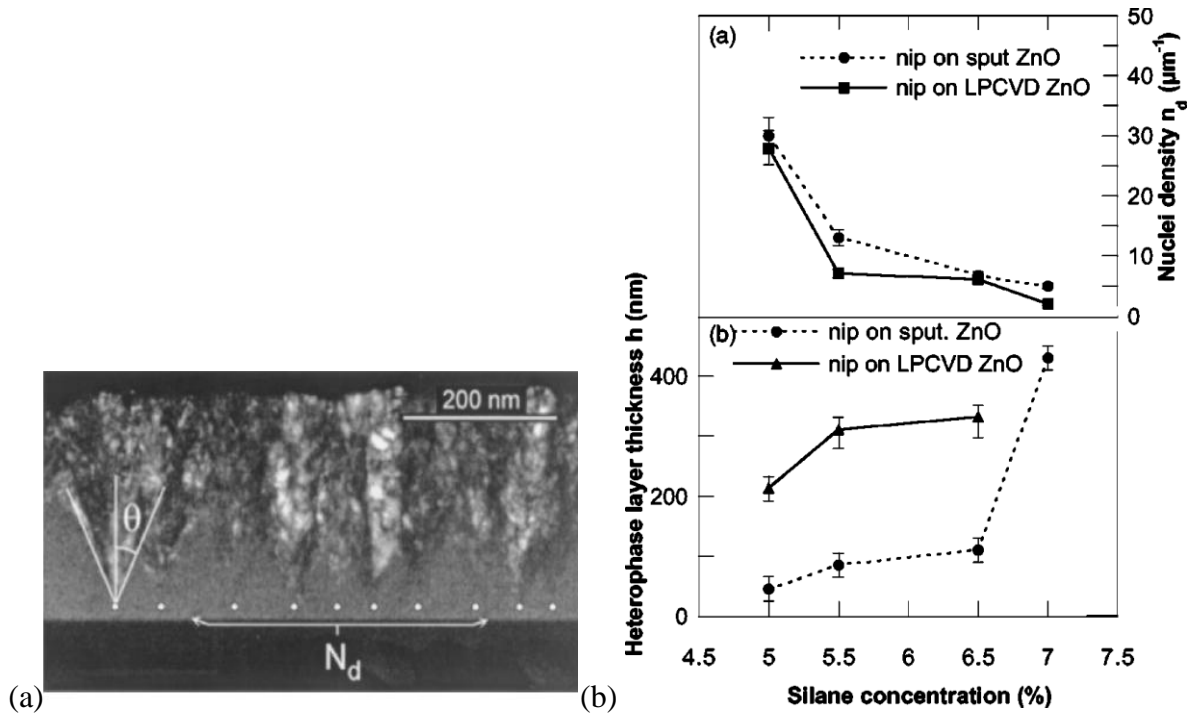
Fig 2.1: The initial growth process in ncSi:H (a) Formation of nucleating sites initially, (b) Nucleation sites depend majorly upon the initial dilution of the gas [16,17].

2.1 Growth Mechanism of ncSi:H

The growth property of ncSi:H depends on various ways of its fabrication techniques such as RF-PECVD, VHF-PECVD and HW-CVD etc. In this report we would be looking at the growth kinetics with respect to VHF-PECVD systems. The primary reaction of the growth process starts with the dissociation of SiH_4 and H_2 molecule with energetic electrons produced from the glow discharge of the plasma. It has been found that several ($\sim$ 5-10 eV) of energy is sufficient to initiate the reaction process. The major advantage of VHF-PECVD system is that we can deposit films at much lower temperatures because of the energetic electrons. Matsuda et. al has suggested that formation of ncSi:H film depends heavily on SiH_3 precursor, atomic hydrogen which plays a vital role on the surface of the forming film,

substrate temperature and power of the ions which are interacting with the film surface [18]. Fig 2.2 shows the relative density of the reactive species formed during the plasma interaction with silane and hydrogen gas. From the fig 2.2 it is evident that apart from SiH_3 and H, the rest of the secondary reaction species are less in number.
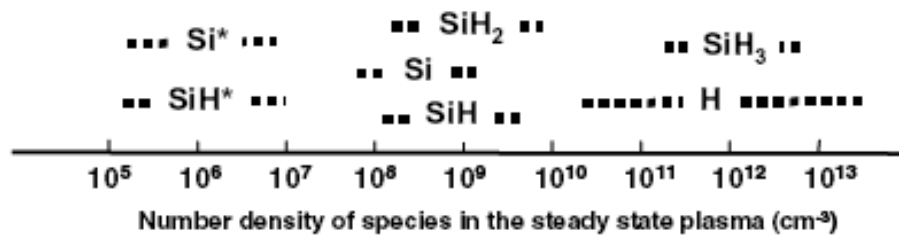
Fig 2.2. Steady state density of the reactive species present in the plasma [8]

There are various models which discusses about the growth kinetics of ncSi:H material. We would be looking at these models one by one and understand the differences and the origin of different school of thoughts.

2.1.1   Surface Diffusion Model:

Matsuda et. al . proposed this model in 1983 [19]. According to this model atomic Hydrogen plays a key role to initiate the growth process. Large amount of local heating happens when locally two hydrogen atoms bond with each other to produce more stable molecule of H_2. The local heating helps SiH_3 radical to diffuse on the film surface to get adsorbed on favorable sites. Fig 2.3 explains the model showing the local heating process and the diffusion of SiH_3 radical. The systematic breakage and formation of Si-Si bond

helps to form the nanocrystals of silicon. Once the nucleation has taken place the rest of the crystal follows the epitaxial growth.
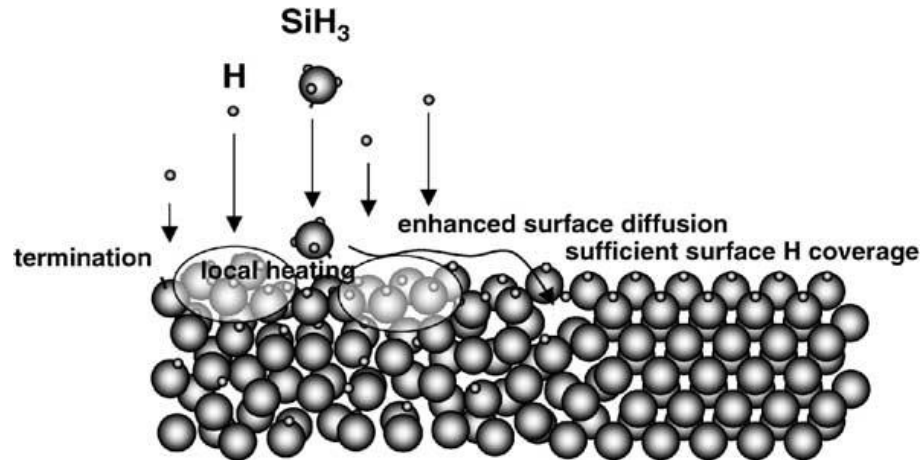
Fig 2.3: Surface diffusion model for the growth of ncSi:H material [19]

Dalal et. al has proposed that breaking Si-H bond from two adjacent SiH_3 is highly unlikely because Si-H bond energy is 2.5eV. The abstraction of hydrogen mainly happens because of the incoming H ion influx which helps to abstract weaker H bonds thus forming Si-Si regular bonds [20].

2.1.2   Etching Model

Tsai et. al proposed the model in 1989 [21]. Etching model came into existence because it was observed that on increasing the dilution growth rate decreases. According to this model as shown in fig 2.4, H atom helps to etch away the weak silicon bonds thus forming new stronger bonds which lead to crystallinity.
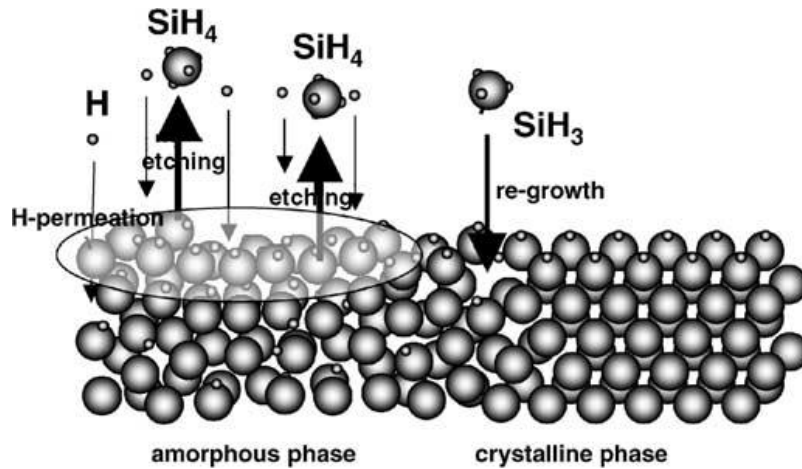
Fig 2.4: Etching model for the growth of ncSi:H material [19]

2.1.3   Chemical-anneal Model:

Nakamura et. al . proposed the model in 1995 [22]. Chemical anneal is an important fabrication technique to produce high quality aSi:H films. It has been observed that while doing the layer by layer growth and subsequently annealing with hydrogen or heavier inert gases the layers could turn crystalline. Fig 2.5 shows the chemical anneal technique where impinging H atom penetrates deep inside the layer breaking the weaker Si-Si bonds and forming crystalline silicon.
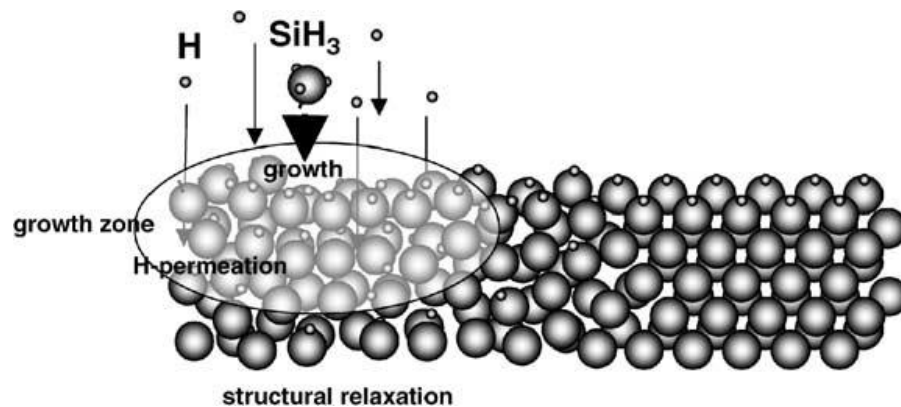
Fig 2.5: Chemical anneal model for the growth of ncSi:H material [19]

2.2 Very high frequency plasma enhanced chemical vapor deposition (VHF-PECVD)

PECVD system is widely used as a fabrication tool for depositing thin film silicon solar cell. The main advantage of VHF-PECVD is the ability to deposit films at much lower temperature. The design of the PECVD system is capacitive coupled plasma generator where voltage is applied in between two parallel plate capacitors as shown in fig 2.6. Electric field in between the plates ionizes the gas, producing an avalanche effect. The benefit of very high frequency over DC deposition was first proposed by Robertson et. al. [23] ever since then it grabbed the attention for further improvements. The benefits of high frequency can be summarized into the fig 2.7 where the variation of various parameters has been shown with increasing plasma frequency. On increasing the frequency of the plasma it reduces ion energy which helps to fabricate better quality film. Deposition rate is also an important parameter which increases if frequency is increased; with high deposition rate fabrication time can be reduced. Electron density increase with frequency helps to increase the deposition rate.

There are 3 major components in a PECVD system, pumps, main reaction chamber and the power supply. There are 3 pump systems involved in the system. The roughing (mechanical pump) is connected to the main chamber which helps to lower down the pressure from atmospheric pressure to 1 torr. A two pump system of turbomolecular pump and a backing (mechanical pump) are used to lower down the pressure further to $1x10^{-7}$ torr. Backing pump helps to maintain a low pressure region at the exit of the turbomolecular pump because we cannot pump out from turbo pump to external atmosphere.

Substrate Heater

Substrate Holder

Shutter

Barometer

Wall baking Heater

View port

Electrode

GND

Nozzle for Gas Outlet

H_2

Match Box

SiH_4

GeH_4

Power Amplifier

Roughing Pump

Ion Gauge

ppm PH_3

ppm TMB

VHF-RF Power

Turbo Pump

Backing Pump

Various gas supply connected to the Cylinders
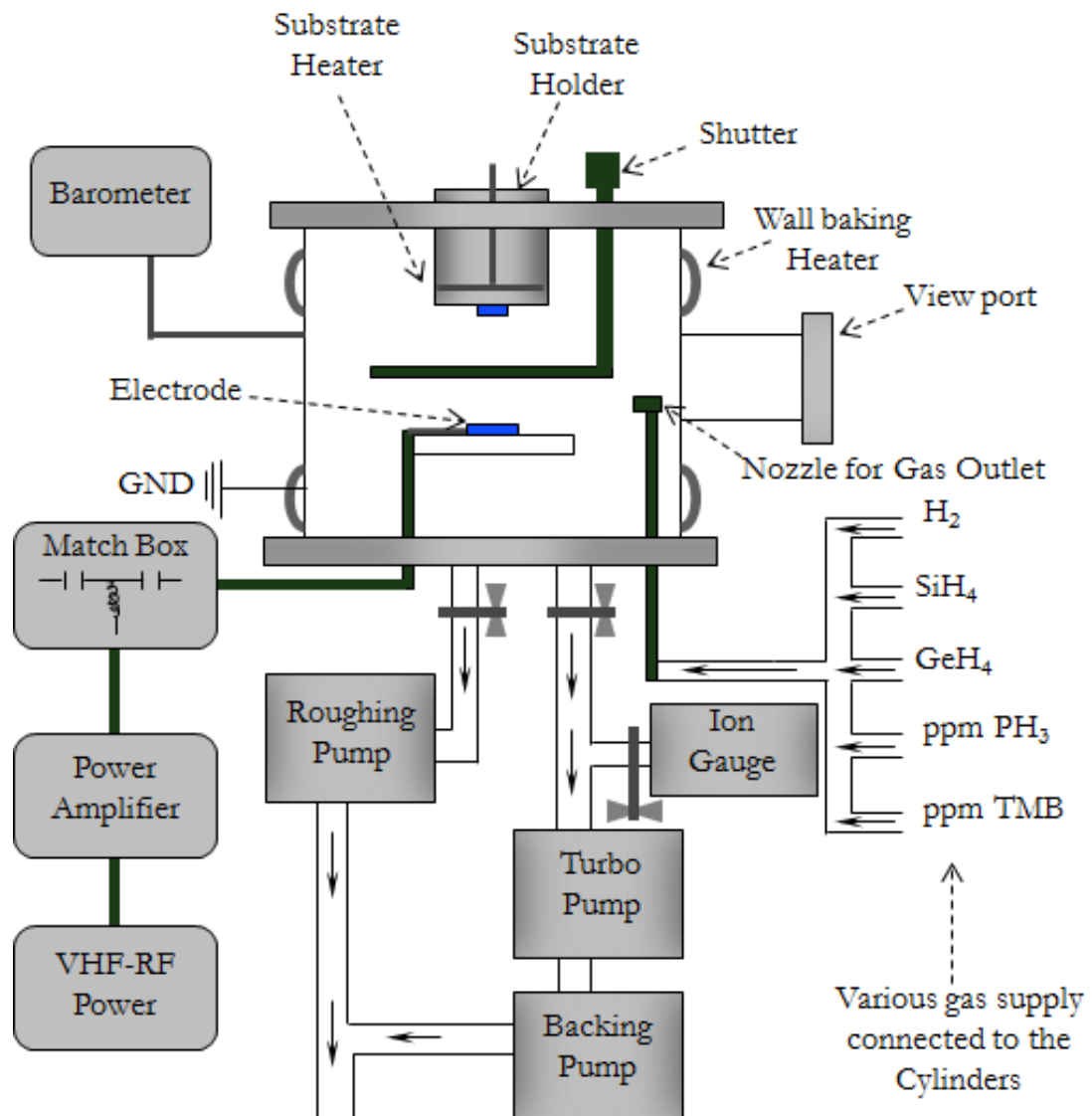
Fig 2.6: Schematic diagram of VHF-PECVD system
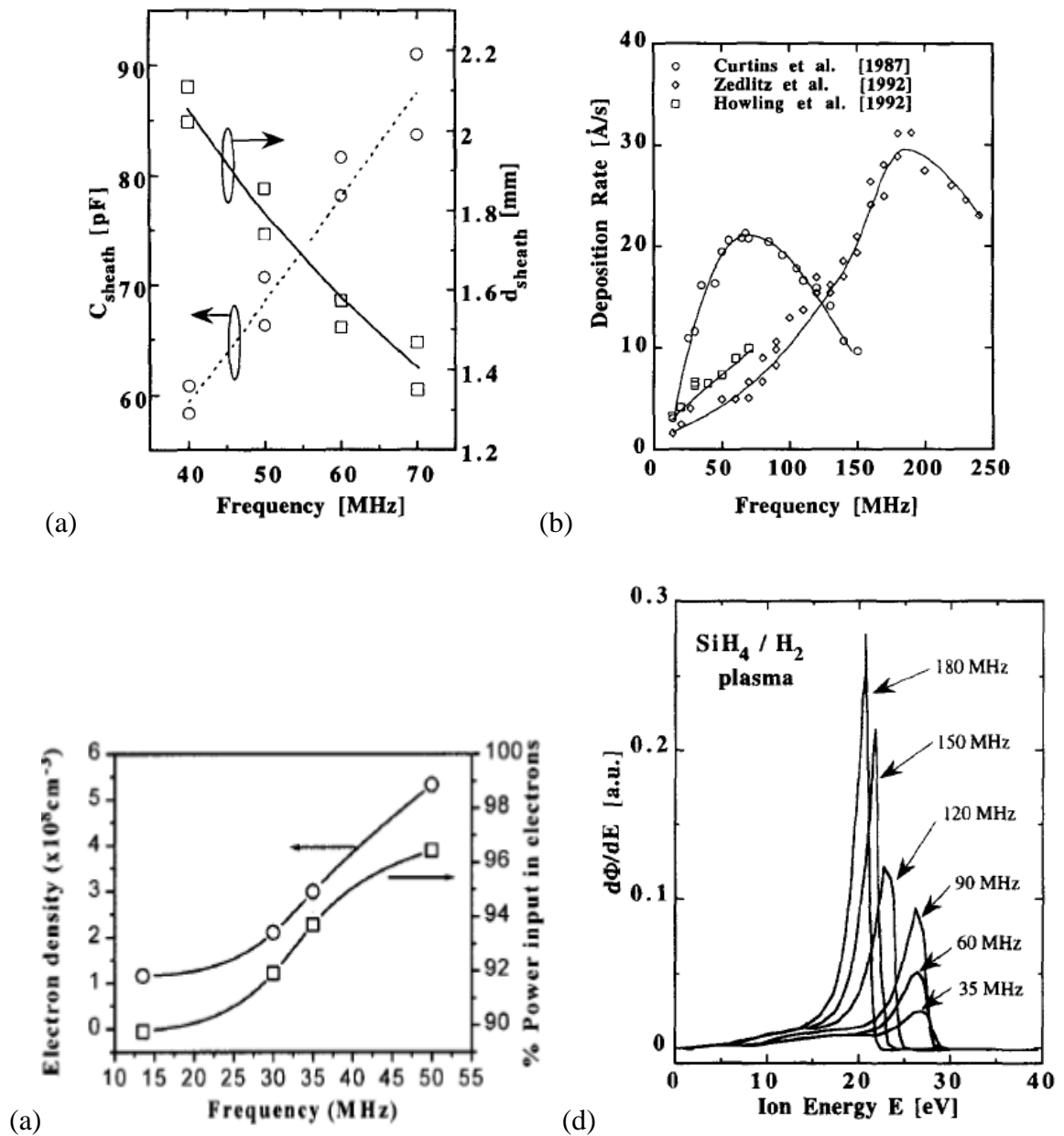
Fig 2.7: Variation of various Plasma parameters with increase in frequency (a) Sheath Capacitance vs. Frequency [24] (b) Deposition rate vs. frequency [25] (c) Electron density vs. Frequency [26] (d) Ion energy vs. Frequency [27]

When a potential is applied across parallel plate capacitor it creates an electric field. To start the plasma there should be some gas molecules present in between the capacitor plate. High electric field causes rapid increase in energy of an electron which gives rise to various secondary reactions. The ignition of plasma can be explained with the help of a pashchen curve where it shows the sweet spot where the gas breaks down. When an energetic electron collides with the molecule it initiates the following reactions:

1) Dissociation:

   The precursor gas dissociates into free radicals which is responsible for the growth of the thin film.

2) Ionization:

   Ionization is caused when the outer shell electron of an atom receives enough energy that it overcomes its electron affinity. Highly energetic electron can knock out the valence band electron and hence ionize the gas into charged particles. Ionization is not favored for the growth of thin film because it may disrupt the growth by ion-bombardment.

3) Excitation:

   Molecule on impact with an electron hold together but they absorb energy and enter into an excited state called metastable state. Plasma glow discharge gets it characteristic color because of the excitation of the electrons in an atom. When an

electron is excited to higher energy level, it comes back to its ground state, releasing characteristic photon in the form of the energy dissipation.

There are various regions present in a glow discharge. In the glow discharge region multiple ionization and recombination excitation takes place. In the dark regions of the plasma no recombination happens. Plasma can be produced either by DC or AC voltage. For conducting films DC plasma can be used because charges don't build up on the substrate. In the case of an insulating film electrons forms shielded cover if DC voltage is used. Alternating voltage at certain frequency helps to prevent the charging. In the industry 13.56MHz is commonly used to prevent any interference with the other communication devices. For thin film deposition we have used very high frequency (VHF) plasma for the film growth. The frequency range is from 45-47MHz. There are other advantages of using VHF voltages. These electromagnetic waves couple energy into the plasma much more efficiently than DC. The major reason of using VHF plasma is to decrease the ion bombardment on the film. The interfaces of the film are prone to damage by highly energetic ions which needs to be avoided. If very low frequency is used then the behavior of the plasma would be similar to DC plasma. Non conducting electrode will be charged up quickly. On the other hand if ultra-high frequency is used then heavy ions will get stuck to their location because now they would be immobile. Therefore, we always work in the moderate range of the frequency.

2.3 Nanocrystalline silicon solar cell designs

A simple solar cell is made up of either p-i-n or n-i-p structure where the intrinsic (i-layer) plays the important role of absorbing the photons and generating power. The electrical equivalent of a solar cell would be a diode. Fig 2.8 shows the schematic of a simple nanocrystalline silicon solar cell.
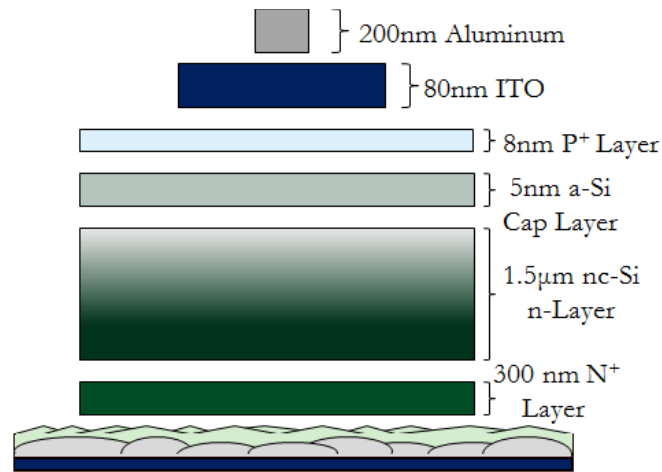
Fig 2.8: Schematic cross sectional diagram of a simple nanocrystalline silicon solar cell

The base of the cell should have few important features such as mechanical stability, sustainability at high temperatures, non-reactive in nature and ability to back-reflect light so that efficiency of the solar cell can be increased. At the bottom we deposit 0.3 um thickness of phosphorus doped aSi:H n+ which acts as the electron collecting layer. On top of n+ a thin buffer layer of aSi:H which acts as the seed layer for the ncSi:H film, seed layer is lightly doped with PH_3 which helps to reduce the series resistance of the cell. The vital function of the buffer layer before starting ncSi:H is to provide nucleation sites for the growth and prevent any diffusion of PH_3 from n+ to the main i-layer. Before depositing p+ another thin buffer layer of aSi:H is deposited which helps to increase the Voc of the cell

and prevents any oxidation of the ncSi:H. Finally after ncSi:H p+, the cell is coated with an anti-reflecting coating of ITO with Aluminum bus bar to reduce the series resistance further.

The unique growth mechanism of ncSi:H helped to drive the development of many novel ncSi:H solar cell designs. These designs evolved to compensate the crystalline fraction in the film. Nanocrystalline silicon unlike amorphous silicon follows a complicated and a specific pattern to evolve. Collins et. al has shown that the material grows in the conical fashion and hence becoming more and more crystalline as it grows [16]. Kocka et. al. has shown further that the high crystallinity at the end of the device gives rise to grain boundary collision of the growing grains as shown in fig 2.9. These grain boundaries are the potential sites of defect where impurities like oxygen, carbon and nitrogen can go and sit. Impurities at the large grain boundaries act as a potential site for recombination which results in reduction of open circuit voltage of the cell. Prevention of the formation of these large grain boundaries can be solved by adopting a suitable solar cell design [28].
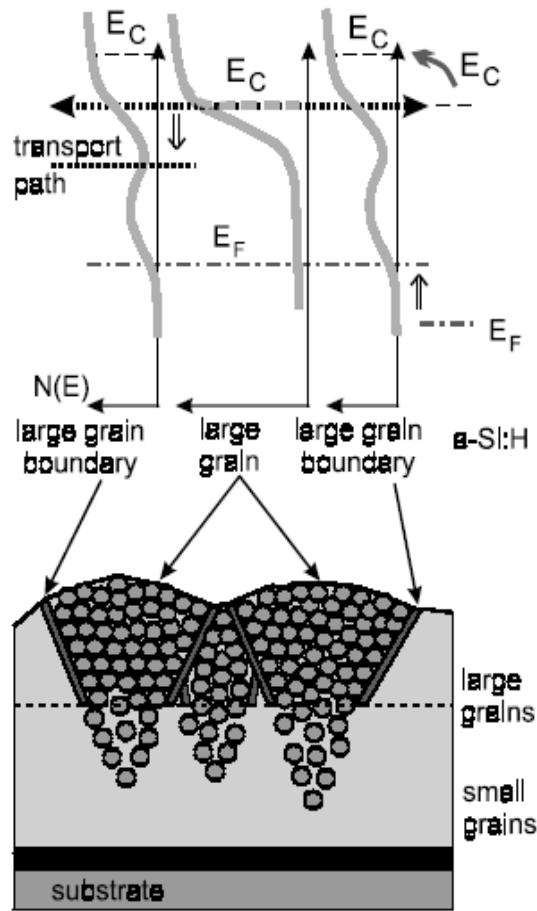
Fig 2.9: Schematic diagram of ncSi:H material with density of states [28]

2.3.1 Hydrogen profile design

Hydrogen profile (HP) technique helps to reduce the large grain boundary formation in ncSi:H solar cells. Yan and Guha et. al. showed successfully that by systematically changing the dilution ratio as the material grows one can control the crystalline volume fraction. Fig 2.10(a) shows the Raman graph of various thickness of ncSi:H material grown by HP technique. It clearly shows similar crystallinity for both thin and thick film. Fig 2.10(b) shows the increase in crystallinity as the film grows thicker if dilution is kept constant [29].
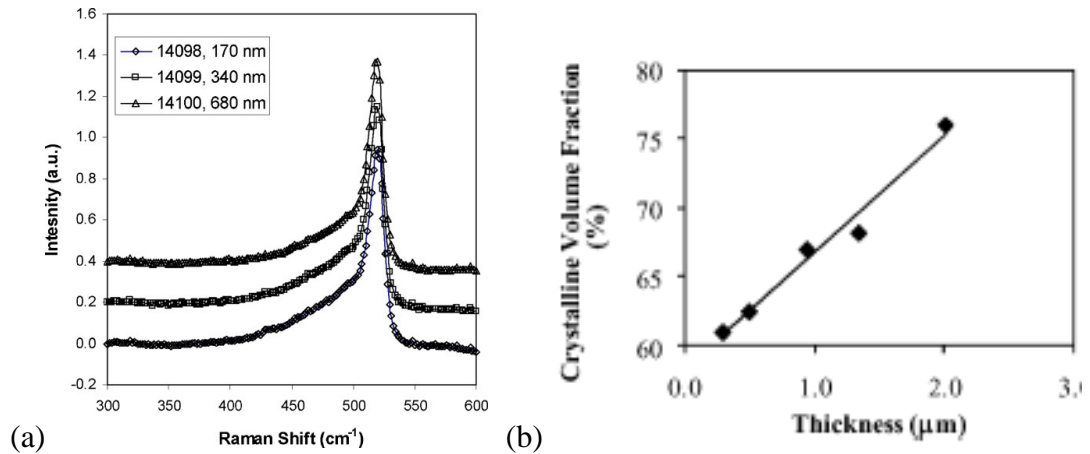
Fig 2.10: (a) Variation of Crystallinity on HP films (b) Crystallinity increases as thickness increases

for constant dilution films [29]

2.3.2 Power profile device

Recently Han et. al. discovered that we can control the crystallinity of the growing ncSi:H film by changing the power. Nanocrystalline silicon becomes more crystalline on increasing the power so we can control the crystallinity by decreasing the power as the film grows. This method not only helps to control the growth of ncSi:H but reduction in power results to reduced ion-bombardment which further helps to improve the film quality [30].
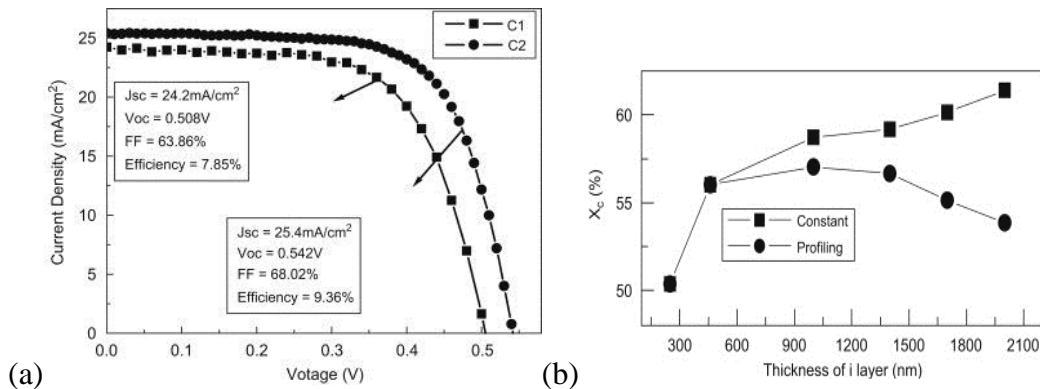
Fig 2.11: (a) Enhancement in the property of cell with power profile, (b) Crystallization variation

with thickness of the film [30]

2.3.3 Superlattice design

Dalal and Atul et. al. proposed that if we could use thin aSi:H film to inhibit the growth of ncSi:H film, that should help to prevent the large grain boundary formation. The idea behind the superlattice structure is to fabricate layer by layer structure where individual ncSi:H film thickness is kept thin around 50-100 nm. Individual aSi:H acts as the new incubation layer for the next ncSi:H. Fig 2.12 is the schematic image of the SL structure with alternating amorphous and nanocrystalline layers. Thin amorphous layer is kept 5-10nm which is good enough to inhibit the growth of underneath ncSi:H. Thicker aSi:H layer may have problems such as tunneling and poor collection of carriers, therefore aSi:H thickness needs to be controlled [31-35]
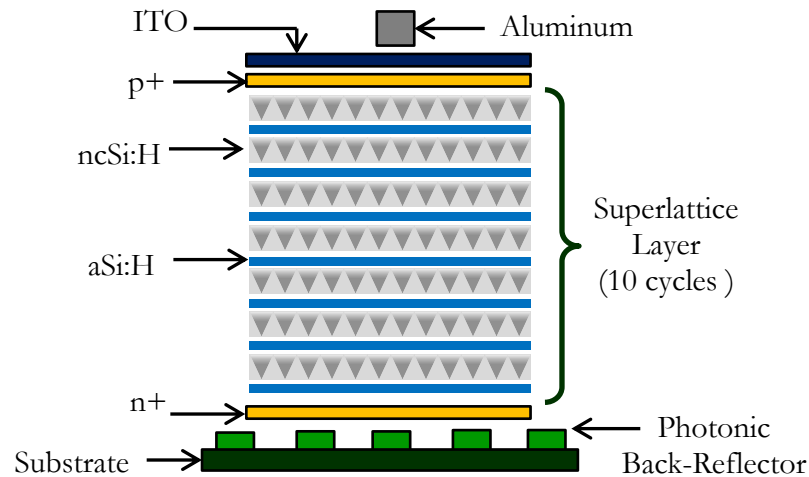
Fig 2.12: Schematic diagram of the superlattice structure showing the layer by layer growth of the film.

CHAPTER 3. CHARACTERIZATION TECHNIQUES

Solar cell properties can be determined by using various electrical and optical characterization techniques [36, 37]. The superior quality of i-layer determines the high efficiency of a solar cell which involves both film quality and device quality [38]. Optimum crystallization and larger grain size are few requirements for a good ncSi:H solar cell, which can only be determined by initial characterization of ncSi:H film. Nevertheless, various device characterizations also help to improve the device quality.

3.1 Current-Voltage experiment (IV)

IV experiment is one of the important experiments of a solar cell device which helps to evaluate its efficiency. It tells us about the open circuit voltage which is the voltage across the load when no current is flowing. Short circuit current is the current when load across the cell is shorted. Fig3.1 is a typical graph of an IV curve with efficiency defined as the ratio of power from solar cell by power input. The equations shown below collectively determine the quality of the solar cell and hence its efficiency [39]

$$Efficiency = \frac{Voc * FF * Jsc}{Pin}$$

$$FF = \frac{ImVm}{IscJsc}$$

$$Voc = \frac{kT}{q}\ln(\frac{Isc}{Io} + 1)$$

$$I = I_L - I_0 \left[\exp\left(\frac{qV}{nkT}\right) - 1 \right]$$
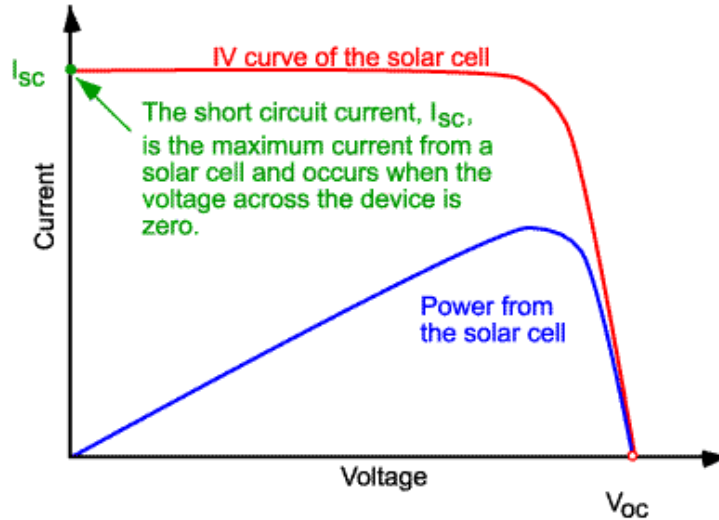
Fig 3.1: Current voltage characteristic of a photovoltaic device.

There are various ways to enhance Jsc, Voc and FF. To increase the current we need thick absorbing layer and efficient light trapping techniques [40]. Back-Reflectors will be discussed in the later chapter; we will discuss the working and various methods to prepare the Back-Reflector. Voc depends mainly on two factors in ncSi:H solar cell, (1) % crystallinity of the i-layer, and (2) Interfaces present in the device which helps to control the reverse saturation current, Jo [41]. Fig 3.2 shows the cross-sectional diagram of a ncSi:H solar cell where all of the interfaces are labeled. We did careful study of each interface to see their effect on Voc variation. Guha et. al. also suggested that by careful passivation of the interfaces we can reduce Jo and hence increase Voc [42,43].
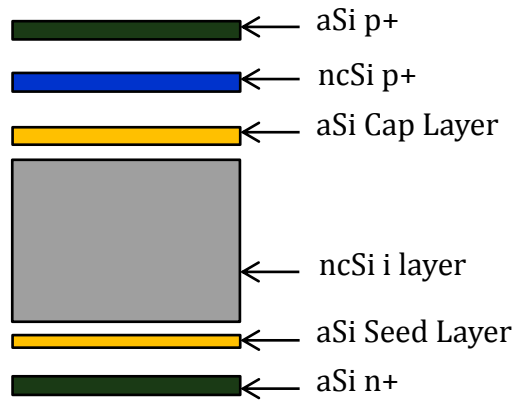
Fig 3.2: Cross-sectional diagram of ncSi:H Solar cell with various layers/interfaces

1) Amorphous silicon seed layer is used to initiate the growth process of ncSi:H. On changing the property of the seed layer we could control the Voc. On making aSi:H seed layer thick we can passivate the n+/i-layer interface properly which helps to increase the Voc. Fig3.3 shows the increase in Voc on decreasing H_2/SiH_4 ratio in the seed layer. The disadvantage of using thick seed layer is increase in series resistance. Fig3.3 shows the variation of Jsc and FF with aSi:H thickness which clearly proves that thick aSi:H leads to lower FF because of high series resistance. The origin of high series resistance can be explained with the help of a band-diagram at the n+/i-layer interface. We observe a barrier for electron, which increases on increasing the seed layer thickness.
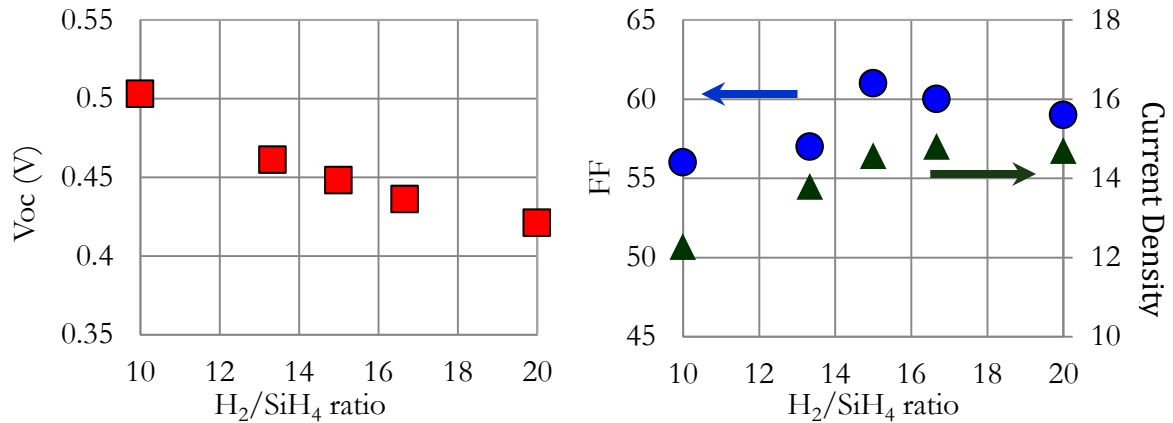
Fig 3.3: Variation of Voc, FF, and Jsc on increasing the dilution of aSi:H seed layer.

2) The i-layer of ncSi:H solar cell is a composition of both amorphous and crystalline phase. On increasing the amorphous phase in i-layer we can increase Voc because Jo reduces. I-layer crystallinity can be controlled by changing the deposition parameters such as dilution ratio, temperature and power. Increasing the amorphous phase beyond a limit makes the material property poor which leads to collection problem. The optimum level of crystallinity should be close to 50% crystalline and 50% amorphous phase for high efficiency solar cells.

$H_2/SiH_4 = 17$
Voc 0.46 , Jsc 14.5mA/cm^2 , FF 73.1
$H_2/SiH_4 = 14$
Voc 0.51 , Jsc 14.02mA/cm^2 , FF 72.2
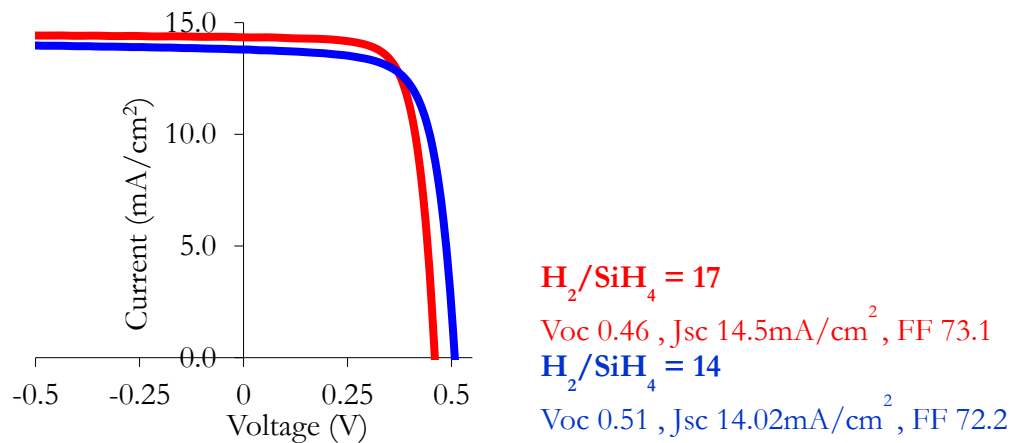
Fig 3.4: I-V curve of two cells with different i-layer dilution.

3) Amorphous silicon is an excellent passivating layer. Before p+ a thin cap layer of aSi:H is used to passivate the i-layer/p+ interface and to prevent any oxidation of ncSi:H i-layer during transfer from one PECVD system to another. Guha et. al. argues that if we could control the thickness of aSi:H cap layer we could decrease the surface recombination. Fig 3.5 shows the effect of aSi:H thickness on Voc. The cap layer thickness is very crucial because if we deposit thick layers then it would form a barrier for hole transfer. Fig 3.5 also shows the I-V curve of identical cells with various aSi:H cap layer.
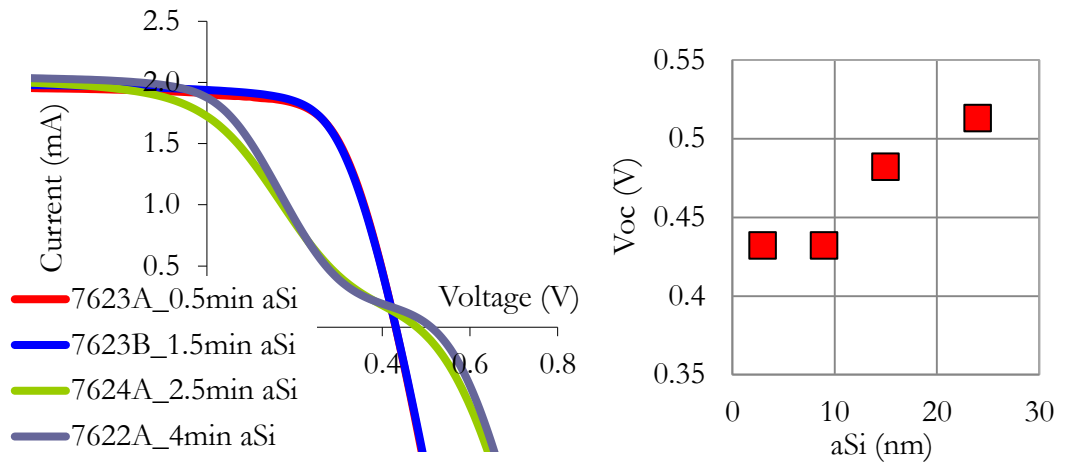
Fig 3.5: I-V curve and Voc variation on increasing aSi:H cap layer thickness.

$$V_{oc} = \frac{kT}{q} ln \left(\frac{I_{sc}}{I_o} + 1 \right)$$

4) The last interface of ncSi:H solar cell is the p+/i-layer interface. Thickness of p+ layer is kept very thin to prevent any loss of current at lower wavelength of light. Nanocrystalline silicon p+ is used because it acts as a transparent window layer for

lower wavelength. Moreover, ncSi:H has high conductivity which helps to achieve high FF in the solar cell. On top of ncSi:H p+ we cap it with thin aSi:H p+ to prevent any oxidation of ncSi:H p+. Fig 3.6 shows the variation of Voc on increasing the thickness of ncSi p+. On increasing thickness of ncSi p+ we observe negligible change in Voc but drop in current density because of loss of lower wavelength photon.
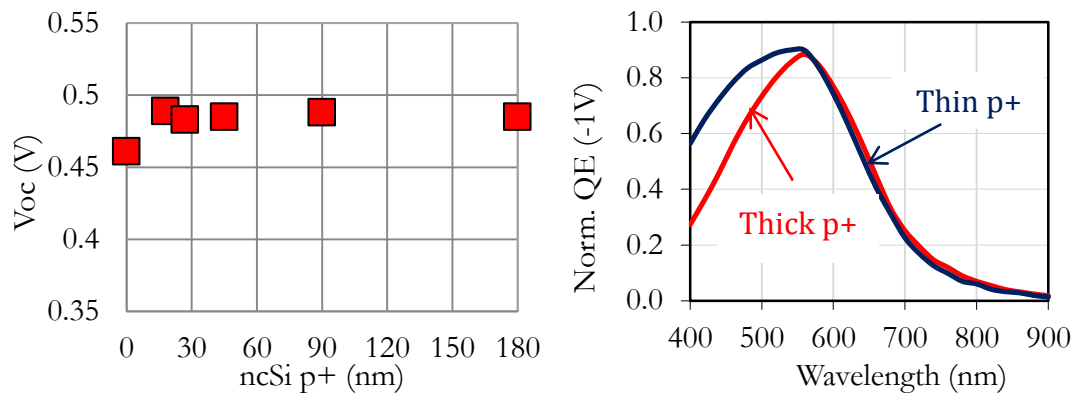
Fig 3.6: Variation of Voc and QE on increasing the thickness of ncSi:H p+

Fill factor of a device primarily depends upon three major properties known as series resistance, shunt resistance and collection property. If we look at the equivalent circuit of a solar cell as shown in fig 3.7 we observe that if series resistance is high then the power loss because of it would be I^2Rs whereas if shunt resistance is low then most of the current will leak and we would end up with lower current density. Collection property of a device is equally important because poor collection will lead to lower output power.
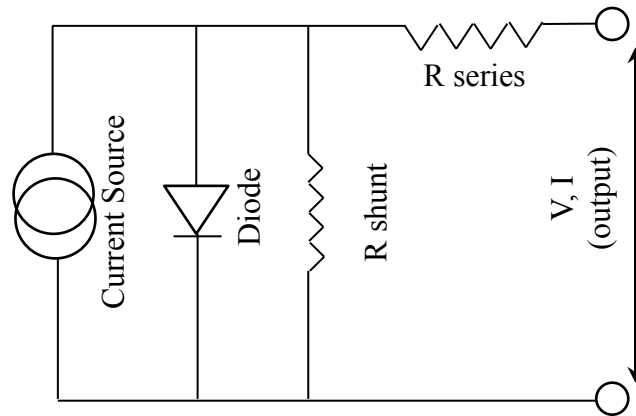
Fig 3.7 : Electrical equivalent circuit of a solar cell.

3.2 Quantum efficiency experiment (QE)

Quantum efficiency experiment explains the behavior of a solar cell at various wavelength of the solar spectrum [44]. QE is a ratio of collected electron or hole with respect to the incident photon. Higher QE gives us higher current density of a device. QE can be done at a bias voltage to study the material property. If ncSi:H is more n-type it leads to hole collection problem, it will be visible on plotting the ratio of QE at 0V and at a bias voltage. If QE ratio is high at 400nm then it is an indication of a very poor interface property in between p and I layer. Similarly if QE ratio is high at 800-900nm then it is an indication of poor material property in bulk of the i layer in an n-i-p cell. To measure QE, we measure the current from the sample, and divide by the current induced at the same wavelength in a reference sample. Fig3.8 shows the schematic diagram of the QE setup clearly showing all of the parts.

The QE setup consists of:

1) A monochromator: It is used to generate light at a particular wavelength by using a grating structure. The wavelength of the incident light can be changed by changing the grating spacing with the help of a knob.

2) Chopper: Monochromator source should be converted to a suitable AC signal so that lock-in amplifier can detect it. Chopper is used to convert the monochromatic light from DC to an AC signal of frequency 13.56 MHz.

3) Filters at 580nm, 700nm, 900nm and 1020nm: The monochromator grating structure fails to isolate the second, third and so forth order of the signal. These filters are used to lower down the noise from the lower harmonics.

4) DC bias light: It is an essential component of a QE system. We use DC bias to fix the quasi fermi levels. If we fail to do so then for each and every wavelength the position of the quasi Fermi level would change, generating more carriers from the trap levels. DC bias light should have sufficiently high intensity as compared to the AC monochromator signal to work effectively.

5) Lock-in amplifier: AC signal of the source is detected by the lock-in amplifier. It only detects the signal flowing at 13.56MHz frequency which helps us to isolate the system from the ambient AC (at different frequency) sources of light.

6) Lens and Mirrors: They play a crucial role to focus and concentrate the monochromatic light on the sample. Special care should be taken while handling the optics. Minor stains or finger prints causes huge change in the reflectivity of the mirrors. It has also been

observed that metal used on the back side of the mirror also affects the spectrum intensity. For Aluminum we use a factor of 0.9 to account for its absorption of the light at the lower wavelength of the spectrum.
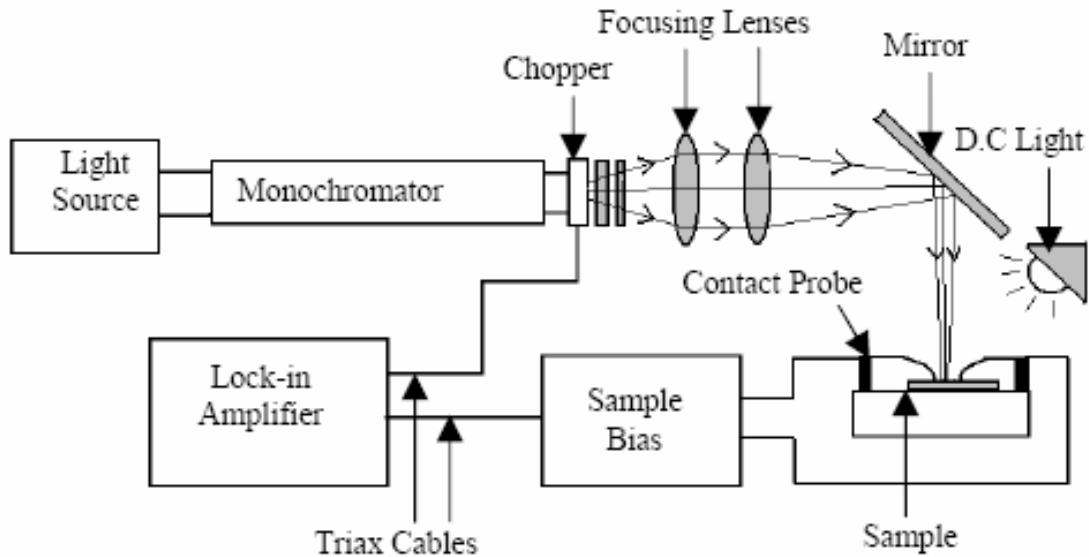
Fig 3.8: Schematic diagram of the QE setup

3.3 Diffusion length calculation

Nanocrystalline silicon is inherently n type material which makes holes the minority carrier. To study the device property and collection of holes we need to calculate the diffusion length. QE vs. bias experiment not only helps to determine the diffusion length but it also graphically shows the ease of collection of holes [45-50].

$$Prob\ of\ absorption = \alpha e^{-\alpha x}$$

$$Prob\ of\ collection = e^{-x/Lp}$$

$$QE \propto 1 - \alpha e^{-\alpha Wd} + \alpha \int_0^t e^{-\alpha x} e^{-x/Lp} dx$$

$$QE \propto \alpha Wd + \frac{\alpha Lp}{1 + \alpha Lp}(1 - e^{(Wd-T)\frac{Lp}{1+\alpha Lp}})$$

$$\frac{QE}{\alpha} \propto Wd + Lp(1 - e^{(Wd-T)Lp})$$

$$Wd = \frac{\epsilon A}{C}$$

The equations involved for the calculation of diffusion length requires both QE vs. bias and high frequency CV data. To calculate the depletion width capacitance value corresponding to the applied bias is used. On plotting both experimental and theoretical QE values we could determine the diffusion length [51-53].

3.4 Capacitance-Voltage experiment (CV)

Nanocrystalline silicon properties critically depends upon the passivation of the grain boundaries with aSi:H and hydrogen. Impurities such as oxygen make the film unintentionally n type in nature. Hole is the minority carrier and its lifetime decreases severely as the film becomes more n type. Calculation of the defect density thus becomes important experiment to evaluate the quality of the absorbing layer. Kimerling et.al. have showed that defect density can be calculated by studying the CV at low frequency (100Hz) [54]. Fig 3.9(a) shows the variation of Capacitance on increasing the reverse bias voltage. Fig 3.9(b) shows the variation of defects on increasing the doping density which correspond one to one increase in defect density on increasing PH_3. For good device quality ppm amount of boron doping is important to counter the unintentional oxygen doping. Extreme

care should also be taken to add exact calculated amount of TMB otherwise after compensating oxygen TMB starts to dope the material.
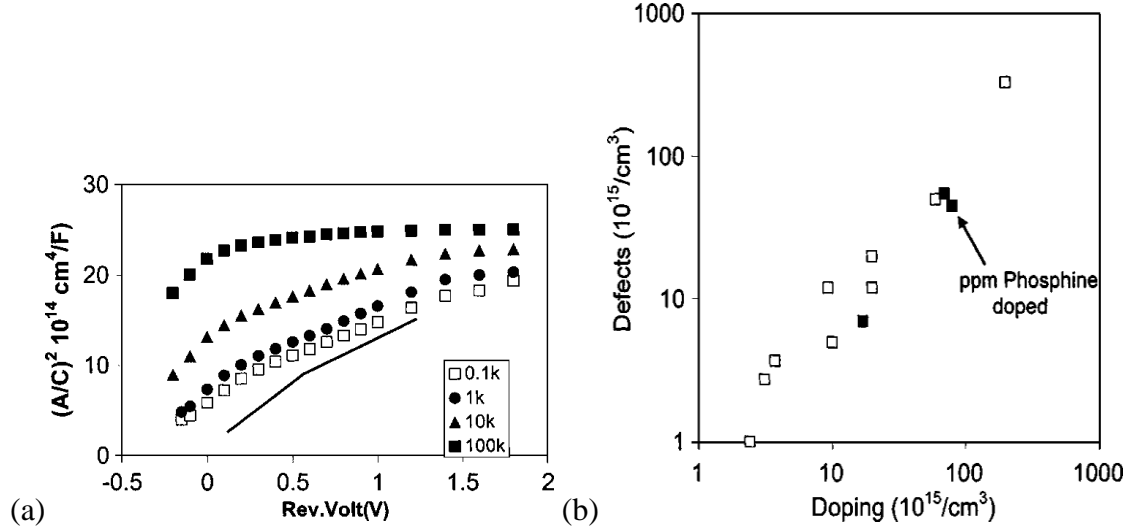
Fig 3.9: (a) Variation of Capacitance with reverse voltage at various frequencies, (b) Variation of defect density on increasing the doping [48]

In fig 3.9(a) there are two distinct regions with different slope at low frequency which suggest the presence of two types of defect states present in the material. Deep level and shallow level traps can be activated at various frequency and reverse bias voltage. At low frequency and low reverse bias only shallow traps play the key role but as the reverse bias voltage increases deep level traps also starts to show up in the experiment. On calculating both the slopes we can calculate the deep and shallow level traps separately by using the equation shown below. C is the capacitance, V is the voltage applied, Na is the defect density.

$$\frac{1}{C^2} = \frac{2}{q\varepsilon_s}\frac{V_a}{N_a}$$

The i-layer thickness of the device can also be calculated by using high frequency CV experiment. At very high frequency such as 100 kHz the carriers fails to see the traps and gets accumulated at the edges of the p+ and n+. On applying simple equation of a capacitor we can get the i-layer thickness at high reverse bias [55].

3.5 X-ray diffraction

Grain size of ncSi:H is determined by XRD experiment [56-59]. By using Braggs law we know that for every plane there exist a characteristic peak at a particular 2Θ angle. The angle corresponds to the constructive interference of the X-rays. Scherer's equation is used to calculate the grain size. For ncSi:H there are two planes of particular interest, <111> and <220>. Study of <220> grain size variation is important because <220> improves the quality of the material by assisting in the carrier transportation. We have also observed that <220> grain size helps to improve the current by absorbing more photons. There are various ways to increase <220> grain size particularly by increasing deposition temperature and pressure. <111> grains are the result of random nucleation. Fig shows the typical graph of XRD with <111> plane at 28, <220> at 46, <311> at 56 and at 44 we are getting the characteristic peak of stainless steel substrate.
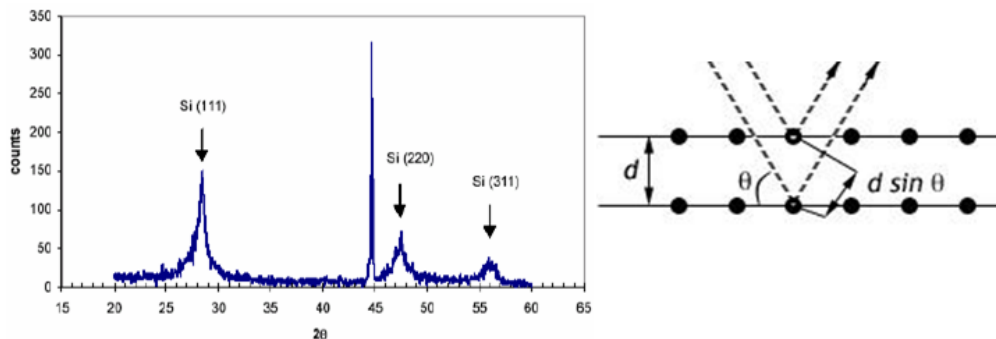
Fig 3.10: XRD graph of ncSi:H material deposited on SS substrate

3.6 Raman experiment

Nanocrystalline silicon is a mixture of both amorphous and crystalline phase. Determining the percentage crystallinity is very important for better device quality. It has been discussed that best material is deposited at the transition of amorphous and crystalline phase. High amorphous content deteriorates the quality by inhibiting the transport property whereas high crystalline fraction will lead to cracks which lead to defect formation. Amorphous silicon tissue contains huge amount of hydrogen which helps to passivate the grain boundaries [60-63].

Raman spectroscopy is used for the measurement of % crystallinity. Wavelength of the laser light is important because different wavelength of laser will show crystallinity of various depths. When laser photons interacts with the material atoms, two types of collision happens. The elastic collision where no loss of energy occurs is known as Rayleigh scattering. The important phenomenon is the in-elastic collision of photons which is known as Raman scattering. When photon interacts with the atom which is at certain vibrational energy it excites the electron to a virtual energy state. On relaxation when the electron comes back to the ground state, either it goes to higher energy state (energy is lost) or it goes to lower energy state (energy is gained). With this shift in energy the resulting photon is slightly shifted to either high or low depending upon stoke or anti-stoke phenomena. Raman machine measures the difference in between reciprocal of the incident and the resulting photon wavelength. Amorphous silicon material doesn't have long range order so we get a Gaussian distribution of signal, distributed over wide range with peak at $480cm^{-1}$.

In the case of crystalline silicon because of the long range order we get sharp lorenztian distribution at $521cm^{-1}$ as shown in fig 3.11.

Virtual Energy State

Stokes   Rayleigh   Anti Stokes

Vibrational
levels

Ground Energy State
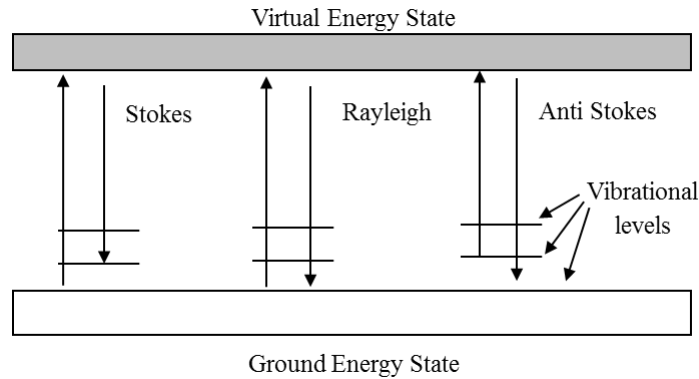
Fig 3.11: Schematic diagram of the Raman and Rayleigh phenomena

Raman measurement involves laser excitation of a particular wavelength. The wavelength of the laser is chosen according to the depth of penetrating required for the analysis. Higher wavelength laser will be absorbed deep in the material hence we could analyze deeper in the film as compared to lower wavelength. Using proper intensity of laser beam is important to prevent any unwanted crystallization because of high power. Fig3.12 shows the variation of three major parameters which we could change during Raman measurement. Laser intensity can be changed according to the film property; organic samples require much lower intensity as compared to inorganic samples. If using lower intensity it may have high noise to signal ratio which could be reduced by high exposure time and large accumulations. Fig3.12 is the power variation on thin film which clearly shows that on using high intensity (25mW) laser it turns the film crystalline. On reducing power and increasing exposure time and accumulations we could get the correct data with little noise.
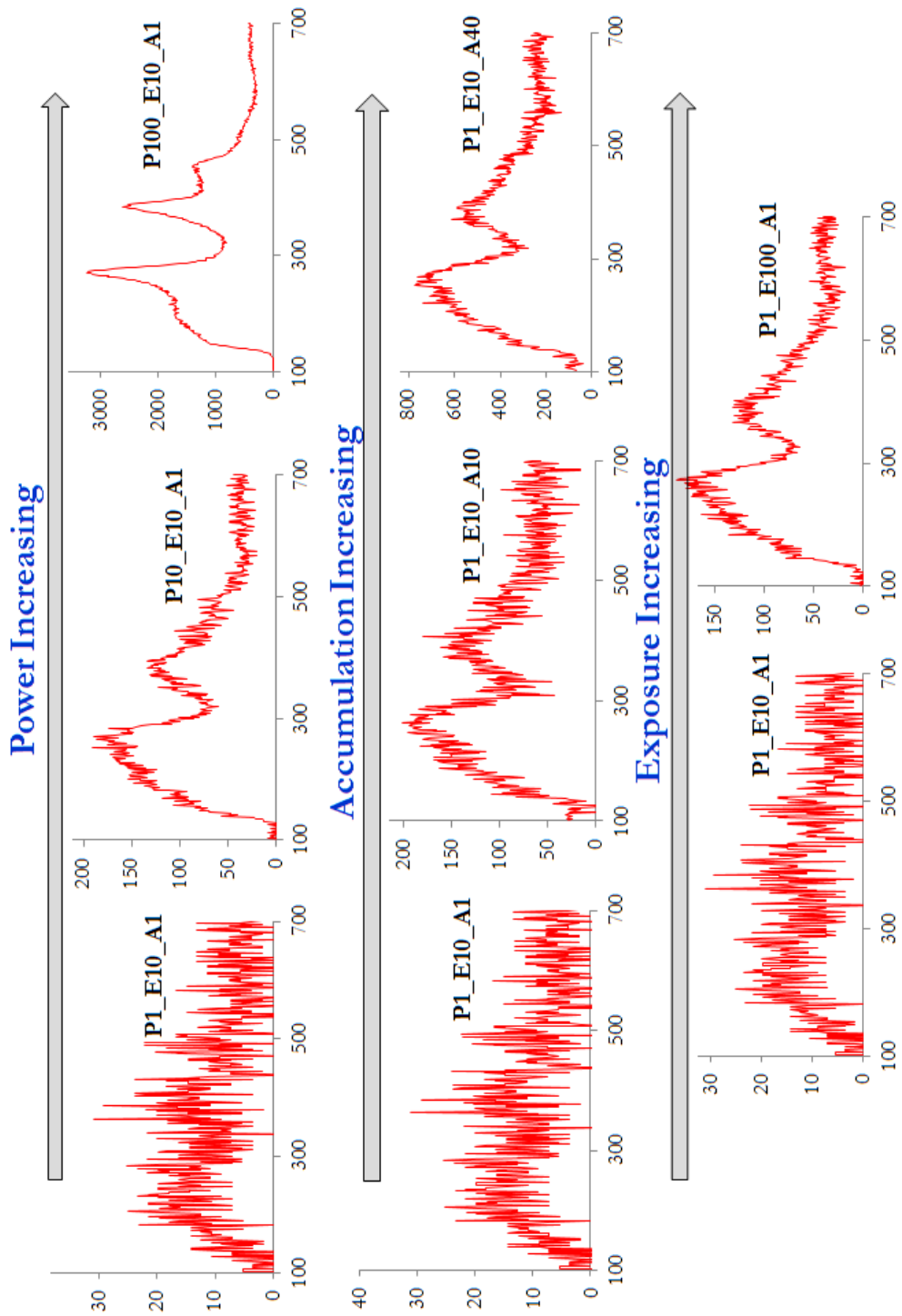
Fig 3.12: Raman measurement done on various samples to show the effect of various components which could affect the measurement

3.7 Optical experiments

Thickness of ncSi:H film is calculated by using spectrophotometry technique. Thin film structures have a series of interferences which forms peaks and valleys at corresponding wavelengths. These peaks and valleys are used to calculate thickness by using the equation shown below where λ1 and λ2 are two adjacent peaks or valleys having refractive index n1 and n2 respectively [64-67]

$$t = \frac{\lambda_1 \times \lambda_2}{2 \times (n_1\lambda_2 \times n_2\lambda_1)}$$

3.8 Capacitance-frequency experiment (Cf)

Cf experiment can be done on thin film solar cell to study the defect density in the absorbing layer. Fig 3.13 showing the schematic image of various transition of carrier which helps to determine shallow and deep level defects

$$N_t(E_\omega) = -\frac{U_d}{qw}\frac{dC}{d\omega}\frac{\omega}{kT}$$

$$E_\omega = kT\ln(\frac{2v_0}{\omega})$$
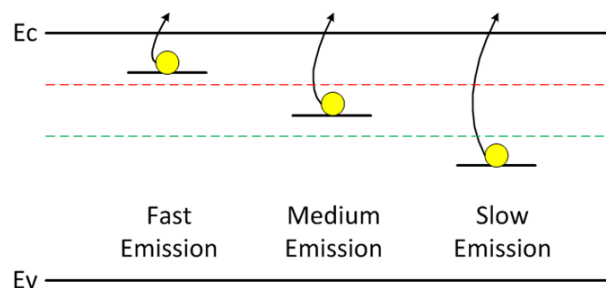
Fig 3.13: Various transitions of electron to evaluate defect density

CHAPTER 4. GROWTH PROPERTY OF aSiGe/ncSi SUPERLATTICE SOLAR CELL

4.1 Motivation for aSiGe:H

Amorphous silicon germanium has great potential in photovoltaic because of its ability to change band-gap on changing the germanium content in the material. Fig4.1 shows the variation of the absorption coefficient of the material on increasing the germanium content.
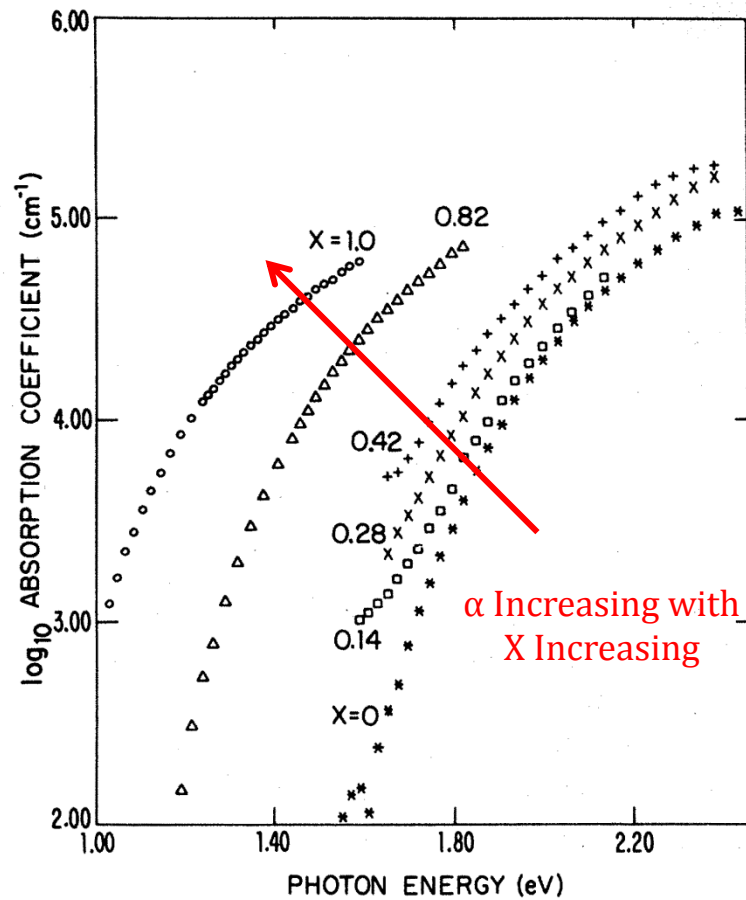
Fig 4.1: Increase in absorption coefficient on increasing the Germanium content in aSiGe:H [70]

The composition of aSiGe:H strongly dependent on the deposition conditions such as SiH_4/GeH_4 ratio, power, temperature and pressure. Generally it is observed that germanium content in the solid state of the film is much higher than the gas phase ratio. It implies that GeH_4 can easily be deposited with higher deposition rate as compared to silicon. The preferential incorporation of germanium makes aSiGe:H an interesting material for solar cell technology [71-76]

Hydrogenated amorphous silicon (aSi:H) and nanocrystalline silicon (ncSi:H) are key materials for the fabrication of low cost thin film solar cells [77]. The structural and electronic properties of amorphous semiconductors have been studied extensively [78], with much understanding of how the electronic properties relate to local structural order [78]. An extensive understanding of the structural and electronic properties of ncSi:H has emerged from atomistic studies[79,80]. These studies have elucidated the phase boundaries between nano-crystallites and aSi:H and the H-distribution in ncSi:H [81] and the temperature dependent evolution of H from ncSi:H [82]. aSi:H and its alloys suffer from the well-known light-induced degradation and metastability or the Staebler-Wronksi effect[83]. Metastability in aSi:H has a rich history of models and theories [78,83]. Atomistic studies have identified the metastability in aSi:H as arising from the breaking of weak silicon bonds [84], accompanied by structural rearrangements in the network, that can account for electron-spin resonance data, defect kinetics [85], charged metstable defects and hysteretic defect annealing[84]. In contrast to the H-collision model [86] has been proposed to explain metastability through the rupture of Si-H, followed by H-motion, leading to H-

induced complexes in the network [86,87]. It has been recognized that H motion can occur by rupture and formation of silicon bonds [88] in the amorphous network, and the role of H has been implicated as the origin of metastability [83]. Local H-motion and flipping of SiH bonds also leads to a metastable state that can account for infrared absorption changes on light soaking [89], in contrast to metastable changes in H-bonding[90] where H bonds to weak silicon bonds.

Stability of aSiGe:H was explained by Stabler and Wronski. The mechanism of the degradation can be explained by the following initiation of the steps:

1) Amorphous silicon is a disordered structure with weak bonds. These bonds break because of the charge-induced action which forms metastable dangling bonds.

2) Weak bond in amorphous tissue can be defined as the trapping of photoexcited electrons and holes in the band tail state of amorphous silicon.

3) The rate of increase of dangling bond depends on increase in disorder structure which increases the tail states.

The advantage of the superior optical properties of aSiGe:H and superior electrical properties of ncSi:H can be utilized to fabricate high efficiency solar cell. Superlattice structure will be used with aSiGe:H as the seed layer for every ncSi:H layer. Before going into details of the experiment we would look at the nucleation process of ncSi:H on aSiGe:H seed layer [91,92]

4.2 Simulation of aSiGe/ncSi superlattice

4.2.1 Constant germanium in superlattice

A simple simulation was done where 12 cycles of aSiGe:H and ncSi:H layers were considered. Fig 4.2 shows the calculation and the enhancement in current of the solar cell. We considered no back reflection and perfect material where every carrier is collected. The individual layer of ncSi is 70nm, aSiGe 5nm and total layer thickness 0.9 um. We have considered 25nm of ncSi p+ to replicate similar QE values obtained in our experiment. We have also considered no reflection from the top ITO surface, to keep the calculations simple.

$$J_1 = qN_o(1 - e^{-\alpha_n t_n})$$

$$J_{23} = qN_o(e^{-(11\alpha_n t_n + 11\alpha_a t_a)})(1 - e^{-\alpha_n t_n})$$
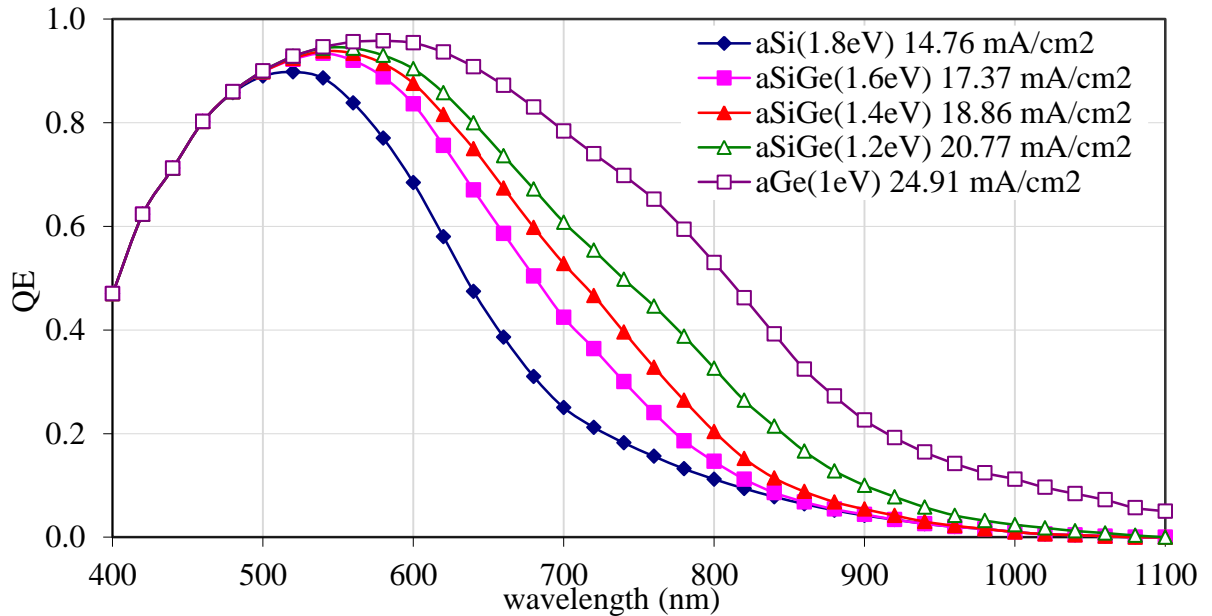
Fig 4.2: Simulation showing the enhancement in current density because of aSiGe:H layer.

4.2.2 Simulation of step graded GeH$_4$ superlattice

A new set of simulation work is done where germanium content is changed in steps. The following simulation is a continuation of the above explained equation but with 4 different absorption coefficients. The inspiration behind the simulation is to imrove the collection of the carriers even further. On grading GeH4, we start with low GeH$_4$/SiH$_4$ ratio changed to higher ratio as the device grows. Fig4.3 shows the schematic diagram of the SL structure. In this simulation we considered band gap variation as 1.8eV, 1.65eV, 1.5eV and 1.35eV. 3 cycles for each band gap of aSiGe with 4 total band-gaps makes 12 cycles, which corresponds to 0.9um of total i-layer thickness. The individual layer thickness of ncSi is 70nm and amorphous layer is 5nm. Device has 25nm of ncSi p+ on the top which absorbs the lower wavelength of the solar spectrum. The detailed equation is explained in the Appendix. Fig is the QE curve and the total current obtained from the simulation. The equation is the current density for the 1st layer and the last 23rd layer.

$$J_1 = qN_o(1 - e^{-\alpha_n t_n})$$

$$J_{23} = qN_o(e^{-(11\alpha_n t_n + 3\alpha_1 t_a + 3\alpha_2 t_a + 3\alpha_3 t_a + 2\alpha_4 t_a)})(1 - e^{-\alpha_n t_n})$$
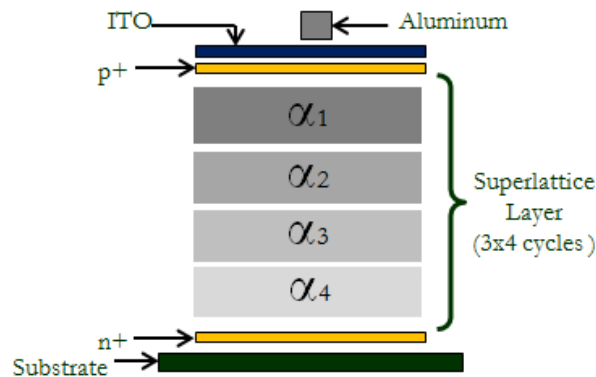
Fig 4.3: Cross sectional image of a SL device with 4 step graded aSiGe band-gaps
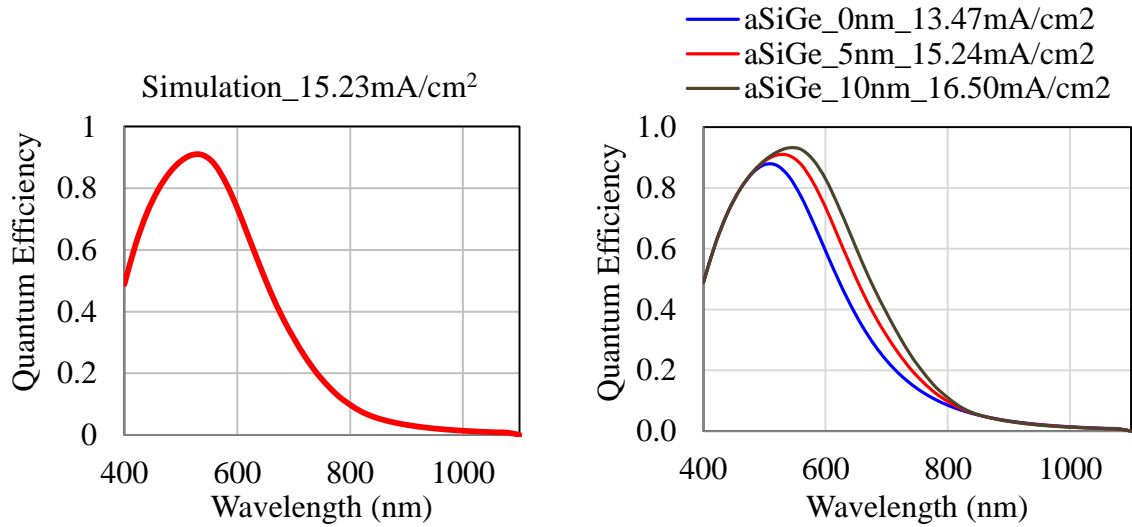
Fig 4.4: QE graph of the step graded simulation and QE comparison of various thickness of the aSiGe layer.

On comparing the QE curves with various thickness of aSiGe it is clearly evident that superior optical property of aSiGe helps to increase the current density from 13.47mA/cm2 (No amorphous layer) to 16.5mA/cm2 (10nm of aSiGe layer). We also observe current enhancement at the right spectral range where aSiGe strongly absorbs photons.

4.3 Growing ncSi:H on aSiGe:H seed layer

Initially we started with a simple hydrogen profile device with aSiGe:H as a seed layer. The experiment showed the unique behavior of aSiGe:H as a seed layer. We found that nucleation process is not same as aSi:H. In the case of aSiGe:H it is difficult to initiate the nucleation process. Fig4.5 shows the IV curve of various hydrogen profile devices made on aSiGe:H. We used high dilution and high power to initiate the nucleation process [93].
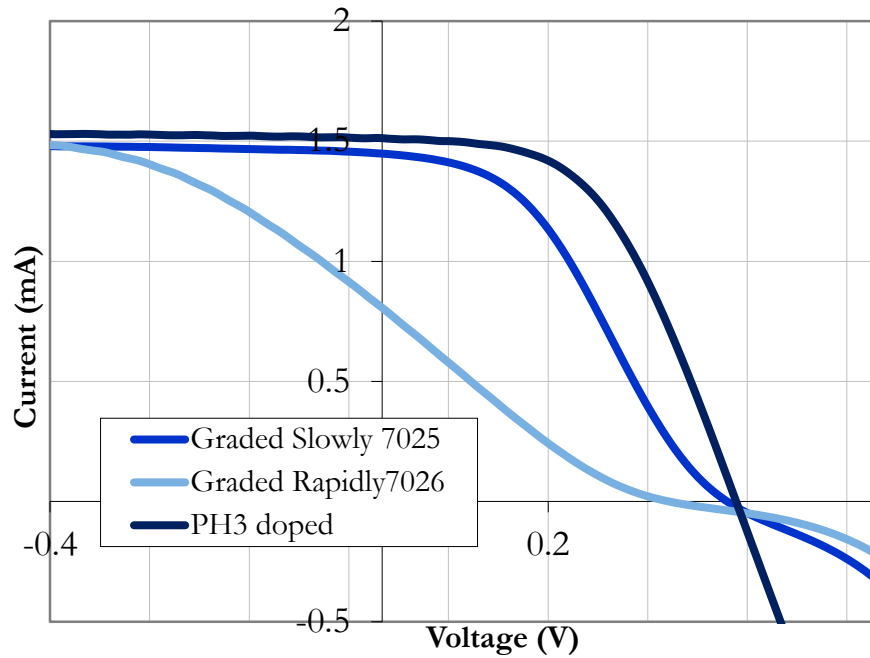
Fig 4.5: IV curve of various hydrogen profile devices made on aSiGe:H seed layer.

The barrier problem was solved by doping the seed layer with high amount of ppm PH_3 and grading GeH_4. PH_3 dopes the seed layer n type hence it helps to lower down Ec which helps electron to get collected in n+ without any restriction. Grading GeH_4 reduces Ge content in the film which helps to initiate the nucleation process. Grading GeH_4 also grades Ev which helps to collect holes generated in the seed layer. Hydrogen profile experiment with aSiGe:H seed layer helped us to understand the nucleation process but it was equally important to study the enhancement in current if we make the SL structure.

4.4 Growth property of (aSiGe/ncSi) Superlattice

Germane was used only in the amorphous cycle and flows were kept from 0 to 10% of the silane flow. High power and high dilution were used specifically because we have already

seen that it is difficult to initiate the nucleation of ncSi:H on aSiGe:H. Fig4.6 shows the variation in crystallinity as germane was increased in the amorphous cycle. This experiment correlated to the hydrogen profile experiment where we showed difficulty in the nucleation process with increase in germanium content in the seed layer. The crystallinity drops sharply from 58% to 38% as germane increases which proves that it is a serious problem during the fabrication process.
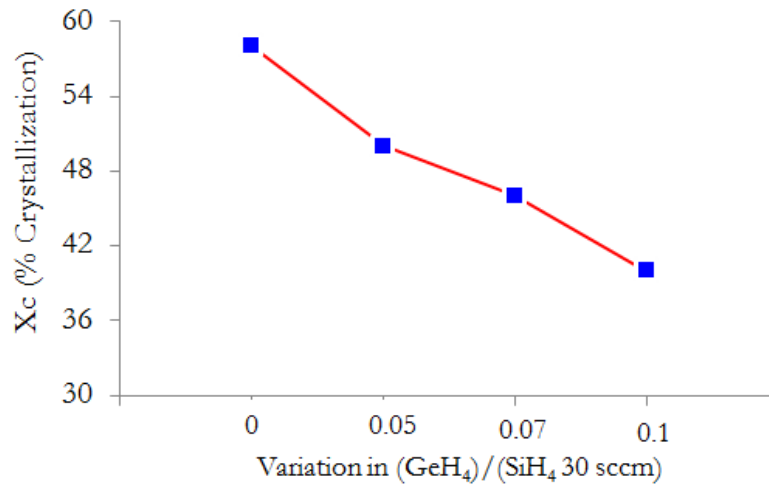
Fig 4.6: Variation in crystallinity on increasing the germane flow in the amorphous cycle

We have also reported the behavior of crystallization on changing the thickness of various layers. Fig4.7 shows the variation of crystallinity on changing ncSi:H and aSiGe:H layers keeping the dilution ratio and power constant. Increase in ncSi:H layer thickness helps to make the material more crystalline whereas increasing the amorphous cycle time increases the amorphous content in the film
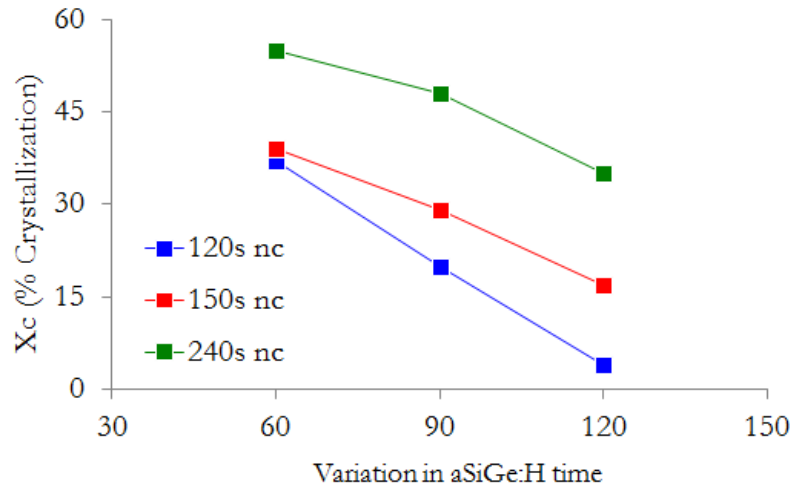
Fig 4.7: Variation in crystallinity for various thickness of aSiGe:H and ncSi:H layer

Superlattice structure helps to control the crystallinity of the material by inhibiting the growth of ncSi:H. The amorphous layer helps to prevent the large grain boundary formation. To show the control of crytsallinity we have deposited SL and constant dilution films for various thickness ranges. On comparing the change in crystallinity as the film grows we can show that SL successfully controls the crystallinity as shown in fig4.8.
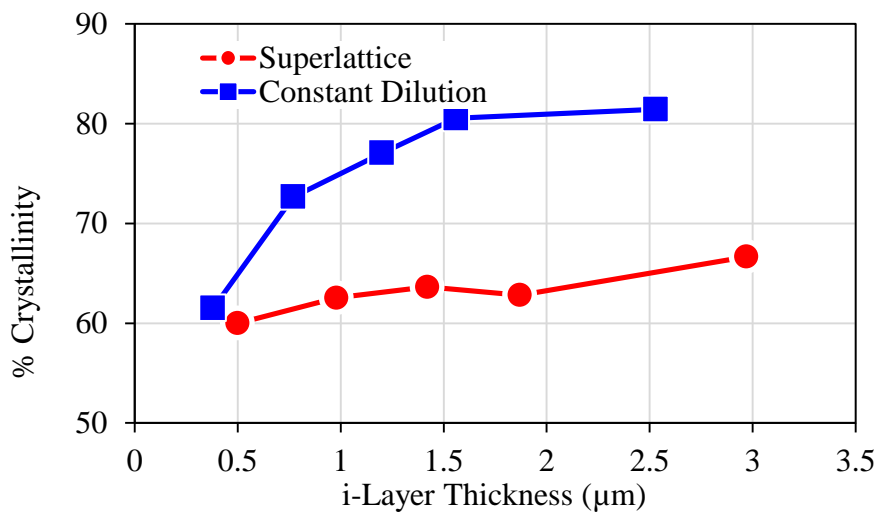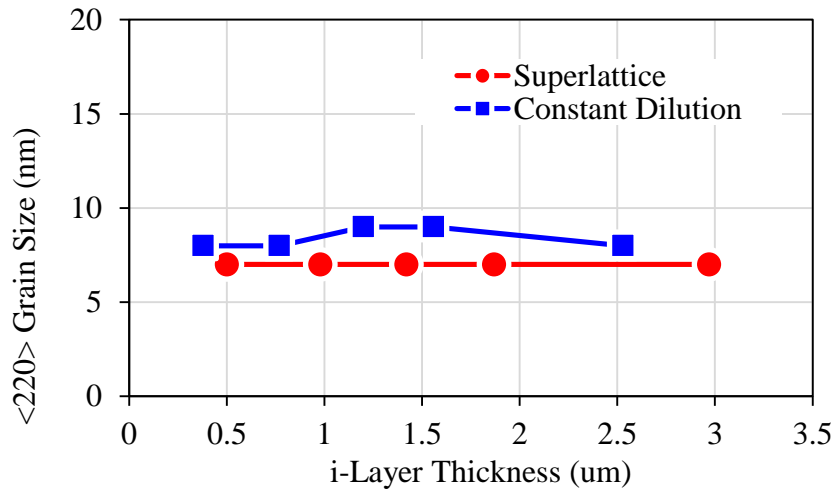
Fig 4.8: Variation of crystallinity and <220> grain size on increasing the thickness of ncSi:H

Germanium content in the film increases on increasing GeH_4 proportion in the reaction zone. Fig4.9 shows the increase in germanium content on increasing % flow of GeH_4 gas in sccm. For this particular experiment deposition condition was kept similar to what we used for SL deposition (H_2 80sccm, SiH_4 4sccm, power 3.5W, temperature 275C and pressure 100mT).
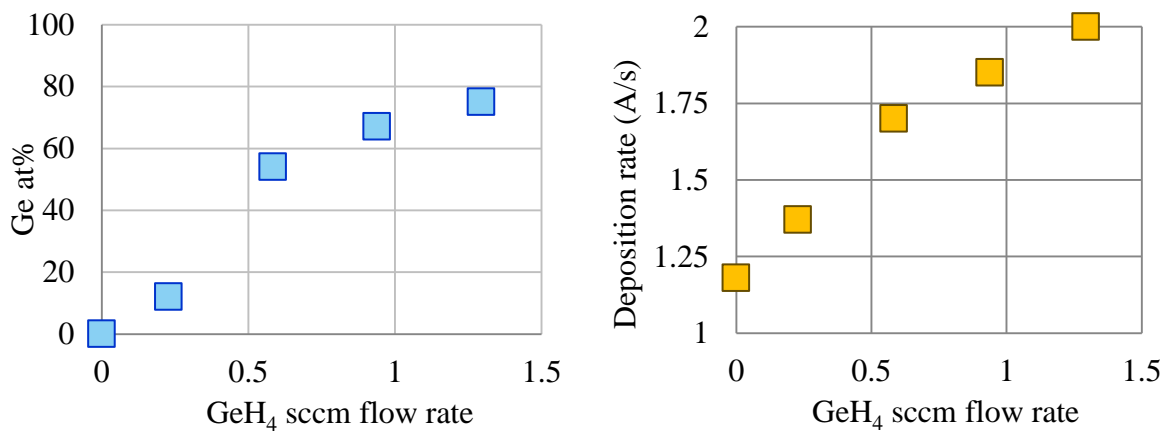
Fig 4.9: Change in at% of germanium in film on increasing GeH_4 flow
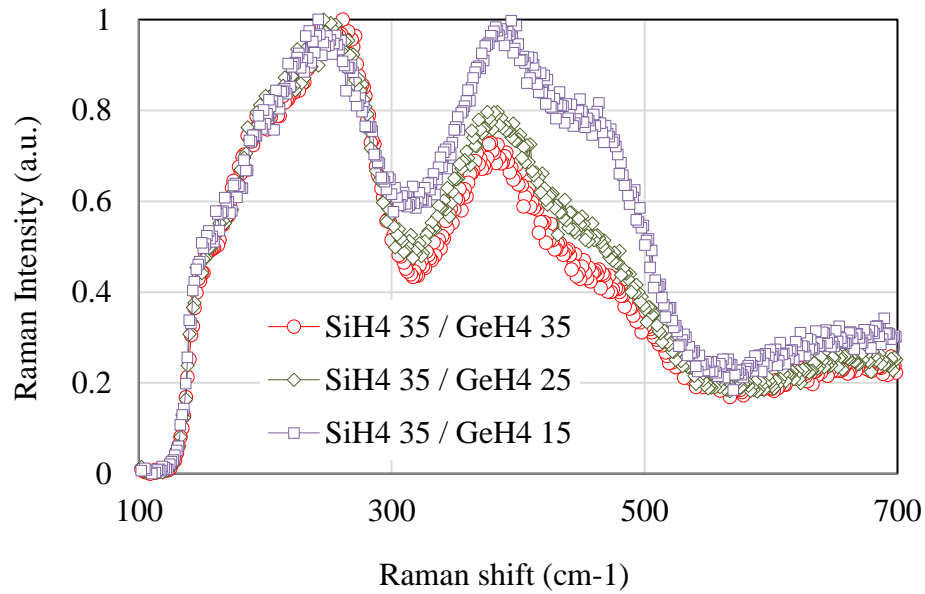
Fig 4.10: Raman comparison of aSiGe:H films with increasing germanium content

Grain size variation is an important study to achieve superior quality ncSi. Larger grains have higher current and better transportation of carriers. SL devices help to control the crystllinity and from the previous study we have also seen thin aSi layer helps to terminate the growth of ncSi. Therefore, amorphous layer thickness and its properties play vital role in determining the growth morphology of ncSi layer. On increasing germanium content in aSiGe:H, it prohibits the growth of ncSi:H. Similarly on comparing aSi/ncSi SL and aSiGe/ncSi SL it is clearly seen that aSiGe/ncSi SL have smaller grain size. It can be explained by the poor nucleation facilitating environment when ncSi is grown on aSiGe.
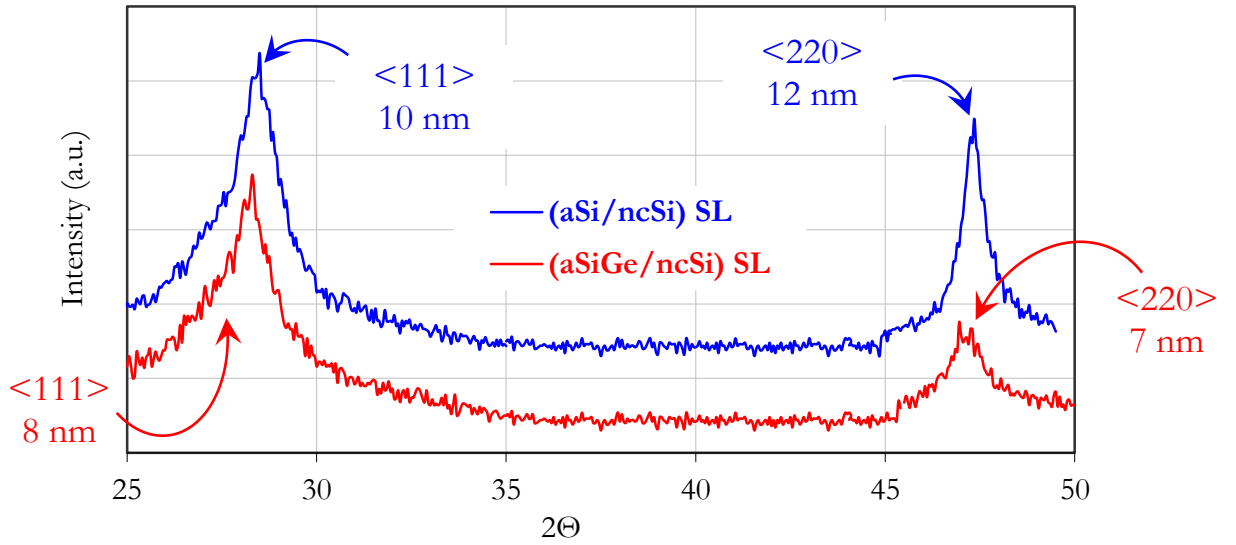
Fig 4.11: XRD graph of aSi/ncSi and aSiGe/ncSi SL with the grain size of <111> and <220>

CHAPTER 5.   DEVICE PROPERTY OF aSiGe/ncSi SUPERLATTICE SOLAR CELL

5.1 (aSiGe/ncSi) superlattice solar cell

(aSiGe/ncSi) SL device is a layer by layer structure of aSiGe:H and ncSi:H. The individual thicknesses of amorphous and nanocrystalline layer can be controlled, which helps to maintain the crsytallinity of the growing film. Fig5.1 is the cross-sectional schematic image of an aSiGe/ncSi SL. Amorphous and nanocrystalline properties are mainly controlled by changing the power. At lower power ~ 3W film is amorphous whereas at high power ~ 30W film grows in the nanocrystalline regime. Dilution of H_2/SiH_4, pressure and temperature are kept constant through the process of SL. We may go for selective doping which we will be discussed in detail later in this chapter.
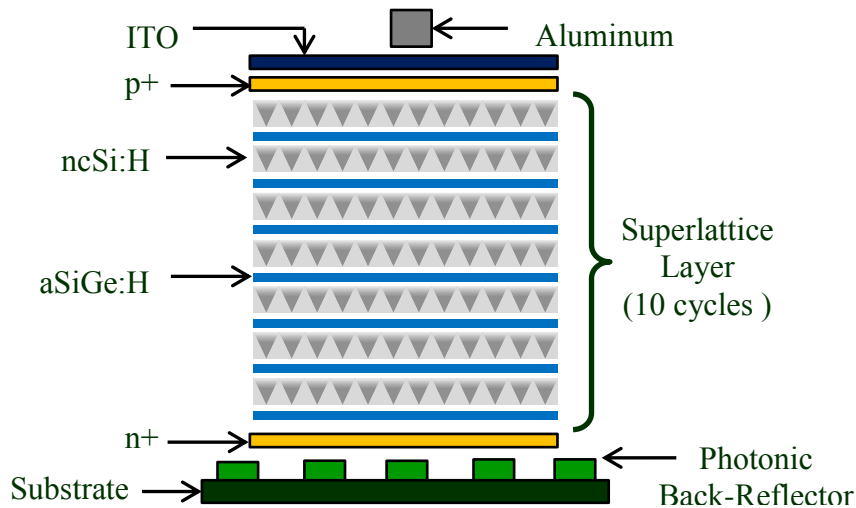
Fig 5.1: Schematic diagram of SL with amorphous and nanocrystalline layers

5.2 Enhancement in QE on increasing germanium content in aSiGe:H Layer

On increasing germanium content in aSiGe:H there is one to one increase in absorption coefficient of the SL which helps to harvest more photons. The simulation result showed an increment of ~ 2mA/cm^2. Experimentally we found the results very much in agreement to the simulation data. Fig5.2 shows the comparison of experimental QE with increase in germanium content in aSiGe:H layer. Current density increases on increasing the germanium content in aSiGe:H amorphous layer. The comparison was done at -1V bias voltage because at high reverse bias we would be able to collect most of the carriers generated in the i-layer. Devices made with aSiGe:H showed severe collection problem at lower reverse bias and forward bias of compared to aSi/ncSi SL. The enhancement is mainly observed in between (550-900) nm range where we should expect to get the enhancement from aSiGe:H.
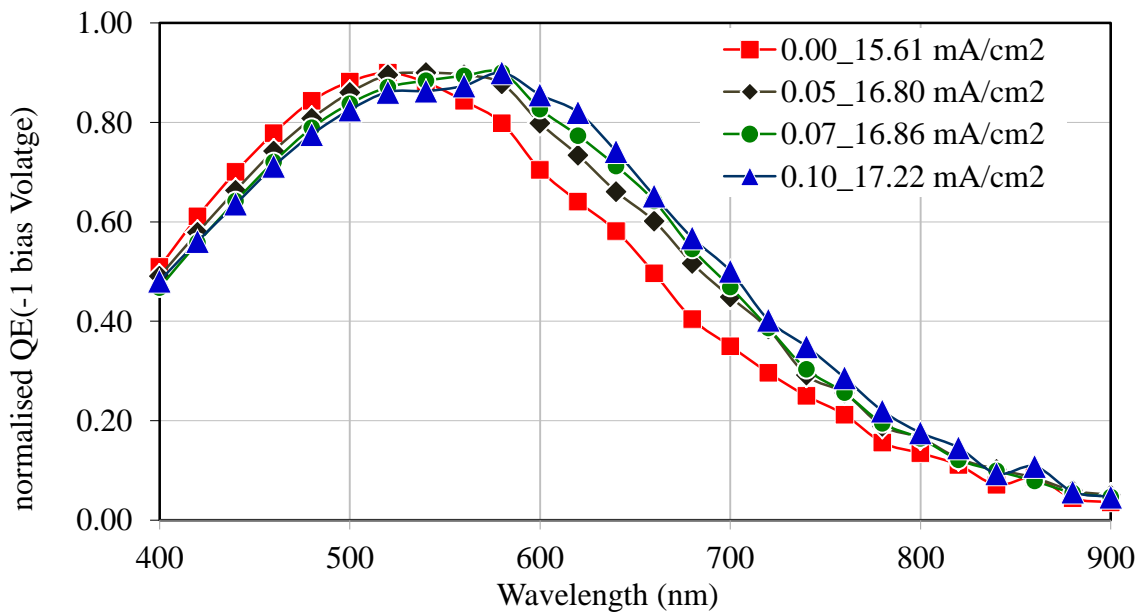
Fig 5.2: Enhancement in QE response on increasing the Ge content in aSiGe:H layer

To solve the collection problem various methods were used during fabrication of the device. We know that SL structure is made up of alternate layers of amorphous and nanocrystalline silicon. Individual amorphous and nanocrystalline layer property are important because they help to collect the carriers. Inherent n-type property of ncSi:H has adverse effect on hole collection. To effectively collect the holes and electrons we can selectively dope the layers with ppm amount of dopants such as TMB and PH_3.

5.2.1 Grading germane in the amorphous cycle

Grading germane help holes to collect from the amorphous layer to ncSi:H layer as shown in fig5.3. Constant ppm TMB was used during the initial growth of SL to compensate residual PH_3 or oxygen contamination.
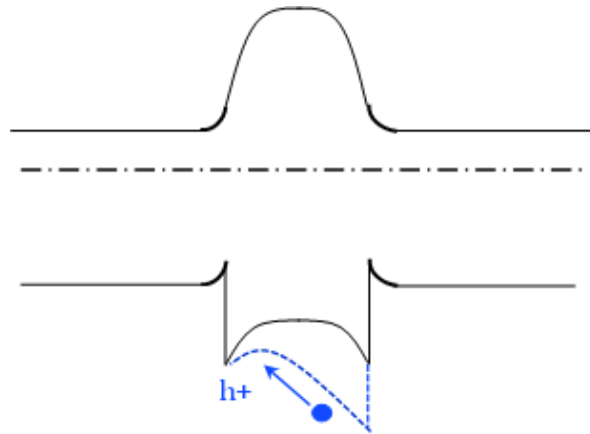
Fig 5.3: Grading of germane helps to assist the hole collection

Collection improves on grading germane in amorphous layer. Grading also helps to assist the nucleation process because for ncSi:H, seed layer would have less germanium content.

Major disadvantage of grading germane is the incorporation of less germane in the amorphous layer hence it result to lower current than expected. Fig5.4 is the best device we have got with grading of Germane. Both QE vs bias and QE ratio suggest hole collection problem.
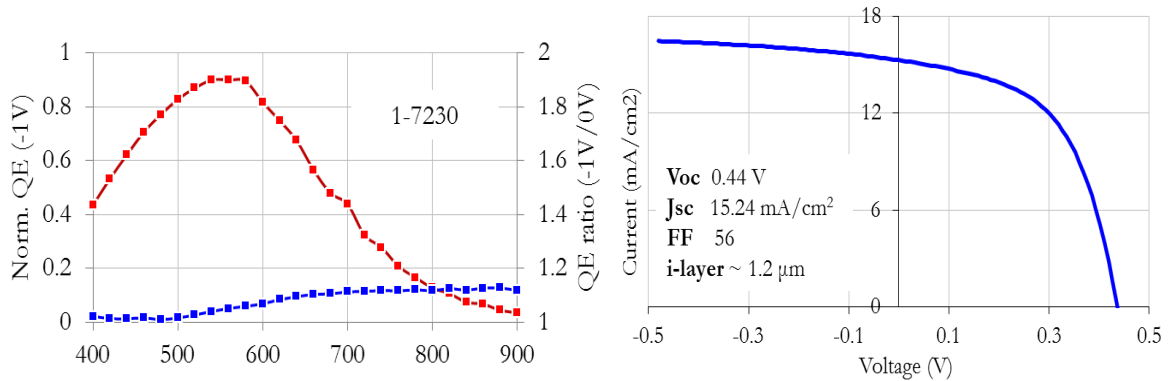
Fig 5.4: QE and IV of the best device got by grading GeH_4 in aSiGe layer

To study the graded aSiGe/ncSi SL in detail we did a series of experiment. Various important parameters of a solar cell such as Jsc, FF and Voc were compared and plotted to see if it has any relation with germanium content in the amorphous layer. Fig5.5 shows the comparison graphs where it clearly shows a trend for each of them. The motivation of carrying this experiment to solve the problem of low Voc. We observed that aSiGe/ncSi SL have lower Voc if compared to aSi/ncSi SL. If we observe the trend of raman crystallization it shows that the material growth is becoming less crystalline on increasing germanium content. On comparing Voc we observe an opposite trend with respect to raman crystallinity. From previous study we know for aSi/ncSi SL on decreasing % crystallinity helps to reduce Jo which helps to increase Voc. The opposite trend in aSiGe/ncSi SL can be explained with the help of Jo. If germanium content is increased in aSiGe:H then it

introduces more defects which increases Jo hence decreases Voc. The increase in defect was also confirmed by doing Cf experiment on similar samples.
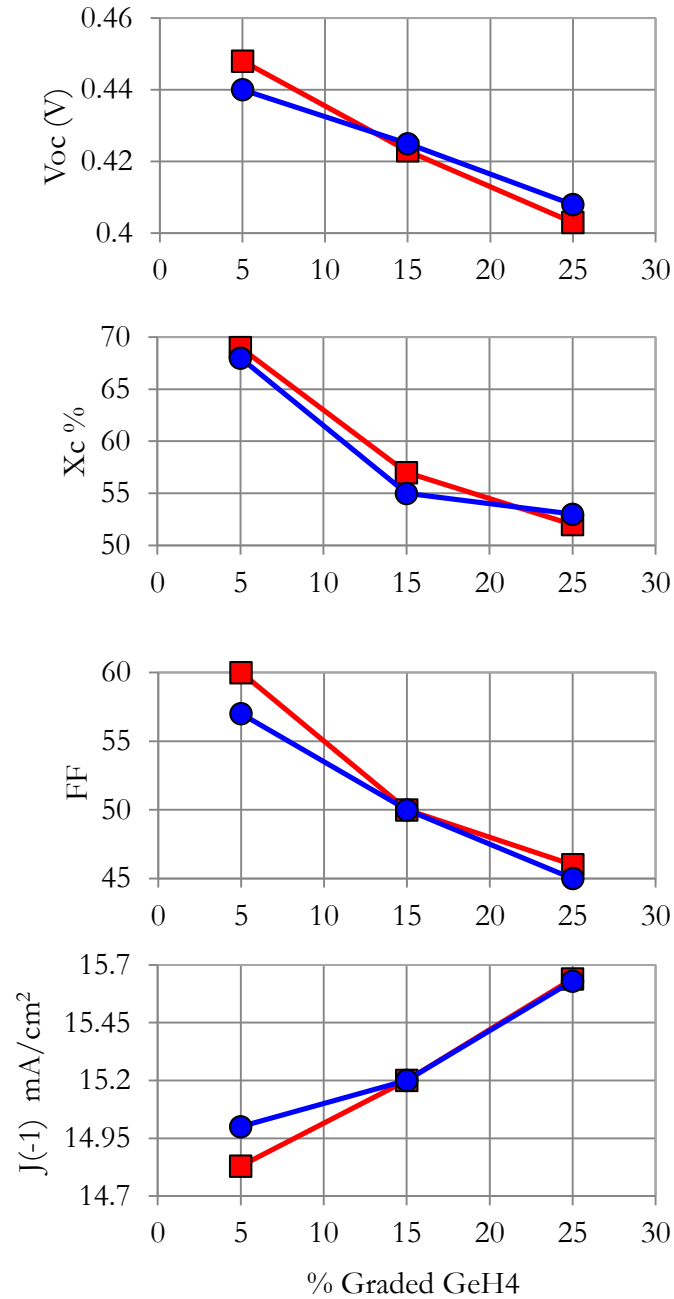
Fig 5.5: Experimental result of graded GeH4 SL devices with two series of experiment shown in red and blue color.

5.2.2 No selective doping of both aSiGe:H and ncSi:H layer

Doping layers selectively may help the collection of carriers with the help of decrease in barrier height. ppm TMB and ppm PH$_3$ were used to dope the layers differently. When we started with aSiGe/ncSi SL we didn't dope anything and the result was a poor quality device. The IV curve in fig5.6 shows the poor collection of carriers and hence low FF. The motivation of doping the layers was definitely driven by the preliminary results where we had problems with carrier collection.
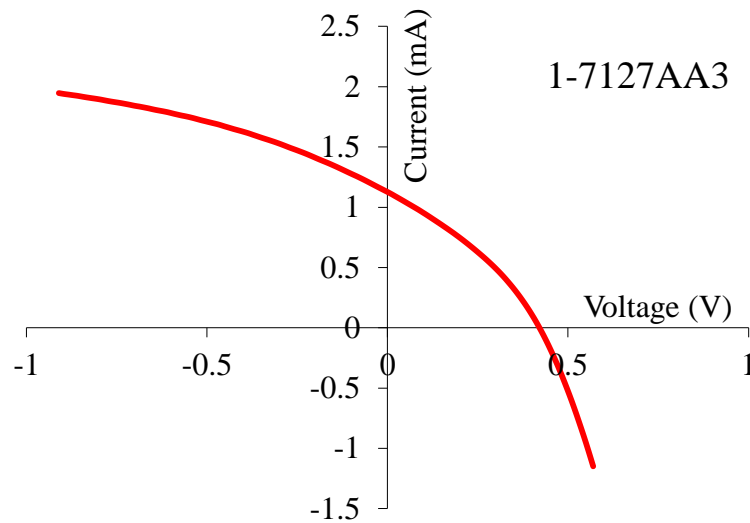
Fig 5.6: IV curve of a poor quality aSiGe/ncSi SL without any selective doping scheme.

5.2.3 Doping only aSiGe:H with ppm TMB

On doping aSiGe:H layer with ppmTMB it raises the height of Ev and Ec as shown in fig5.7. On raising the level of Ec and Ev, it increases the barrier for both the hole and the electron generated in aSiGe:H layer.
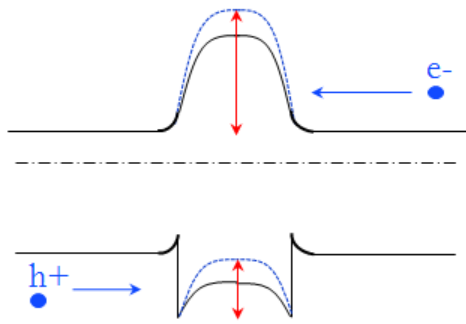
Fig 5.7: Doping aSiGe:H only with ppm TMB

QE curve and QE vs. bias curve shows clearly the electron collection problem as shown in fig5.8. The Quantum efficiency experiment was done at -1V and 0V bias where we see high collection problem at lower wavelength. The lower wavelength light absorbed near the p-i interface of the device, there is no problem for the hole collection near p-i interface but electrons have to diffuse through the n-layer to get collected in n+. If we see collection problem near 400nm then it implies electron collection problem. QE vs bias data explains how effectively we are collecting the holes. Fig5.8 QE vs bias data does show poor collection of holes in the forward bias when the electric field is weak.
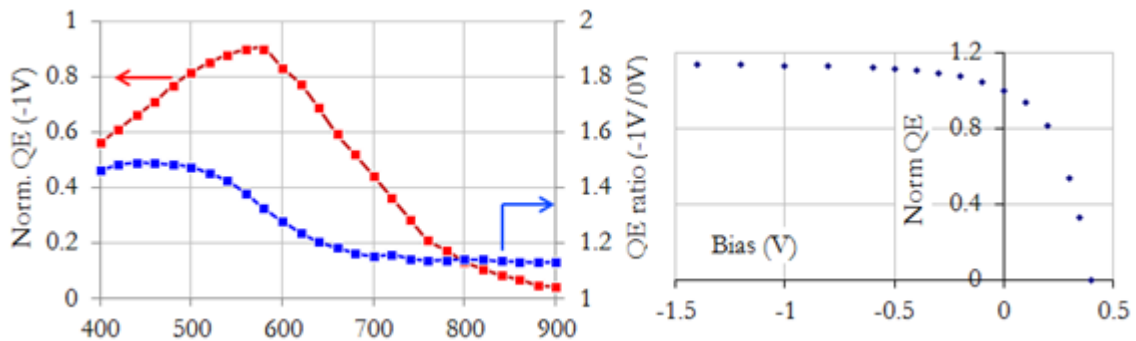
Fig 5.8: QE and QE vs. bias graph of the device with ppm TMB doped aSiGe:H layer

5.2.4 Doping aSiGe:H with ppm TMB and ncSi:H with ppm PH₃

We have already discussed earlier the inherent n type nature of the nanocrystalline silicon. Doping ncSi:H with ppm PH_3 makes the material more n type and lifetime of holes decreases drastically. Fig5.9 is the band diagram of the ncSi:H layer doped with PH_3 and aSiGe:H doped with ppm TMB. Fig5.10 is the QE and QE vs. bias graph of the device which shows drastic hole collection because of decrease in the diffusion length.
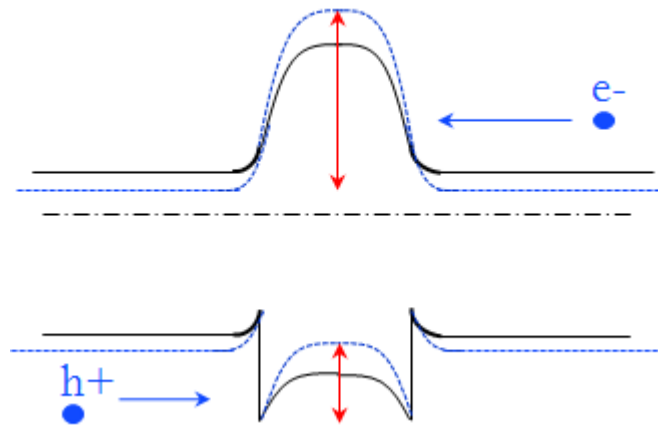
Fig 5.9: Band diagram of ncSi:H doped with ppm PH_3 and aSiGe:H doped with ppm TMB
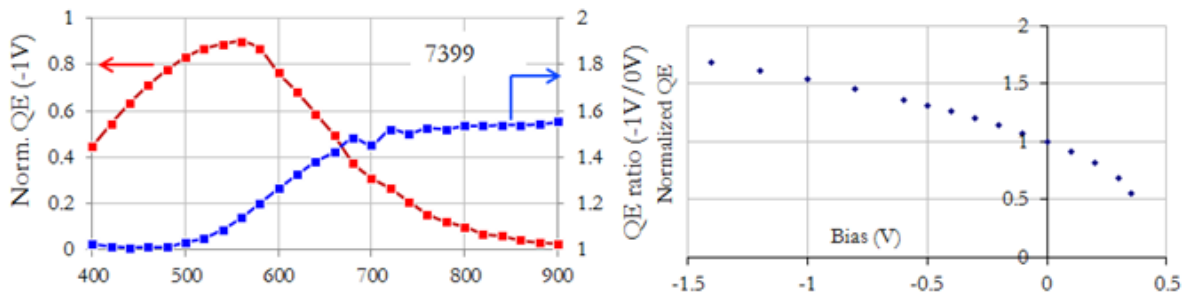
Fig 5.10: QE and QE vs. bias graph of ncSi:H doped with ppm PH_3 and aSiGe:H doped with ppm TMB

If there is hole collection problem in the device then it would appear as high QE ratio at higher wavelengths. The reason is the high absorption length of high wavelength photon.

Higher wavelength photons gets absorbed near the n-i interface of the device. There is no problem for the electron collection but for holes they have to diffuse through the i-layer to reach p+. Doping ncSi:H reduces the lifetime and hence reduces the diffusion length of the holes. QE vs bias data also shows the characteristic problem of hole collection. Even at high reverse bias we see the hole collection problem.

5.2.5   Doping aSiGe:H with ppm PH$_3$ and ncSi:H with ppm TMB

Figure 5.11 shows the band diagram of the SL doped with ppm PH$_3$ in aSiGe:H and ppm TMB in ncSi:H. ppm PH$_3$ helps to decrease the barrier height for both electron and holes. The main purpose of adding TMB in the ncSi:H cycle is to compensate any contamination of PH$_3$. It has been observed that ncSi:H gets very easily contaminated with PH$_3$, for the same reason we do a dummy run with TMB after initial PH$_3$ grading. In this set of experiment optimizing the dopants is very crucial to obtain a good device.
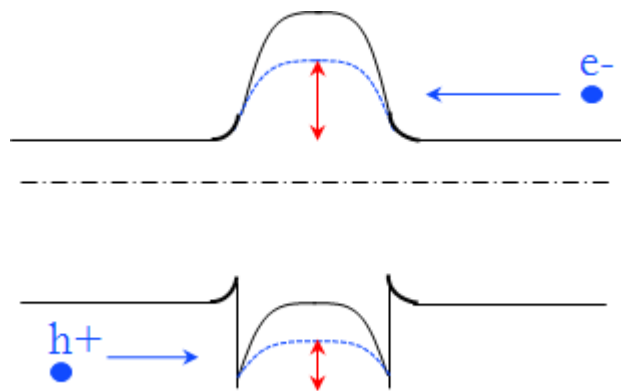
Fig 5.11: Band diagram of aSiGe:H doped with ppm PH3 and ncSi:H with ppm TMB

Fig5.12 shows the QE and QE vs bias graph along with the IV curve. There is hole collection problem which could be solved by further optimization of the dopant quantity. The QE current at -1V bias is 15.65 mA/cm2 which is high as compared to aSi:H SL devices made with similar parameters.
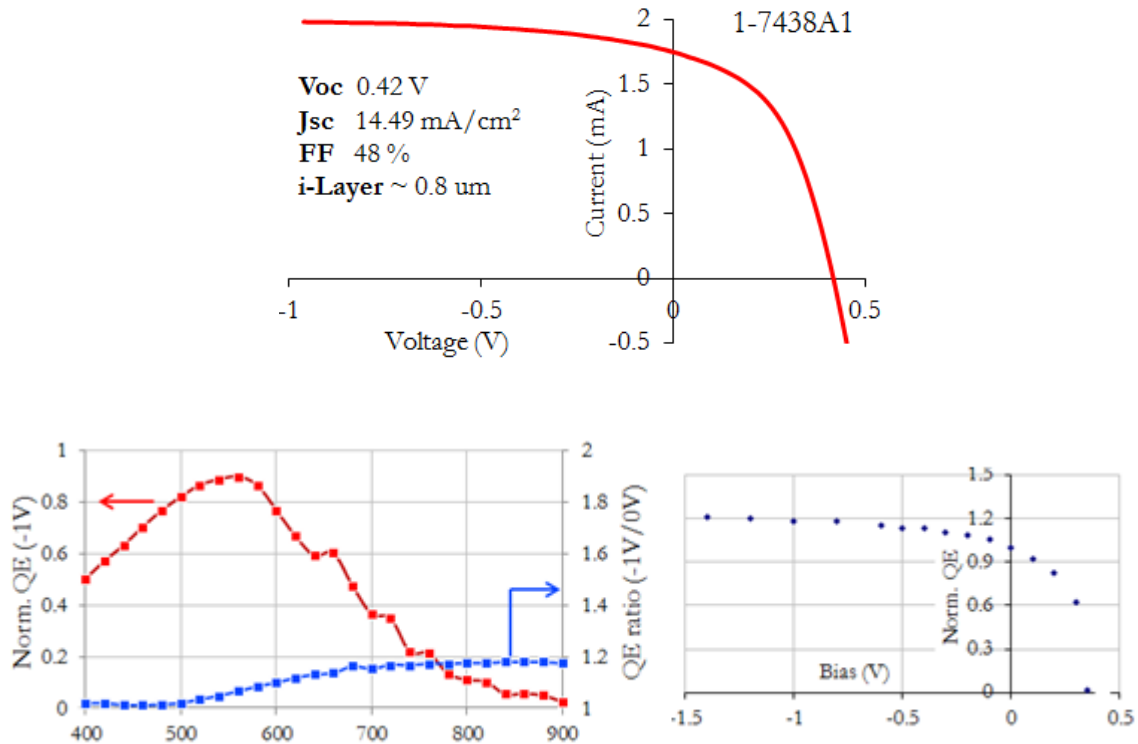
Fig 5.12: IV, QE and QE vs. bias data of the device doped with ppm PH_3 in aSiGe:H and ppm TMB in ncSi:H

5.2.6   Doping only ncSi:H with ppm TMB

On doping only ncSi with ppm TMB it causes electron collection problem similar to case (b). Adding TMB in the device is vital and tricky at the same time. To understand the device behavior we need to first study the compensating and doping nature of TMB. The ppm amount of TMB always help to compensate residual oxygen present in the reator

chamber. It helps to increase the hole lifetime. At the same time if TMB amount exceeds the required amount then it starts to dope the material. This affects the electron collection and we see drop in FF.

5.3 Increasing aSiGe:H layer time (thickness)

Increasing Germanium content helps to increase the current. If we could make thicker aSiGe:H layers then it would absorb more photons. A systematic set of experiment was done in which aSiGe:H layer thickness was increased while keeping rest of the parameters same. It was observed that on increasing the thickness we could further improve the current density by 2mA/cm^2, provided we maintain the crystallinity. In the previous study it was shown that on increasing either Germanium or thickness of aSiGe:H layer, it inhibits the growth of ncSi:H.
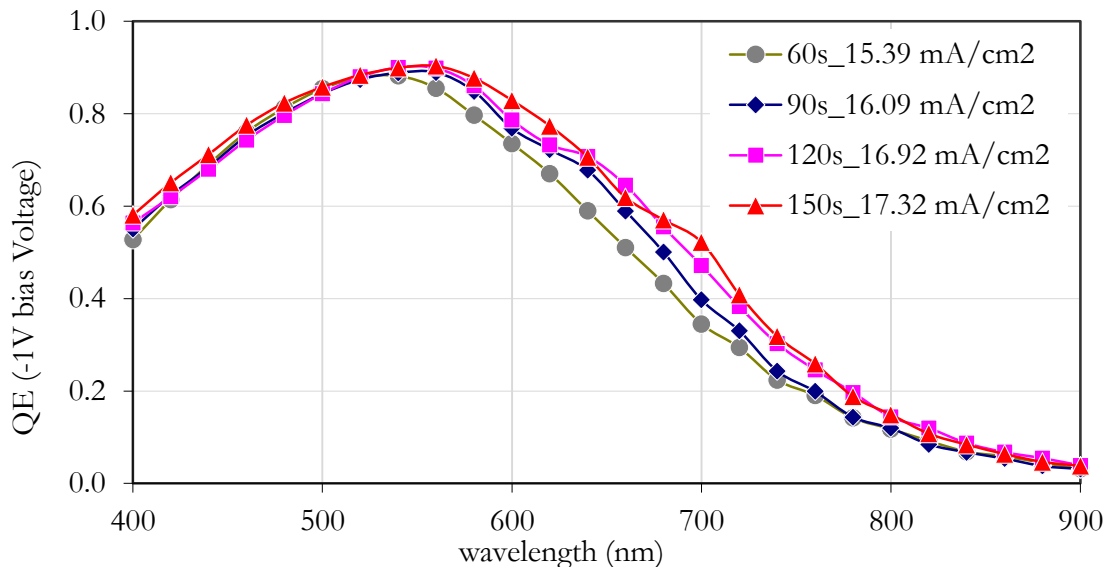
Fig 5.13: Experimental QE curves showing the enhancement in the current density on increasing aSiGe:H thickness.
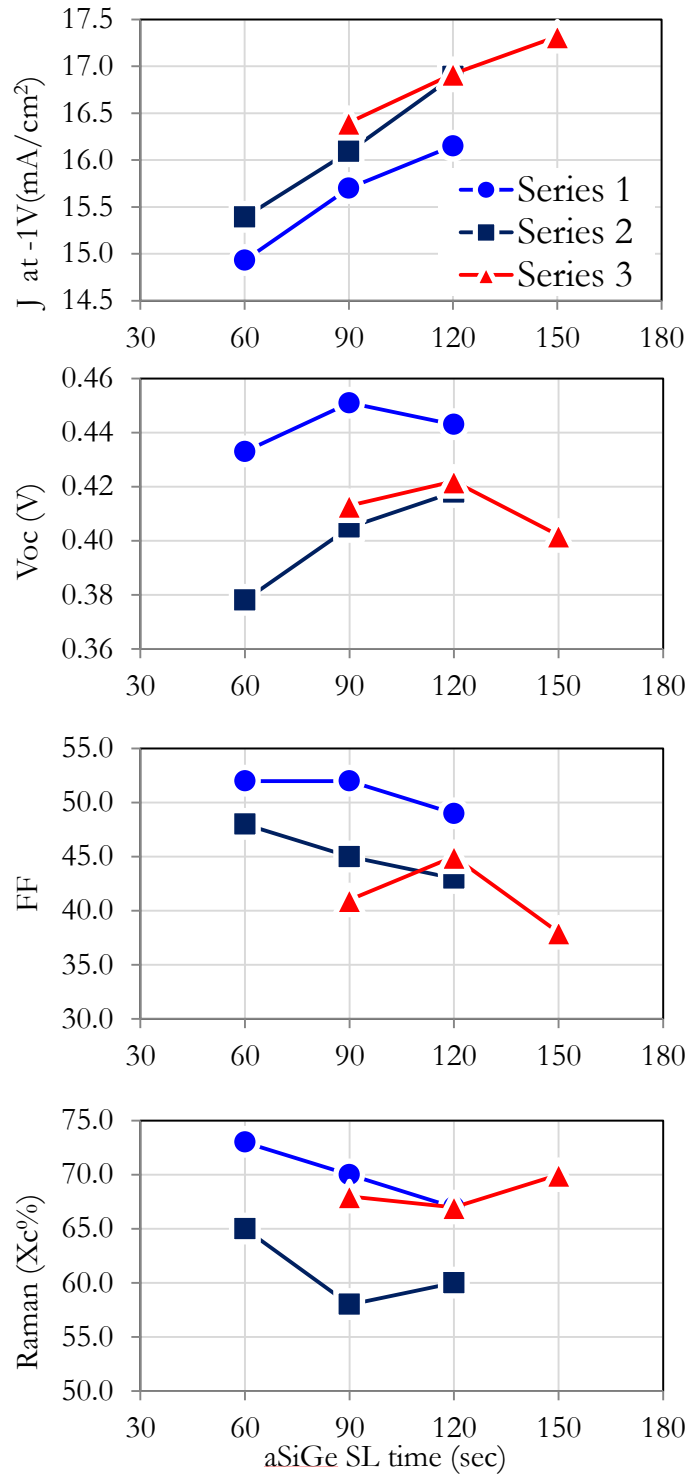
Fig 5.14: Different series in which aSiGe:H layr was increased.

5.4 Grading GeH₄ along cycles in SL

To further improve the collection of holes we came up with an innovative design by applying the principal of grading and selective doping. Holes generated near n+ have most difficulty for the collection because they have to diffuse through the i-layer to get collected in p+. From previous set of experiments we know that aSiGe:H provides poor electrical properties so we can use less GeH4 in the initial cycles and increase it gradually towards the end. By doing so we would be using high Ge content in aSiGe:H near the depletion width of the device which would further help in the collection. Nevertheless we would also be implementing selective doping (ppm TMB in ncSi layer only). Fig5.15 shows the schematic image of the grading scheme with the IV curve. With this new scheme we were able to achieve over 60% fill factor in aSiGe/ncSi SL devices.
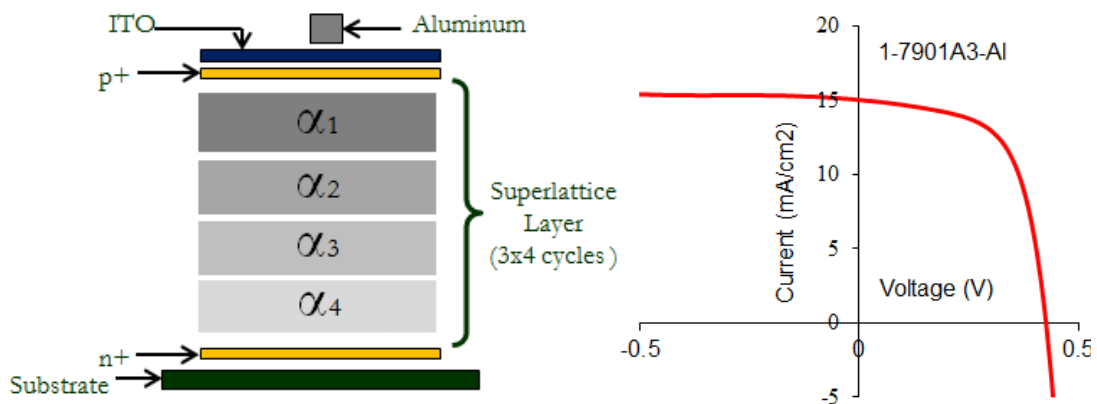
Fig 5.15: Schematic structure of the graded GeH4 SL structure with 4 different step grading showed as 4 different absorption coefficient. IV curve of the best SL device obtained with Voc 0.43, FF 64% and J 15.2mA/cm2.

5.5 Comparison of Experimental and Theoretical Result

To prove that aSiGe/ncSi SL helps to increase the current we compared aSi/ncSi SL and aSiGe/ncSi SL. They have similar i-layer thicknesses for the comparison. Simulation was laso done by keeping the i-layers 0.95um with ncSi layer 70nm and amorphous layer 5nm. From fig5.16 we can see that simulation result matches very closely to what we get experimentally. The enhancement is exactly at the predicted solar spectrum range which helps to prove that thin aSiGe:H definitely helps to increase the current.
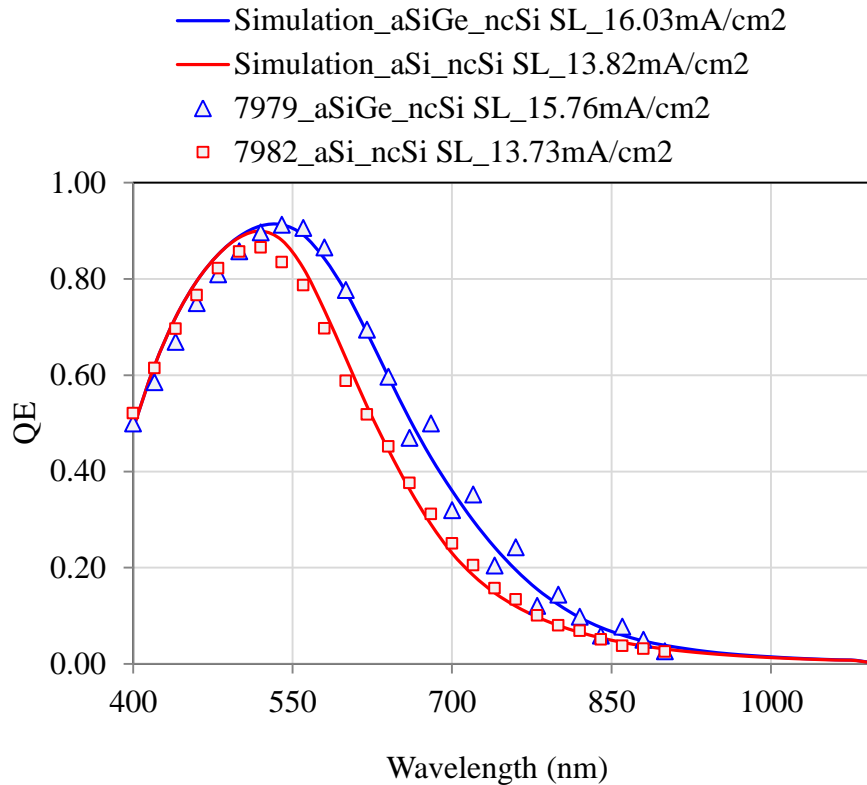
Fig 5.16: QE comparison of theoretical and experimental work done on aSi/ncSi SL and aSiGe/ncSi SL with same i-layer thickness.

On comparing other device properties we see that aSiGe/ncSi SL have lower Voc as compared to aSi/ncSi SL. Raman experiment explains that it is not the crystallinity which is responsible for lower Voc, since both the devices have similar % crystallinity ~ 55%. Various other experiments were done on these germanium SL to find out the variation of defects. An interesting result was shown by the Cf experiment. It is apparently increase in defect states in the material which could be the reason for lo Voc. Cf experiment shows that on increasing germanium content in the amorphous layer we observe increase in defect density. Fill factor is comparable for both the devices which could have been possible because of step grading and preferential doping of amorphous and nanocrystalline layers.
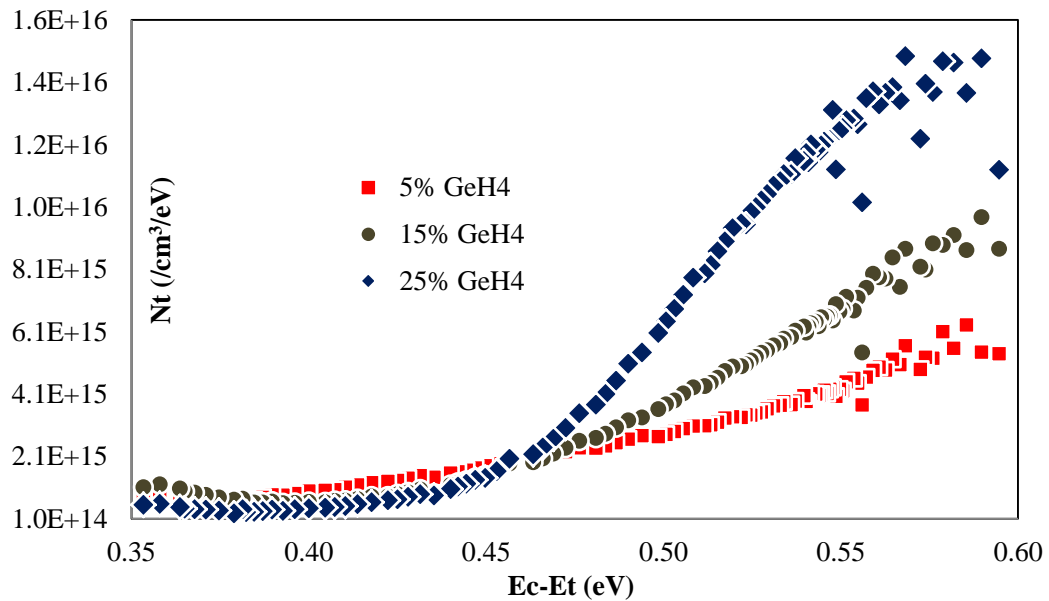
Fig 5.17: Cf experiment done on (aSiGe/ncSi) SL with various germanium content in the amorphous layer.

CHAPTER 6. NOVEL WAYS TO INCREASE EFFICIENCY OF SOLAR CELLS

6.1 Introduction

Thin film solar cells hold a lot of potential in photovoltaic industry by lowering the cost and processing time. Thin absorbing layer of these solar cells lack the ability to capture all incoming photons. Therefore, light trapping schemes are needed for proper harvesting of the near infra-red wavelengths of light. BR can be used to trap the incoming light with the help of multiple reflections, and scattering which mostly depends on the surface texture of BR. There are various ways to harvest light such as:

1. Annealing silver to form island like structures.

2. Etching ZnO:Al to form irregular craters.

3. Photonic periodic structures.

Nanocrystalline silicon has slightly higher absorption co-efficient than crystalline silicon, typical diffusion lengths are only around 4μm, which in turn implies the intrinsic layer should be around the same thickness. Being an indirect bandgap material thickness of more than 100μm needed for efficient absorption to have efficiencies comparable to that of crystalline silicon solar cells. BR help in minimizing process time by utilizing thinner layers and also increase the absorption by scattering the unabsorbed photons which leads to light trapping and thus increased photo generation.
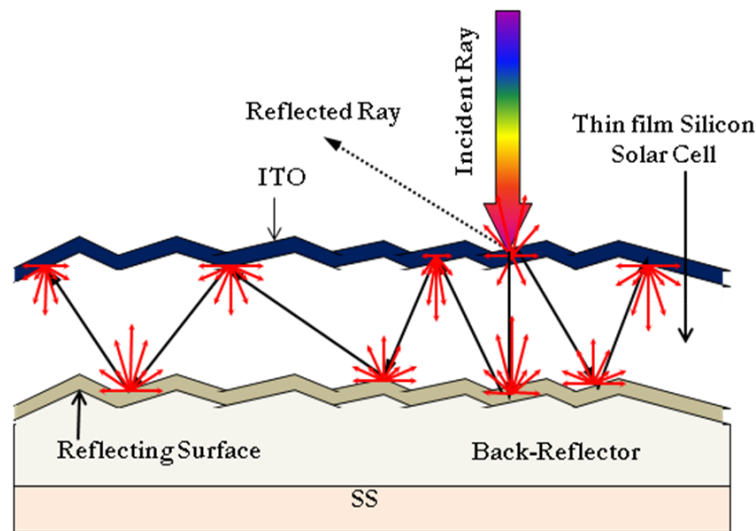
Fig 6.1: Schematic Diagram of the Integrated Back-Reflector with the thin film Solar cell.

Figure 6.1 is the schematic diagram of a solar cell with a BR at the bottom. BR has various important components such as, a textured surface which will help to scatter light, a reflecting surface to reflect light without any absorption, and a TCO barrier to prevent silver diffusion in the device. BR is mainly used to harvest the higher wavelength of light because they require large absorption length before they gets absorbed [94]

Transparent Conducting Oxide (TCO) is an essential component in a thin film solar cell. TCO has a crucial role as the front contact for thin film solar cells because the lateral conductance of p/n doped silicon layers is not high enough to avoid resistive losses over typical distances of 1cm or so [95]. Some of the TCOs used as front contacts are Indium Tin Oxide (ITO) and alumina doped Zinc Oxide ($ZnO:Al_2O_3$). When used as a front contact the TCO needs to be highly transparent in the region of operation of a solar cell as they need to effectively couple light into silicon absorber layer and also posses' high conductivity and carrier mobility to enhance carrier collection. The absorption losses need

to be minimized. Conductivity depends on the carrier concentration, mobility and thickness of the film. To increase the conductivity we need high mobility. Increasing the carrier concentration also decreases transmission, so a trade-off has to be made. TCO's should have an inert chemical property because they are coated at the top surface of a solar cell. Silicon thin film solar cells are typically grown in hydrogen rich plasma and etching of ZnO will lead to deterioration in the light trapping abilities. Thus the requirements for a proper choice of TCO can be summarized as

1) High transparency in the visible and infrared wavelengths

2) Effective light coupling into silicon

3) High conductivity and carrier mobility

4) Ability to be textured

5) Chemical stability against hydrogen plasmas

6) Abundant availability

7) Low cost of processing

8) Non-toxic

ZnO is an oxide, naturally occurring as the rare mineral called as zincite. ZnO has grown to prominence in recent years because of its application in thin film solar cells both as a front and back contact as well as its ability to be textured and also due to limited availability of Indium (ITO). ZnO can be deposited using a variety of techniques like RF magnetron sputtering [96], DC sputtering [97], LPCVD [98] and spray pyrolysis [99]. ZnO and its doped alloys have a high transparency in the region of operation for solar cells because of

their high optical band-gap (> 3.3eV). ZnO by itself has the resistivity of 10^{-4}cm^{-1}, but when alloyed with Al_2O_3 the resistivity drops to $2*10^{-5}$ cm^{-1}.
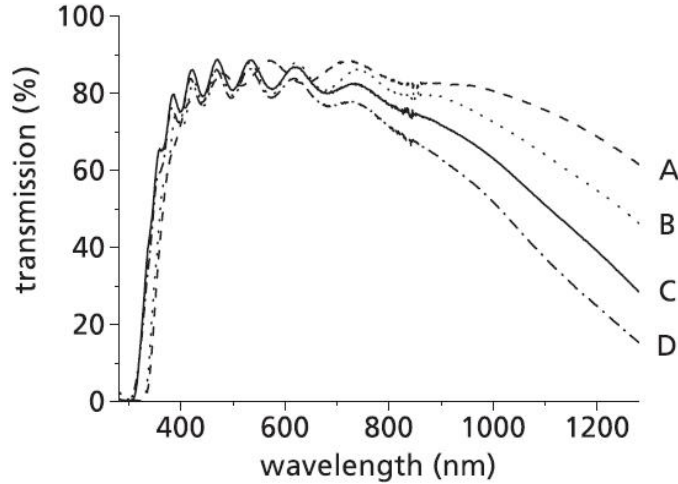
Fig 6.2: Spectral response of ZnO:Al films with varying Al_2O_3 concentrations, (A-0.2% and D-2%) [100]

Magnetron sputtered ZnO films are smooth after deposition but can be textured using wet etching techniques. Doping with Al_2O_3 increases carrier mobility in ZnO films up to 42cm^2/V-s [100] for a 0.5wt% doped Al_2O_3. The target aluminum concentration (TAC) determines the number of free carriers available in ZnO films. However heavily doped ZnO reflects light in the infrared region due to free electron oscillations. For high doping levels, parasitic free carrier absorption mechanism significantly reduces transmission in the infrared region. While a compromise has to be arrived between the transmission and the conductivity, it is the surface roughness, feature shape and size that are crucial for light scattering.

6.2 Annealed Silver as a Back-Reflector

Silver nano-particles are widely used in various fields such as chemical and biology. They have become currently an important field of study because of their plasmonic behavior which has been reported recently [105,106]. Nano-silver helps to enhance the signal because of the collective oscillation of the electrons (plasmons), which are excited by incident electromagnetic radiation. The process can be co-related to diffusion and nucleation phenomena of the silver atoms as shown in Figure 6.3.

De-sorption
[Re-evaporation]
Adsorption
Diffusion
Adsorption at
Defect Sites
Nucleation
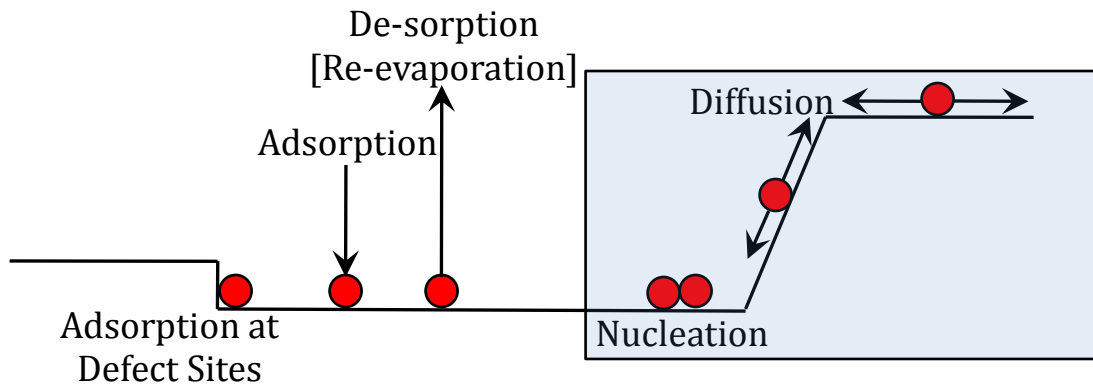
Fig 6.3: Schematic diagram showing silver texturing process at high temperature.

Annealed silver was fabricated by evaporating 200nm silver on Stainless Steel (SS) followed by heat treatment inside the furnace at high temperature for different times. Since silver agglomerates at high temperatures, therefore a systematic procedure was followed to study the behavior. Silver was annealed at different temperature for different times. Fig6.4 shows SEM images of silver film after the heat treatment. Clearly we see the nucleation and growth (agglomeration) of silver. Annealing at 400°C for 30min gave us the optimum texturing for the BR. On annealing silver at lower temperature for less time gave us in-adequate texturing. Whereas over annealing results in poor coverage of SS.

Atomic Force Microscopy (AFM) was used to evaluate the RMS roughness of the annealed silver. Islands were uniformly distributed over the area having height around 200-300nm. The lateral sizes of the islands were around 0.5-1μm (sub-micron) range. We have also observed that the distribution, size and height of the islands can be largely varied with the thickness and heat treatment of silver.
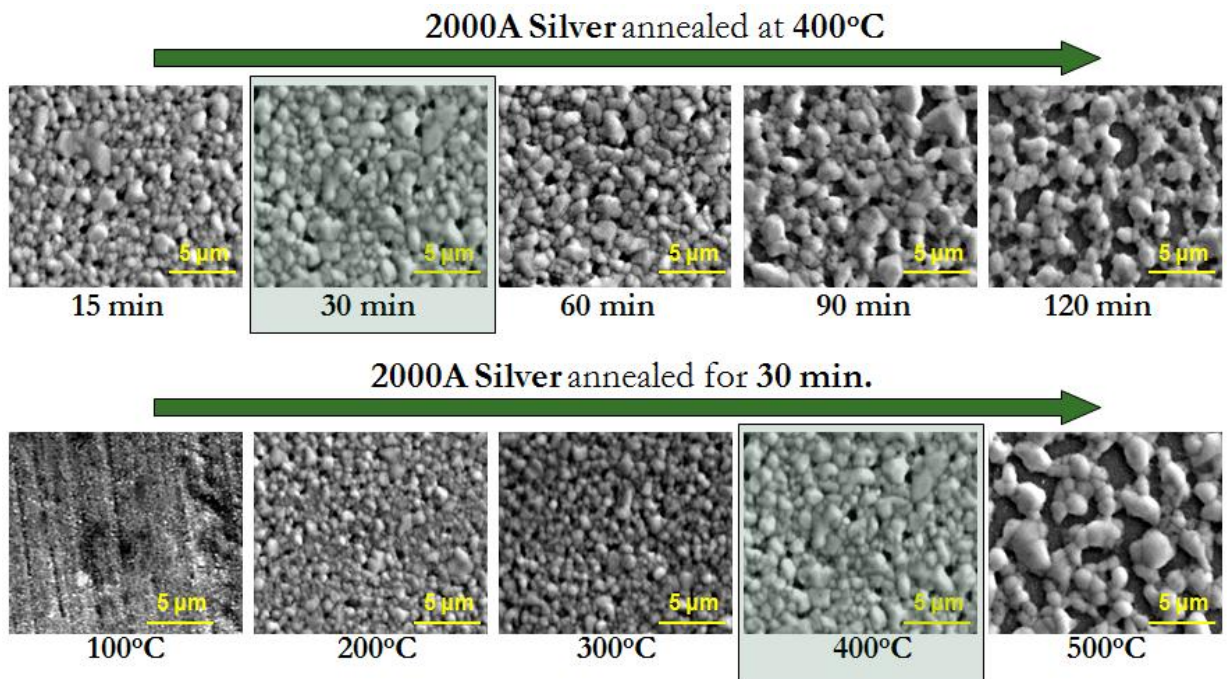
Fig 6.4: *SEM images of the annealed Silver after heat treatment at various temperature for various time.*
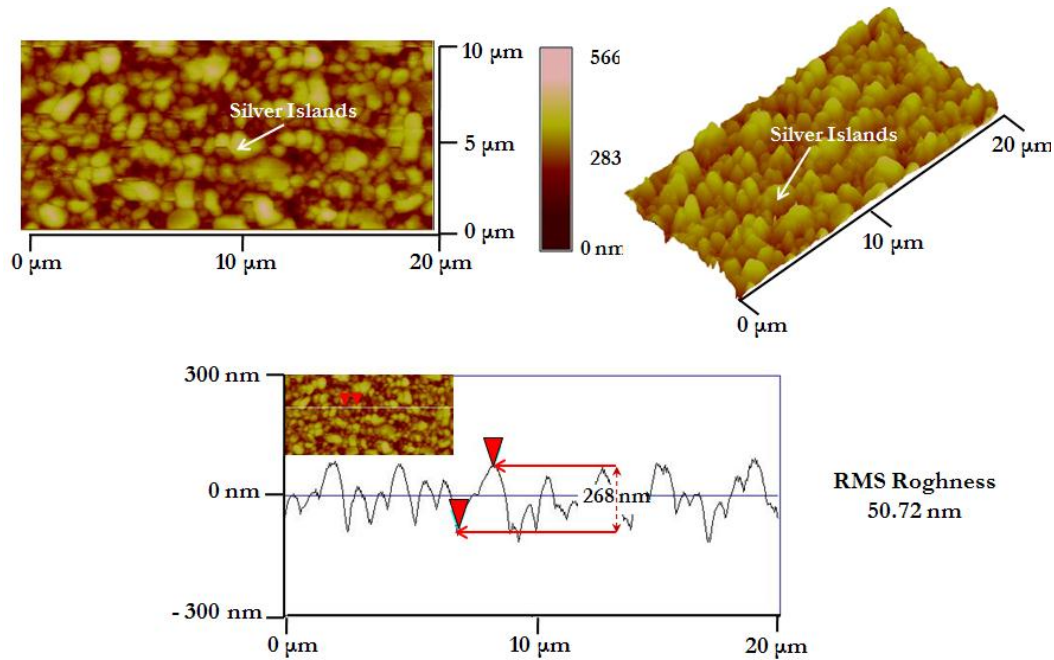
Fig 6.5: AFM analysis of Silver annealed at 400°C for 30min

6.3 Etched ZnO as a Back-Reflector

Texturing ZnO BR by using wet etching is a widely used method to prepare random textured BR. Typically sputter deposited ZnO films are very smooth and produce adequate texturing by using dil. HCl. The initial features and duration of the etch; control the morphology of the etched surface. Thus the morphology of the etched film can be controlled to provide enhanced light trapping abilities for the thin film solar cell. ZnO crystals readily undergo chemical etching [101]. The etching behavior is dependent on the crystal planes and the etching solution [102]. The etching model was predicted by Mariano et al. way back in 1969, using a model for polar III-V semiconductors. The etching takes place when the ions from the solution (OH$^-$ in the case of a basic solution and H$_3$O$^+$ in the case of an acidic solution) attach themselves to the available dangling bond as shown if figure 6.6(a).

The sputtering and the consequent wet etching of ZnO films can be linked to the Thronton model postulated by J.A.Thronton [103] in 1974. Kluth et. al [104] have proposed a modified version of the Thornton model to accommodate the variations in ZnO films [118]. Originally the Thornton model was proposed to model the growth of sputtered metals using two basic parameters, substrate temperature and deposition pressure. It uses a normalized ratio of the substrate temperature to the melting temperature of a metal (TS=TM). In the case of ZnO TS is around 150 - 400 C, and so the ratio becomes very small, instead the Julich group considers the substrate temperature instead of the normalized ratio (TS=TM). Also it has been seen that the TAC wt % also plays an important role. Pressure also seems to have a profound effect on the morphology produced after etching. Fig6.6 illustrate the variation in the deposited ZnO film at various temperature and pressure.
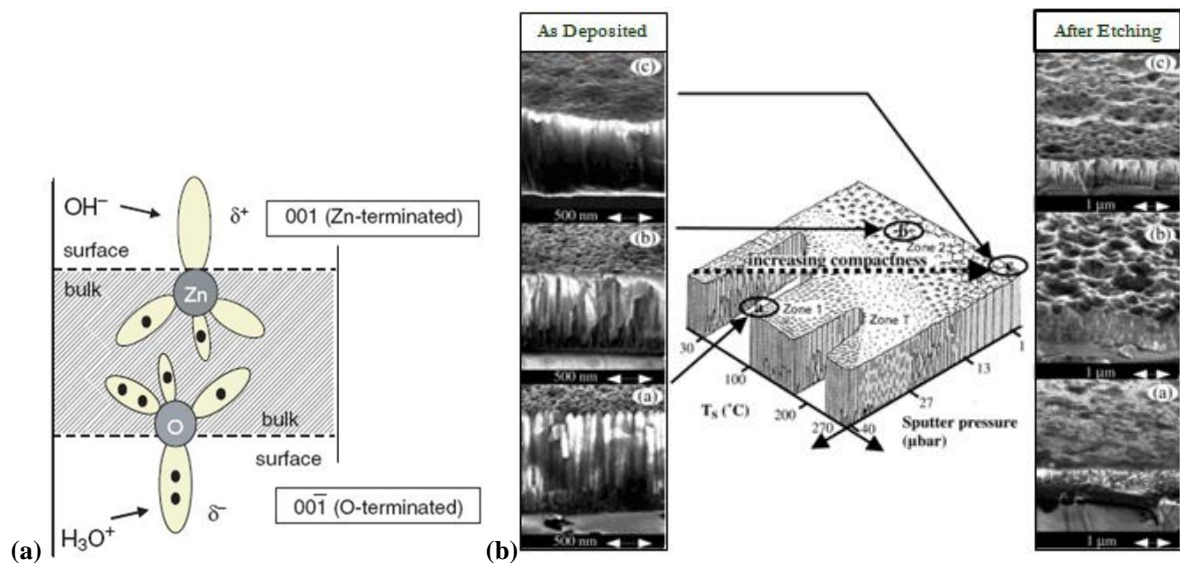
Fig 6.6: Etching mechanism of ZnO by using either base or acidic solution [118]

Initially deposited ZnO films were smooth and typical surface roughness around 10nm. After a short dip in 0.5% HCl, film starts developing small hexagonal craters. Few more seconds will texture the film to an optimum surface roughness and crater diameters. Typical root mean square surface roughness after texturing is around 100 - 150nm. Fig6.7 shows the SEM images of surface morphology with increasing etching time. The crater diameters around 0.5-1μm formed after acid etching the film. 0.185% conc. HCl solution was used to etch the ZnO film. Etching in basic solutions like KOH does not produce a uniform surface morphology; possibly due to the lesser number O⁻ terminated bonds in RF magnetron sputtered ZnO films hence we have used acidic solution to etch the film.
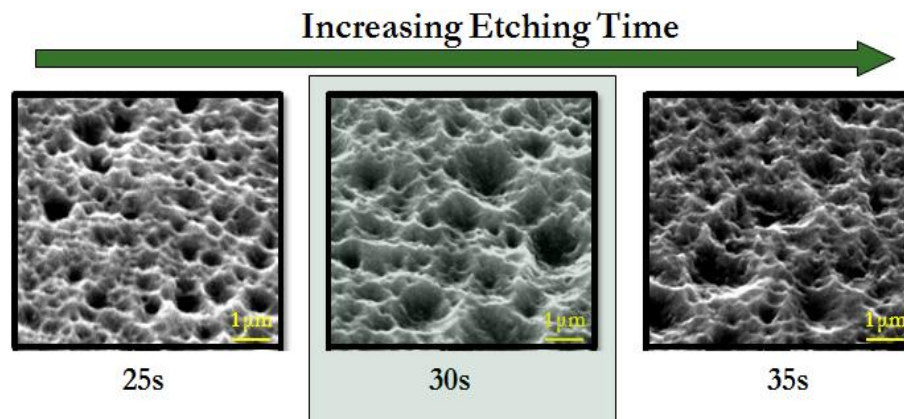
Fig 6.7: SEM images of the etched ZnO film, etched with dil. HCl for various times.

Fig6.8 shows the AFM images of the etched ZnO. On increasing the etching time from 25s to 35s we find that RMS roughness increases from 74 nm to 111 nm. But we also need to be careful not to over-etch the film. Etching for longer time leads to larger size of the crater which has been shown in the figure with varying angle θ. An optimum etching leads to superior BR property because too small or too large angle θ leads to poor BR property. This phenomenon can be explained by the total internal reflection [128,129].
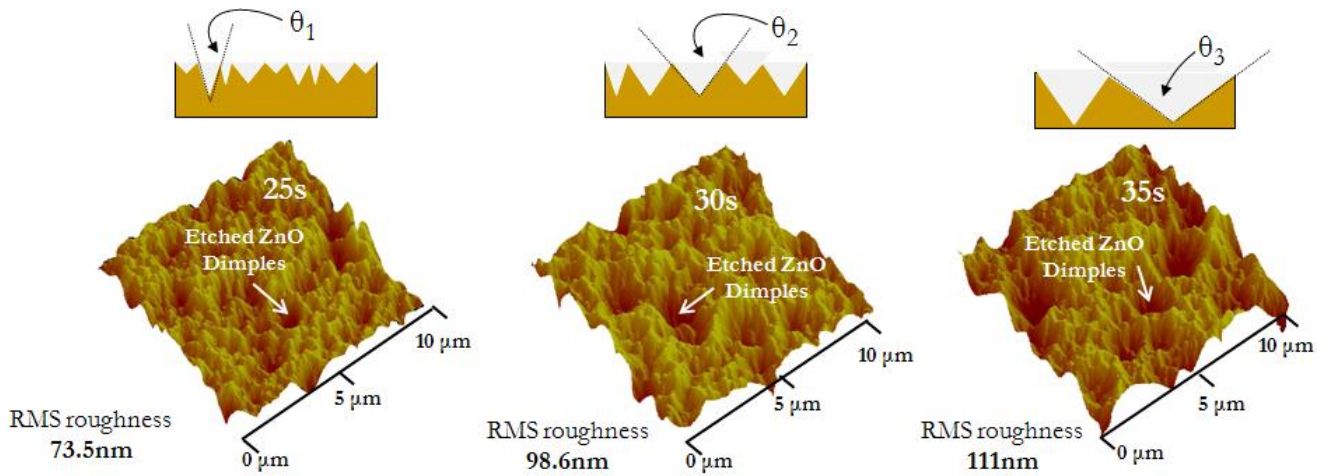
Fig 6.8: AFM images of the etched ZnO with varying etching time

6.4 Thin film solar cell on randomly textured back-reflector

Annealed Silver BR was successfully integrated with a thin film silicon solar cell to check the increment in the Quantum Efficiency response and increase in current. Fig6.9a is the comparison of the QE curves for amorphous and nano-crystalline silicon solar cell respectively. QE was measured at high reverse bias, -0.5V for amorphous silicon cell and -1V for nano-crystalline silicon cell to ensure complete collection of the carriers. The i-layer thickness for amorphous silicon was 0.3μm and for nano-crystalline it was 1.2μm. For amorphous cell we found the QE increment at 700nm from 0.08 to 0.25. Nano-crystalline cell showed enhanced QE improvement at 800 nm from 0.1 to 0.38. BR is very effective for nano-crystalline silicon solar cell because nano-crystalline silicon has better absorption coefficient as compared to amorphous silicon. On comparing the effective absorption coefficient to the actual absorption coefficient we found an enhancement of 8 times at the higher wavelength of the spectrum. Enhancement was calculated using QE at high reverse bias (-1V) with the help of the equation 1. R is the % reflection from the ITO, α is the effective absorption coefficient, t_1 is the P+ layer thickness (negligible in our case) and t_2 is the thickness of the i-layer.

$$\mathbf{QE} \sim (1\text{-}R)[\exp(\alpha t_1)][1\text{-}\exp(\alpha t_2)]$$
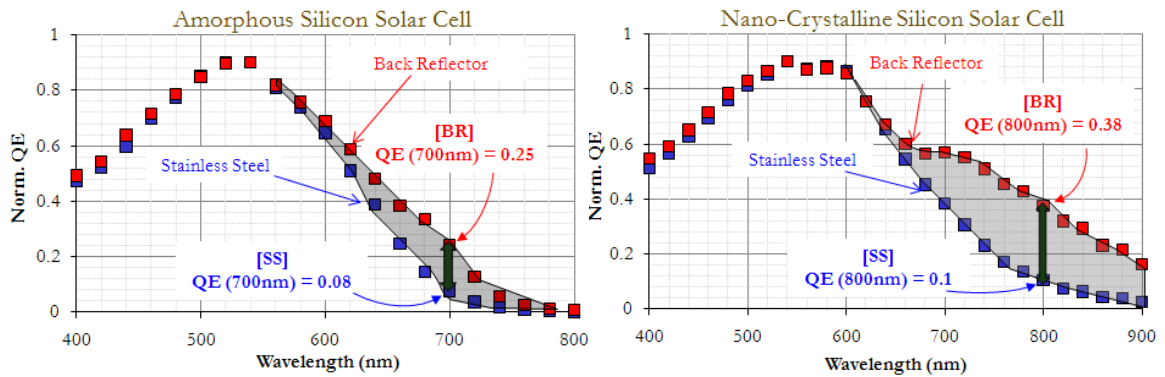
Fig6.9a : QE enhancement in aSi and ncSi solar cell due to annealed silver back-reflector

Etched ZnO BR has similar QE enhancement curve as we have already seen in the case of annealed silver BR. The typical i-layer thickness was 0.25 μm for amorphous silicon and 1.2 μm for nano-crystalline silicon solar cells. Nano-crystalline silicon solar cell showed striking enhancement at the higher wavelength of the spectrum because of better absorption coefficient.
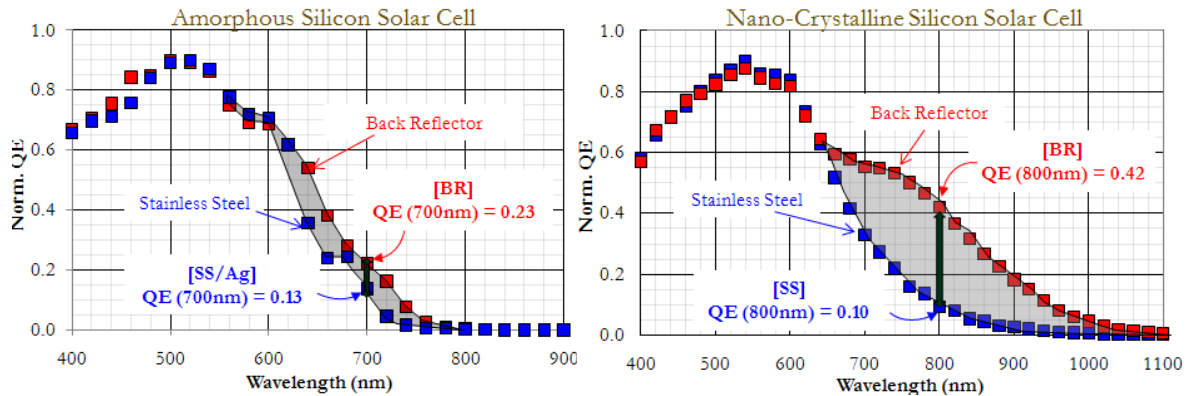
Fig6.9b : QE enhancement in aSi and ncSi solar cell due to etched ZnO back-reflector

6.5 Tandem solar cell:

The absorption of the solar spectrum is limited by the band-gap of the semiconductor. The efficiency of a solar cell can be increased by having a tandem structure, where 2 or more solar cells are connected in series. The band-gap of the absorbing layer decreases as we go from top to bottom of the solar cell. Simple electrical equivalent of a tandem solar cell

would be diodes connected in series. For tandem solar cell, efficient BR is absolutely required. We have fabricated nanocrystalline silicon/amorphous silicon tandem solar cells on nano-imprinted photonic structures. Fig6.10 shows the schematic structure of the tandem solar cell with IV curve. The best efficiency attained was ~10% on flexible substrate [124-127].
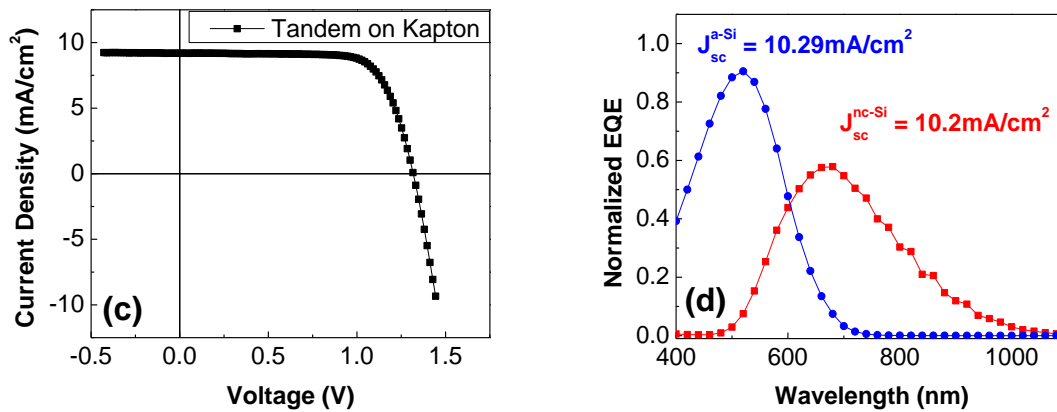
Fig 6.10: IV and QE graph of aSi:H solar cell/ ncSi:H solar cell, tandem cell with overall efficiency ~10% before light induced degradation

6.6 Nanodots on silicon wafer and SS

Major limitation in all thin film solar cell is the absorbance of near band-gap light which is ineffective, in particular for an indirect band gap semiconductor silicon. Recently plasmonic silver nanoparticles being used with an inorganic thin film solar cell. Reports by Catchpole, Green, Pillai, and Nakayama suggest that silver nanoparticle has promising advantage in the thin film industry [105]. There are two important aspects of a silver nanoparticle, size and shape. As the name suggests nanodots, these particles are in the nanometer range. Moreover Catchpole has argued that shape of the nanodot plays a vital

role in the plasmonic phenomena. For plasmonic it becomes important that the nanodots should carry high charge carriers which is only possible in the case of metals such as silver gold and etc. The scattering from the metal nanoparticles near their localized plasmon resonance is a promising way of increasing the light absorption in the solar cells.

We did few series of experiments to find out the morphology/structure of the nanoparticles and its optical property. The first experiment was to see optical property and hence the plasmonic behavior of silver nanodots. On cleaned (regular standard cleaned) glass slides 25A of silver was deposited and then it was annealed at 200C and 250C for 15min and 45min. Specular transmission was done on the Cary spectrophotometer from 400nm to 900nm. The spectral response is shown in fig6.11.
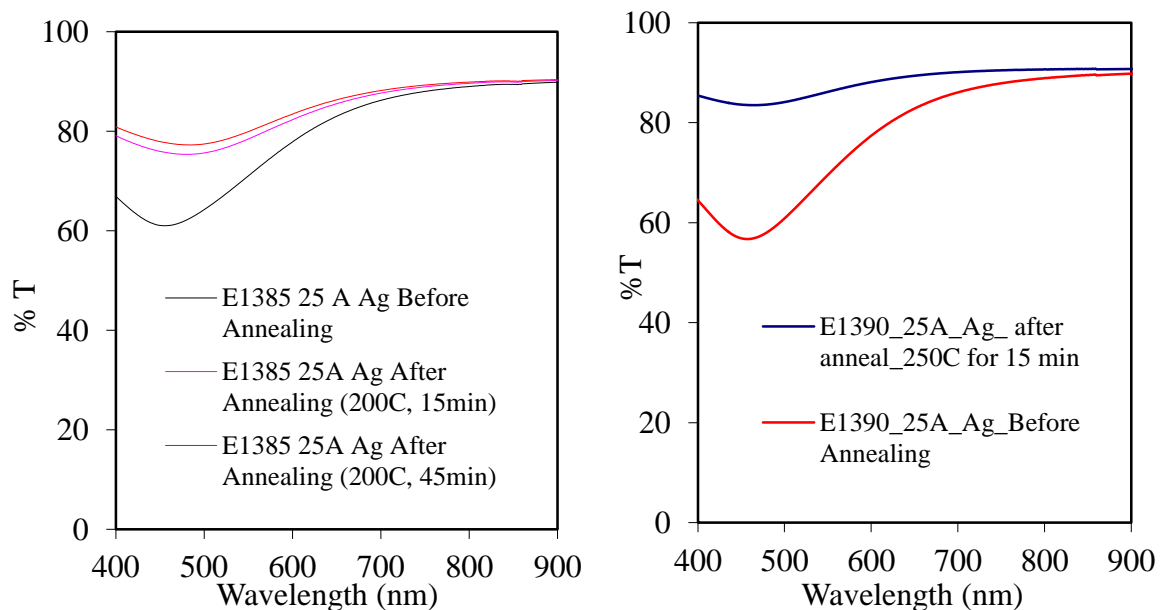
Fig 6.11: %T vs wavelength of 25A Ag before annealing and after annealing for 15min and 45min at 200C/250C.

From figure 6.11(a) it is clearly evident that first few minutes are the crucial moments for the formation of the nanodots which remains unaffected on further annealing. Figure 6.11(b) shows %T vs wavelength variation of 25A silver deposited on cleaned glass and annealed at 250C for 15 min. On comparing fig6.11(a) and figure 6.11(b) it is clear that 250C anneal time improves the %T to almost 90% near infrared region and around 85% near 480nm, unlike 200C annealed sample which showed an improvement to 78% at 480nm. Second set of experiment was a detailed study of the nanodots with the help of SEM. From optical transmission curves it is evident that after annealing there is most likely the formation of island structure which helps to improve %T. Nevertheless SEM images would suggest us the dimension and moreover distribution of nanodots on the substrate.
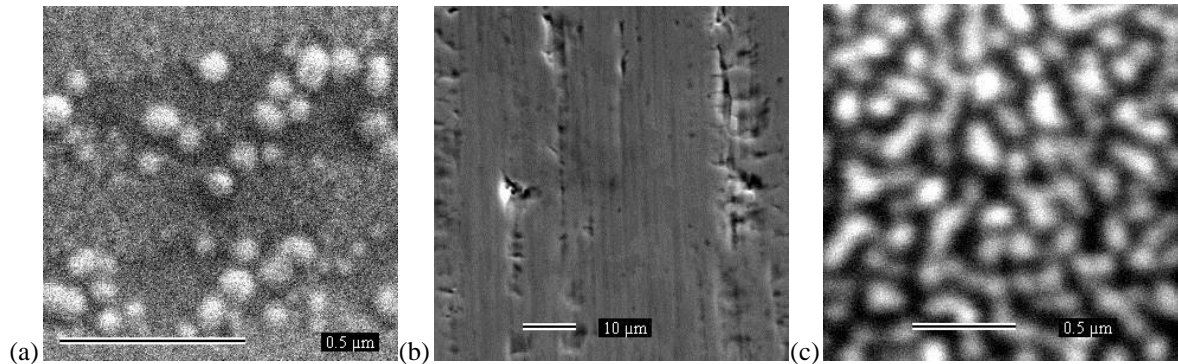
Fig 6.13: SEM images of (a) 25A silver annealed at 250C for 15min on si wafer (b) 25A silver annealed 250C for 15 min on SS (c) 25A silver annealed at 250C for 15min on nc-Si thin film solar cell.

For the SEM imaging samples were prepared on SS and silicon wafer. Wafer provides a smooth and a flat surface for the test which helps to image the nanodots effectively. It is also true that the devices are made on SS therefore it would be interesting to see the nanodots distribution. Fig6.13 shows the distribution of nanodots on a wafer, SS and nc-Si device respectively. Dimension of the nanodots varying from few nanometers to 50nm.

Wafer is smooth and flat it is easier to image the nanodots whereas ridges on SS have dimension of several microns which act like huge trench for the nanodots makes imaging difficult. Fig6.13(c) shows the presence of features but it is mostly the microcrystals of the silicon. P+ layer is thin and because of that microcrystalline silicon can be seen with the SEM because ncSi:H is rough textured material which is shown in the fig6.14. This SEM image was taken on a ncSi:H device having a BR at the bottom.
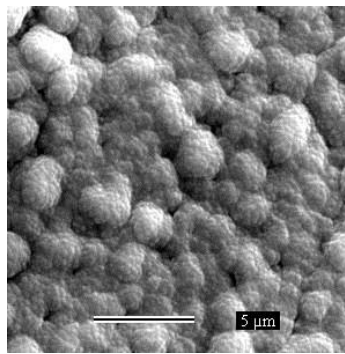
Fig 6.14: SEM image of a ncSi:H device with a B-R at the bottom of the cell.

Nucleation and growth largely depends on the defects especially surface defects and surface energies. This explains that the nucleation and growth on SS and wafer would be largely different. On looking at the height profile of the AFM images, it is clear that the height of the agglomeration is different for SS and wafer. For SS height is near 20nm while for Si wafer it is 10nm, just half of the SS. This can be explained from the rough terrain of SS which provides many favorable locations for the agglomeration of silver. Figure 6.15 shows the 3 dimensional variation of the agglomerated silver. The variation of the nanodots looks evenly distributed on the smooth Si wafer as compared to the rough SS.

(a)   (b)
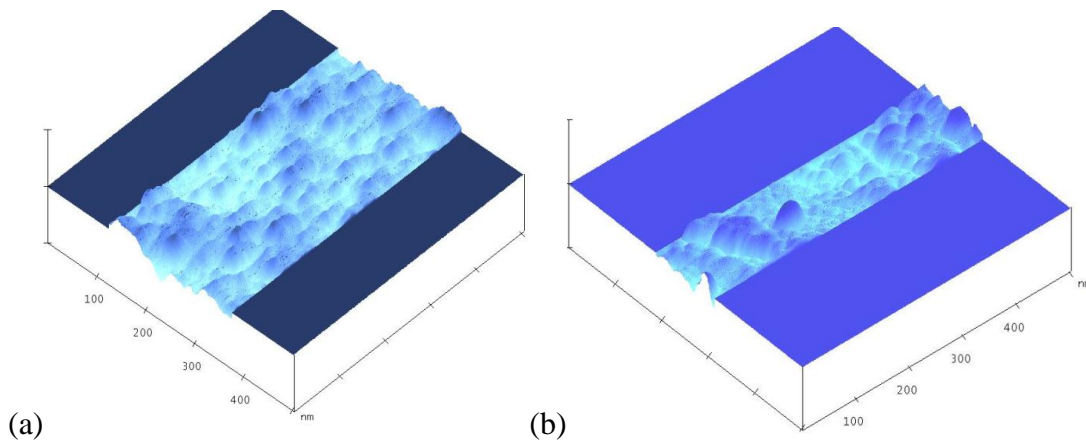
Fig 6.15: 25A silver annealed at 250C for 15 min on (a) Si Wafer and [X and Y axis 1div = 100nm, on Z axis 1div = 8nm] (b) SS [X and Y axis 1div = 100nm, on Z axis 1div = 30nm]

6.7 Various ways of increasing grain size

Nanocrystalline silicon electrical properties improve if the grain size increases. SCLC experiment can be used to prove that electron mobility increases as the grain size increases [140]. We have also observed increase in absorption coefficient when nanocrystalline silicon fabricated at high temperature. Increase in absorption coefficient is because of the increase in the grain size [141]. On changing pressure we can manipulate the ion bombardment on the growing nanocrystalline silicon material. When pressure is increased it decreases ion energy and that improves the device quality. Films prepared at higher pressure show an enhanced <220> grain growth. A series of systematic experiment was done by using PECVD system to see the effect of pressure on grain size variation. Fig 6.16 is the grain size enhancement graph at various temperature and pressure. The grain size increase at high pressure can be attributed to low ion energy bombardment.
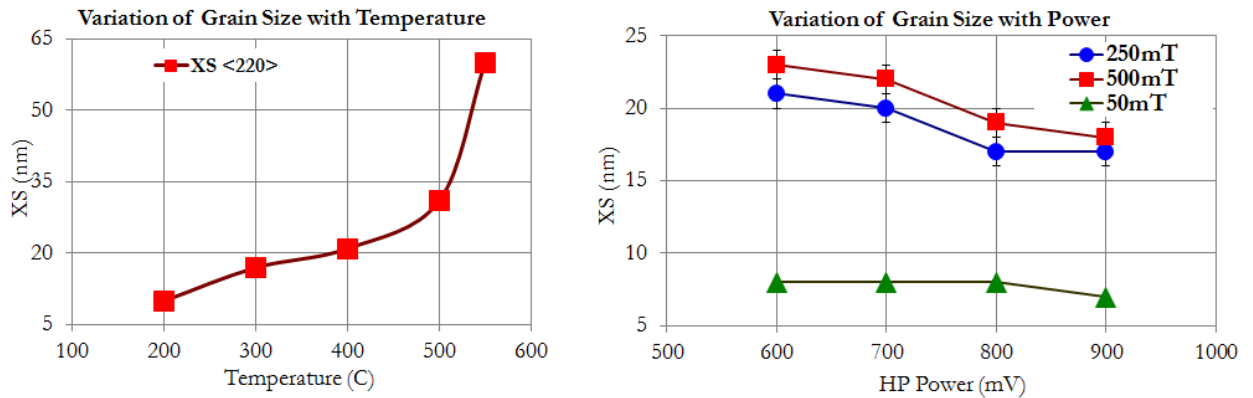
Fig 6.16: Increase in <220> grain on increasing temperature and pressure

For better quality ncSi:H larger grains are required. It also helps to enhance the current. Fig 6.17 showing the absorption coefficient increase with grain size and corresponding increase in QE current.
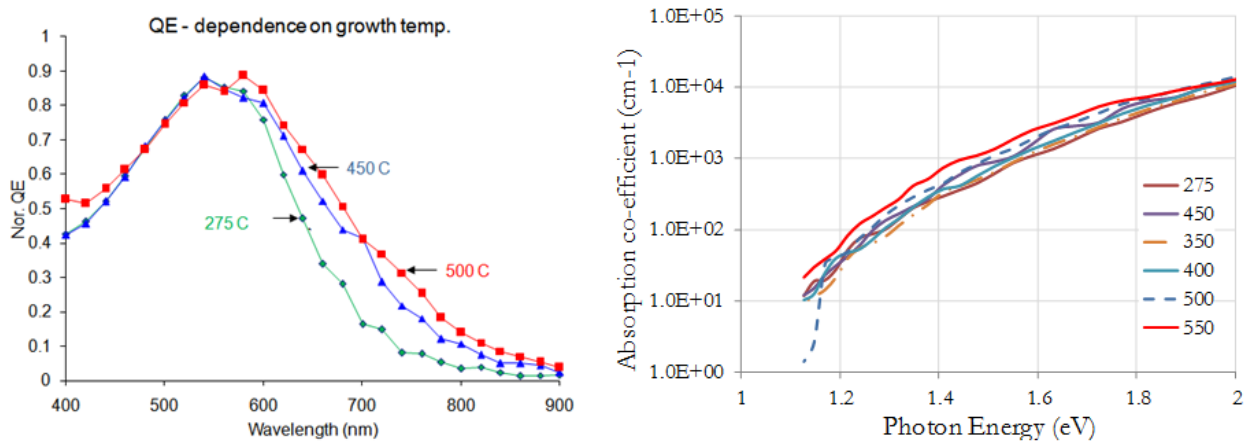
Fig 6.17: Increase in QE current and absorption coefficient on increasing the temperature [21]

To enhance the grain size and the quality of aSi:H SL devices we fabricated some of the devices at higher pressure and got an encouraging result. For the first time we were able to get <220> grain size around 20nm at 250C made at 250mT with excellent device quality.

Fig 6.18 shows the IV and XRD graph of the SL device made at 250mT. Making SL devices at 100mT limits the grain size to 10-12 nm.
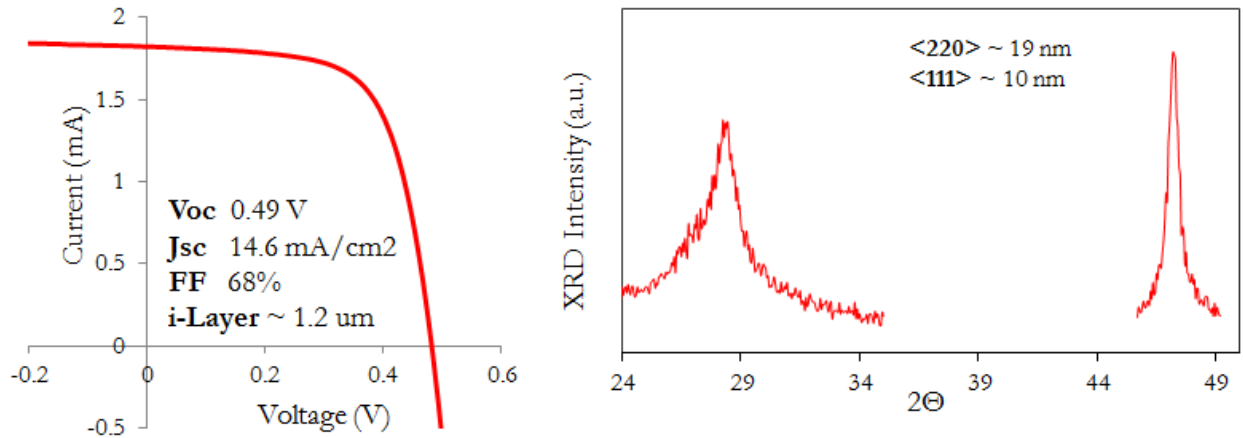
Fig 6.18: aSi/ncSi SL device made at 250mT pressure showing excellent device quality with <220> grain size 19 nm.

6.8 Reducing oxygen contamination

Nanocrystalline silicon is inhenrently n type because of un intentional oxugen doping. To compensate oxygen it is therefore essential to dope the I layer with ppm TMB. On adding TMB it forms a complex compound with oxygen which helps to reduce the recombination effect. In the previous study we have seen that on eliminating oxygen device property improves drastically. To prove the above argument we did an experiment where I layer was intentionally doped with ppm oxygen. It showed poor device property and poor collection of carriers. On adding calculated amount of ppmTMB w improved the device quality significantly [142, 143].
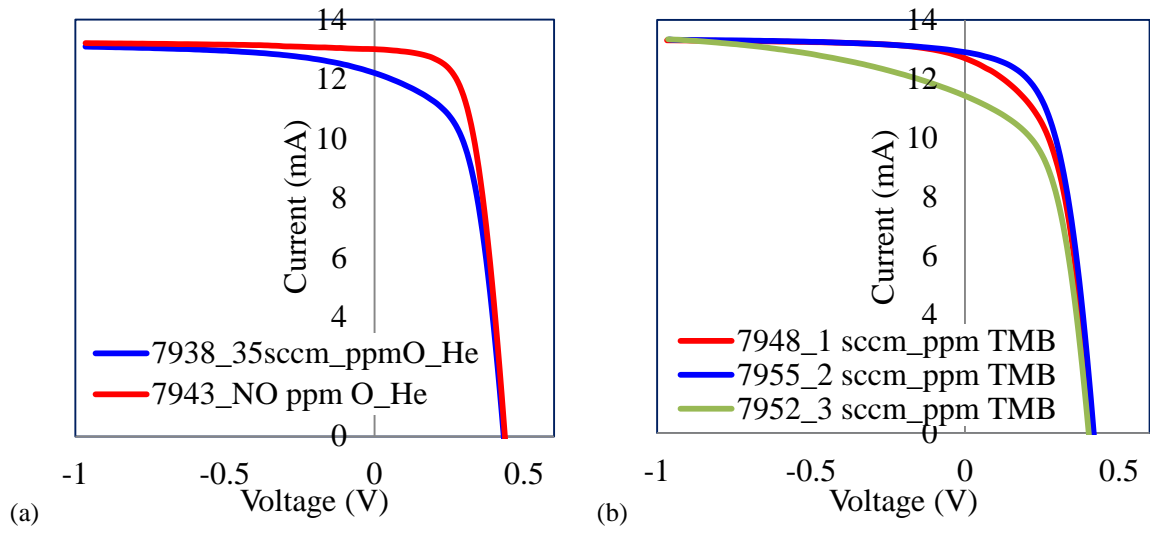
Fig 6.19: IV comparison of ppm oxygen doped and un-doped ncSi:H solar cell, (b) Improvement in the collection of carriers on adding calculated amount of ppm TMB along with fixed ppm oxygen doped ncSi:H solar cell

CHAPTER 7. SUMMARY & FUTURE WORK

1. We have got encouraging results by showing the enhancement in QE current on implementing aSiGe:H layer in the SL structure. Nonetheless we have also observed problems with the nucleation process. Our main focus would be to optimize the deposition parameter so that we could consistently get nanocrystalline films. High dilution and high power is required but Voc goes down so we have to equally focus on getting high Voc.

2. The main issue with aSiGe/ncSi SL devices is the collection of carriers. We tried to grade germane so that it could assist the hole collection but the main drawback was less enhancement in current because of less Ge incorporation. aSiGe:H layers are very thin around 10nm, to get enough enhancement in current we need to incorporate more Ge. The challenge would be to maintain the crystallinity of the film while increasing the Ge content in aSiGe:H.

3. The other method which we have tried was the selective doping of the layers. It could be possible that we are not able to collect the holes effectively generated in aSiGe:H layers. With the help of the band diagram and using various doping conditions we have showed that doping aSiGe:H with ppm PH_3 and ncSi:H with ppm TMB may assist the collection of the minority carriers.

We have tried various doping configuration such as:

1) No doped layers

2) ncSi layer with TMB and aSiGe with PH3

3) ncSi layer with PH3 and aSiGe layer with TMB

4) Only aSiGe with TMB

5) Only ncSi layer with TMB

Doping each layer selectively helped us but to understand the collection property. We keep rest of the parameters same such as dilution ratio, power levels and pressure for better comparison.

4. Step graded germane concentration in SL structure also helped to optimize the device. We used 4 different band-gaps of aSiGe:H where germane concentration was increased as the device grew. The benefit of this structure is that higher germane concentration is near p+/i interface, we know that electric field is strong in that region so it helps to collect the holes efficiently.

5. The grain size of aSiGe/ncSi SL was measured by using XRD. It showed decrease in <220> grain size if compared to aSi/ncSi SL devices. For aSiGe:H grain sizes were in the range 7-9 nm whereas for aSi:H SL grain sizes varied from 10-12 nm prepared at 100mT pressure.

From the previous experiment we have observed that grain size increases as temperature goes above 400C or by increasing the deposition pressure. Both the

cases are not favorable for the deposition of high quality aSiGe:H. High temperature lead to loss of Ge-H bond and high pressure decreases the ion energy which makes it difficult for GeH$_3$ radical to diffuse on the film. High pressure can help us to attain larger grain size in aSiGe/ncSi SL. To overcome lower ion energy we need to increase the power of the deposition or increase dilution with hydrogen to facilitate nanocrystalline silicon formation.

6. The whole purpose of making a SL structure is to curb the large grain boundary formation. We optimized the device and looked at various variations listed below.

   a) Variation of crystallinity as SL thickness increases

   b) Variation in diffusion length as SL thickness increases

   c) Variation in grain size as SL thickness increases

   d) Variation in defect density as SL thickness increases

   e) Variation of crystallinity on changing various layers of the SL

We have showed the variation of crystallinity as Ge content increases. It is difficult to form the nanocrystalline silicon film if we increase the Ge content. We have also showed the variation of crystallinity as the individual layer thicknesses changed. For optimum SL film with equal crystalline and amorphous phase longer ncSi:H cycles are required.

7. With the help of a simple model we have showed that definitely there is an increment in the current density on incorporating Ge in aSiGe:H layer. We will further develop the device model to explain the experimental data. Developing a model helps to understand the physics of the device.

8. Instead of thick devices we realized that it is best to make thin aSiGe:H layers to further improve the collection problems. ncSi:H is an indirect band-gap so it requires thicker layers to absorb all of the photons. Therefore if we are relying on thin SL then it would be essential to integrate the devices with suitable back-reflectors so that effective light path increases.

9. Different types of back-reflectors were developed to improve photon harvesting in a solar cell. Textured silver and ZnO have been discussed in detail, their preparation and optical properties. Plasmonic structures have been used to compare with the randomly textured substrates. It has been shown that periodic structures may give higher QE currents as compared to randomly textured substrates. We would also like to investigate more on combining both randomly textured substrates with periodic structures.

10. Tandem solar cell is another way to increase the efficiency. We developed thin film tandem solar cell of aSi and ncSi solar cells. Efficiency close to 10% have been reported on flexible substrates.

REFERENCES

[1] M. A. Green, "Recent developments in photovoltaics", Solar Energy, 76(1-3):38, (2004)

[2] A. V. Shah, R. Platz, and H. Keppner, "Thin film silicon solar cells: a review and selected trends", Solar energy materials and solar cells, 38(1-4):501, (1995)

[3] A. V. Shah, H. Schade, M. Vanecek, J. Meier, E. Vallat-Sauvain, N. Wyrsch, U. Kroll, C. Droz, and J. Bailat, "Thin film silicon solar cell technology. Progress in photo-voltaics research and applications", 12(23):113, (2004)

[4] J. Yang, A. Banerjee, and S. Guha, "Triple-junction amorphous silicon alloy solar cell with 14.6% initial and 13.0% stable conversion efficiencies", Applied Physics Letters, 70:2975, (1997)

[5] R. W. Collins, A. S. Ferlauto, G. M. Ferriera, C. Chen, J. Koh, R. J. Koval, Y. Lee, J. M. Pearce, and C. R. Wronski, "Evolution of microstructure and phase in amorphous, protocrystalline, and microcrystalline silicon studied by real time spectroscopic ellipsometry", Solar energy materials and solar cells, 78(1-4):143, (2003)

[6] A. Matsuda, "Microcrystalline silicon. Growth and device application", Journal of Non-Crystalline Solids, 338:1, (2004)

[7] V.L. Dalal, "Fundamental considerations regarding the growth of amorphous and microcrystalline silicon and alloy films", Thin Solid Films, 395(1-2):173, (2001)

[8] M. Kondo, M. Fukawa, L. Guo, and A. Matsuda, "High rate growth of microcrystalline silicon at low temperatures", Journal of Non-Crystalline Solids, 266:84, (2000)

[9] M. A. Green, "Crystalline and thin film silicon solar cells: state of the art and future potential", Solar energy, 74(3):181, (2003)

[10] M. A. Green, "Photovoltaics: technology overview", Energy policy, 28(14):989, (2000)

[11] S. Veprek, V. Marecek, "The preparation of thin layers of Ge and Si by chemical hydrogen plasma transport", Solid State Electron. 11 (1968) 683.

[12] G. Lucovsky, C. wang, R. J. Nemanich, M. J. Williams, "Deposition of μc-Si and μc-SiC thin films by remote plasma-enhanced chemical-vapor deposition", Solar Cells 30 (1991) 419.

[13] M. Faraji, S. Gokhale, S. M. Choudhari, M. G. Takwale, S. V. Ghaisas, "High mobility hydrogenated and oxygenated microcrystalline silicon as a photosensitive material in photovoltaic applications", Appl. Phys. Lett. 60 (1992) 3289.

[14] J. Meier, P. Torres, R. Platz, S. Dubail, U. Kroll, J.A.A. Selvan, N. P. Vaucher, C. Hot, D. Fischer, H. Keppner, "Microcrystalline silicon and micromorph tandem solar cells", Mater. Res. Soc. Symp. Proc, 420 (1996) 3.

[15] N. Beck, P. Torres, J. Fric, Z. Remes, J. Kocka, A. Shah, "Material and solar cell research in microcrystalline silicon", Proc. Mater. Res. Soc. Symp. 452 (1997) 761.

[16] R.W. Collins, A.S. Ferlauto, G.M. Ferreira, Chi Chen, Joohyun Koh, R.J. Koval, Yeeheng Lee, J.M. Pearce, C.R. Wronski, "Evolution of microstructure and phase in amorphous, protocrystalline, and microcrystalline silicon studied by real time spectroscopic ellipsometry ", Solar Energy Materials & Solar Cells 78 (2003) 143–180

[17] J. Bailat, E. Vallat-Sauvain, L. Feitknecht, C. Droz, and A. Shah , "Microstructure and open-circuit voltage of n−i−pmicrocrystalline silicon solar cells", Journal of appl phys 93 (2003)

[18] Y. Mai, S. Llein, R. Carius, J. Wolff, A. Lambertz, F. Finger, and X. Geng, "Microcrystalline silicon solar cells deposited at high rates", J. Appl. Phy, 97 11493 (2003)

[19] A. Matsuda, "Formation kinetics and control of microcrystallite in μc-Si:H from glow discharge plasma ", J. Non-Cryst. Solids 59 (1983) 767.

[20] V.L. Dalal, "Fundamental considerations regarding the growth of amorphous and microcrystalline silicon and alloy films ", Thin Solid Films 395 (2001) 173

[21] C.C. Tsai, G.B. Anderson, R. Thompson, B. Wacker, "Control of silicon network structure in plasma deposition", J. Non-Cryst. Solids 114 (1989) 151

[22] N. Fukata, S. Sasaki, K. Murakami,"Hydrogen molecules and hydrogen-related defects in crystalline silicon", Phys. Rev. B 56, 6642–6647 (1997)

[23] U Kroll, J Meier, P Torres, J Pohl, A Shah, "From amorphous to microcrystalline silicon films prepared by hydrogen dilution using the VHF (70 MHz) GD technique ",Journal of Non-Crystalline Solids Volumes 227-230, Part 1, May 1998, Pages 68-72

[24] U. Kroll, A. Shah, H. Keppner, J. Meier, P. Torres, D. Fischer, "Potential of VHF-plasmas for low-cost production of a-Si: H solar cells ",Solar Energy Materials and Solar Cells, 1997:343, (2001)

[25] B. Kalache, A. I. Kosarev, R. Vanderhaghen, and P. Roca i Cabarrocas, "Ion bombardment effects on microcrystalline silicon growth mechanisms and on the film properties,J. Appl. Phys. 93, 1262 (2003)

[26] Hiromu Takatsuka, Matsuhei Noda, Yoshimichi Yonekura, Yoshiaki Takeuchi, Yasuhiro Yamauchi ,"Development of high efficiency large area silicon thin film modules using VHF-PECVD ",Solar Energy, Volume 77, Issue 6, December 2004, Pages 951-960

[27] V. Dalal and A. Madhavan ," Alternative designs for nanocrystalline silicon solar cells ", J. Non-Cryst. Solids 354:2403, (2008)

[28] J. Kočka, A. Fejfar, H. Stuchlíková, J. Stuchlík, P. Fojtík, T. Mates, B. Rezek, K. Luterová, V. Švrček, and I. Pelant,"Large grain boundary formation inncSi:H growth",Sol. Energy Mater. Sol. Cells 78, 493 (2003)

[29] B. Yan, G. Yue, J.M. Owens, J. Yang, and S. Guha, " Light-induced metastability in hydrogenated nanocrystalline silicon solar cells", Applied Physics Letters, 85:1925, (2004)

[30] X. Han, G. Hou, X. Zhang, C. Wei, G. Li, J. Zhang, X. Chen, D. Zhang, J. Sun, Y. Zhao, X. Geng, "Improvement of hydrogenated microcrystalline silicon solar cell performance by VHF power profiling technique", Sol. Ener. Mat. And sol. Cells, 94 (2010) 254

[31] Atul Madhavan, "Alternative design for solar cells", Iowa State University, Thesis, (2009)

[32] V.L. Dalal, J. Graves, and J. Leib. Influence of pressure and ion bombardment on the growth and properties of nanocrystalline silicon materials. Applied Physics Letters, 85:1413, 2004.

[33] V.L. Dalal and A. Madhavan. Alternative designs for nanocrystalline silicon solar cells. Journal of Non-Crystalline Solids, 2008.

[34] P. Sharma. Study of nano-crystalline silicon deposited by VHF-PE CVD for solar cell devices. PhD thesis, Iowa State University, 2005.

[35] V.L. Dalal, K. Muthukrishnan, S. Saripalli, D. Stieler, and M. Noack. Growth and Electronic Properties of Nanocrystalline Si. In Materials Research Society Symposium proceedings, volume 910, page 293. Warrendale, Pa.; Materials Research Society; 1999, 2006.

[36] S. Usui and M. Kikuchi, "Properties of heavily doped GD-Si with low resistivity", Journal of Non-Crystalline Solids, 34(1):1, (1979)

[37] I.C. Cheng and S. Wagner. "Hole and electron mobilities in nanocrystalline silicon deposited at 150 C", Applied Physics Letters, 80:440, (2002)

[38] S. Veprek, Z. Iqbal, RO Kuhne, P. Capezzuto, FA Sarott, and JK Gimzewski, "Properties of microcrystalline silicon. IV. Electrical conductivity, electron spin resonance and the effect of gas adsorption", Journal of Physics C: Solid State Physics, 16(32):6241, (1983)

[39] S. Soedergren, A. Hagfeldt, J. Olsson, and S.E. Lindquist. "Theoretical models for the action spectrum and the current-voltage characteristics of microporous semiconductor _lms in photoelectrochemical cells", J. Phys. Chem, 98(21), (1994)

[40] R. Fluckiger, J. Meier, M. Goetz, and A. Shah, "Electrical properties and degradation kinetics of compensated hydrogenated microcrystalline silicon deposited by very high-frequency-glow discharge", Journal of Applied Physics, 77:712, (1995)

[41] J. Bailat, E. Vallat-Sauvain, L. Feitknecht, C. Droz, and A. Shah, " Microstructure and open-circuit voltage of n- i- p microcrystalline silicon solar cells", Journal of Applied Physics, 93:5727, (2003)

[42] G. Yue, B. Yan, C. Teplin, J. Yang, S. Guha, "Optimization and characterization of i/p buffer layer in hydrogenated nanocrystalline silicon solar cells", Journal of Non-Crystalline Solids 354:2440–2444, (2004)

[43] M. Ito, M. Kondo, A. Matsuda, "The effect of superlattice buffer of microcrystalline silicon solar cells", 3rd world conference on photovoltaic energy conversion, 2726, (2003)

[44] V. Dalal, M. Leonard, J. Booker, A. Vaseashta, "Quantum efficiency of aSi:H alloy solar cells", IEEE, 837, (1985)

[45] D.P. Stieler, "Measurement of mobility in nanocrystalline semiconductor materials using space charge limited current", PhD thesis, Iowa State University, (2005)

[46] D. Ritter, E. Zeldov, and K. Weiser, "Steady-state photocarrier grating technique for diffusion length measurement in photoconductive insulators", Applied Physics Letters, 49:791, (1986)

[47] A.M. Goodman, "A Method for the Measurement of short minority carrier diffusion lengths in semiconductors", Journal of Applied Physics, 32:2550, (1961)

[48] V.L. Dalal and P. Sharma, "Defect density and diffusion length of holes in nanocrystalline silicon devices", Applied Physics Letters, 86:103510, (2005)

[49] V.L. Dalal, P. Sharma, D. Staab, M. Noack, and K. Han. "Defect densities, diffusion lengths and device physics in nanocrystalline Si: H solar cells. In amorphous and nanocrystalline silicon science and technology", MRS Spring Meeting, 569-574, (2004)

[50] S. Saripalli, "Transport in nanocrystalline silicon and silicon germanium", PhD thesis, Iowa State University, (2008)

[51] P.D. Reusswig, "Measurement of minority carrier lifetimes in nanocrystalline silicon devices using reverse-recovery transient method", Master thesis, Iowa State University, (2008)

[52] S. Saripalli, P. Sharma, P. Reusswig, and V. Dalal, "Transport properties of nanocrystalline silicon and silicon-germanium", Journal of Non-Crystalline Solids,354(19-25):2426, (2008)

[53] D. Stieler, V.L. Dalal, K. Muthukrishnan, M. Noack, and E. Schares, "Electron mobility in nanocrystalline silicon devices", Journal of Applied Physics, 100:036106, (2006)

[54] L.C. Kimerling, "Influence of deep traps on the measurement of free-carrier distributions in semiconductors by junction capacitance techniques", Journal of Applied Physics, 45:1839, (2003)

[55] F. Finger, S. Klein, T. Dylla, A.L.B. Neto, O. Vetterl, and R. Carius, "Defects in microcrystalline silicon prepared with hot wire CVD", MRS Symposium Proceedings, 715:123, (2002)

[56] Y. Sun, T. Miyasato, and J. K. Wigmore, "Possible origin for (110)-oriented growth of grains in hydrogenated microcrystalline silicon films", Applied Physics Letters,70:508, (1997)

[57] W. H. Zachariasen, "A general theory of X-ray diffraction in crystals", Acta Cryst., 23:558, (1967)

[58] B. D. Cullity and J. W. Weymouth, "Elements of X-Ray diffraction", American Journal of Physics, 25:394, (1957)

[59] http://pvcdrom.pveducation.org/celloper/quantum.htm.

[60] C. Smit, R. van Swaaij, H. Donker, A. Petit, WMM Kessels, and MCM van de Sanden, "Determining the material structure of microcrystalline silicon from Raman spectra", Journal of Applied Physics, 94:3582, (2003)

[61] H. Richter, Z. P. Wang, and L. Ley, "The one phonon Raman spectrum in microcrystalline Silicon", Solid State Communications, 39(5):625, (1981)

[62] Z. Iqbal and S. Veprek, "Raman scattering from hydrogenated microcrystalline and amorphous silicon", J. Phys. C(Solid State Phys.), 15(2):377, (1982)

[63] S. Veprek, F.A. Sarott, and Z. Iqbal, "Effect of grain boundaries on the Raman spectra, optical absorption, and elastic light scattering in nanometer-sized crystalline silicon", Physical Review B, 36(6):3344, (1987)

[64] Y. Fukuda, Y. Sakuma, C. Fukai, Y. Fujimura, K. Azuma, and H. Shirai, "Optical emission spectroscopy study toward high rate growth of microcrystalline silicon", Thin Solid Films, 386(2):256, (2001)

[65] M.R. Esmaeili-Rad, A. Sazonov, A. G. Kazanskii, A. A. Khomich, and A. Nathan, "Optical properties of nanocrystalline silicon deposited by PECVD", Journal of Materials Science: Materials in Electronics, 18:405, (2007)

[66] T. Tiedje, E. Yablonovitch, G.D. Cody, and B.G. Brooks, "Limiting effciency of silicon solar cells", IEEE Transactions on Electron Devices, 31(5):711, (1984)

[67] P. Sheng, "Optical absorption of thin film on a Lambertian substrate", Electron Devices, IEEE Transactions on, 31(5):634, (1984)

[71] J. Meier, P. Torres, R. Platz, S. Dubail, U. Kroll, J.A.A. Selvan, N.P. Vaucher, C. Hot, D. Fischer, H. Keppner, "Amorphous silicon technology", MRS ,420: 3, (1996)

[72] A. Matsuda, "Microcrystalline silicon. Growth and device application", Journal of Non-Crystalline Solids, 338:1, (2004)

[73] M. Heintze and R. Zedlitz, "Control of a-Si: H deposition by the ion flux in a VHF plasma", Journal of non-crystalline solids, 164:55, (1993)

[74] M. Heintze, R. Zedlitz, and G. H. Bauer, "Analysis of high-rate a-Si: H deposition in a VHF plasma", Journal of Physics D: Applied Physics, 26:178, (1993)

[75] R. Zedlitz, M. Heintze, and G. H. Bauer. "An approach to high quality a-Ge:H by VHF deposition", MRS, 297:55, (1993)

[76] H. Curtins, N. Wyrsch, and A. V. Shah, "High-rate deposition of amorphous hydrogenated silicon: effect of plasma excitation frequency", Electronics Letters, 23(5):228, (1987)

[77] D. E. Carlson and C. R. Wronski, "Amorphous semiconductors", ed. by MH Brodsky, Appl. Phys, 36, (2000)

[78] R. A. Street, Hydrogenated Amorphous Silicon, Cambridge Solid State Science Series (1986).

[79] B.C. Pan and R. Biswas, "Structure and simulation of hydrogenated nanocrystalline silicon", J. Appl. Physics. 96, 6247 (2004).

[80] B.C. Pan and R. Biswas, "Simulation of Hydrogen evolution from nano-crystalline silicon", Journal of Non-Crystalline Solids 333, 44 (2004).

[81] D. L. Staebler and C. R. Wronski, "Reversible conductivity changes in discharge-produced amorphous Si", Appl. Phys. Lett. 31, 292 (1977).

[82] M. Stutzmann, W. Jackson, C. Tsai, "Light-induced metastable defects in hydrogenated amorphous silicon: A systematic study", Phys. Rev. B 32, 23 (1985).

[83] R. Biswas, B.C. Pan, and Y. Ye, "Metastability of amorphous silicon from silicon network rebonding", Phys. Rev. Lett. 88, 205502 (2002).

[84] R. Biswas, B.C. Pan, "Defect kinetics in new model of metastability in a-Si:H", Journal of Non-Crystalline Solids, 299-302, 507 (2002).

[85] H. Branz, "H collision model", Phys. Rev. B 59, 5498 (1999).

[86] R. Biswas and B.C. Pan, "Microscopic nature of Staebler-Wronski defect formation in amophous silicon", Appl. Phys. Lett. 72, 371 (1998).

[87] R. Biswas, Q. Li, B.C. Pan, Y. Yoon, "Mechanism for hydrogen diffusion in amorphous silicon", Phys. Rev. B. 57, 2253 (1998).

[88] Q. Li and R. Biswas, "Hydrogen Rebonding and defect formation in a-Si:H", Phys. Rev. B 52, 10705 (1995).

[89] R. Biswas, and Y.P. Li, "H-flip model of light induced changes of amorphous silicon", Phys. Rev. Lett. 82, 2512 (1999).

[90] F. Leblanc, J. Perrin, and J. Schmitt, " Numerical modeling of the optical properties of hydrogenated amorphous-silicon-based p-i-n solar cells deposited on rough transparent conducting oxide substrates", Journal of Applied Physics, 75:1074, (1994)

[91] M. Zeman, R. van Swaaij, J. W. Metselaar and R. E. I. Schropp, "Optical modeling of a-Si:H solar cells with rough interfaces: Effect of back contact and interface roughness", Journal of Applied Physics, 88:6436, (2000)

[92] H. W. Deckman, C. R. Wronski, H. Witzke, and E. Yablonovitch, "Optically enhanced amorphous silicon solar cells", Applied Physics Letters, 42:968, (1983)

[93] L. Houben, M. Luysberg, P. Hapke, R. Carius, F. Finger, and H. Wagner, "Structural properties of microcrystalline silicon in the transition from highly crystalline to amorphous growth, Philosophical Magazine A, 77(6):1447, (1998)

[94] D Zhou and R Biswas, "Photonic crystal enhanced light-trapping in thin film solar cells," Journal of Applied Physics, (2008)

[95] DE Carlson and CR Wronski. In: Amorphous Semiconductors, ed. By MH Brodsky. Topics Appl. Phys, 36

[96] Y Igasaki and H Saito, "The effects of deposition rate on the structural and electrical properties of ZnO films deposited on (1120) oriented sapphire substrates", Journal of Applied Physics, (1991)

[97] ZC Jin, I Hamberg and CG Granqvist, "Optical properties of sputter-deposited ZnO thin films", Journal of Applied Physics, (1988)

[98] S Fay, U Kroll, C Bucher, E Vallat-Sauvain, and A Shah, "Low pressure chemical vapor deposition of ZnO layers for thin films solar cells: Temperature induced morphological changes", Solar energy Materials and Solar Cells, (2005)

[99] J Aranovich, A Ortiz, and RH Bube, "Optical and electrical properties of ZnO films prepared by spray pyrolysis for solar cell applications", Journal of Vacuum Science and Technology, (1979)

[100] J Hupkes, B Rech, S Calnan,O Kluth, U Zastrow, H Siekmann, and M Wuttig, "Material study on reactively sputtered zinc oxide for thin film silicon solar cells", Thin solid films, (2006)

[101] AN Mariano and RE Hanneman, "Crystallographic polarity of ZnO crystals", Journal of applied physics, (1969)

[102] G Heiland and P Kunstmann, "Polar surfaces of zinc oxide crystals", Surface science, (1969)

[103] JA Thronton, "Influence of apparatus geometry and deposition conditions on the structure and topography of thick sputtered coatings", Journal of vacuum science and technology, (1974)

[104] O Kluth, B Rech, and H Wagner, "Sputtered zinc oxide films for silicon thin film solar cells", Material properties and surface texture, (2001)

[105] S Pillai, KR Catchpole, T Trupke, "Surface plasmon enhanced silicon solar cells", Journal of applied physics, (2007)

[106] F. Meillaud, A. Shah, C. Droz, E. Vallat-Sauvain, and C. Miazza, "Effciency limits for single-junction and tandem solar cells", Solar Energy Materials and Solar Cells, 90(1819):2952, (2006)

[107] Y. Igasaki and H. Saito, "The effects of deposition rate on the structural and electrical properties of ZnO:Al lms deposited on sapphire substrates", Journal of Applied Physics, 70:3613, (1991)

[108] Z.C. Jin, I. Hamberg, and C. G. Granqvist, "Optical properties of sputter-deposited ZnO:Al thin films", Journal of Applied Physics, 64:5117, (1988)

[109] S. Fay, U. Kroll, C. Bucher, E. Vallat-Sauvain, and A. Shah, "Low pressure chemical vapour deposition of ZnO layers for thin-film solar cells: temperature-induced morphological changes", Solar Energy Materials and Solar Cells, 86(3):385, (2005)

[110] J. Aranovich, A. Ortiz, and R.H. Bube, "Optical and electrical properties of ZnO films prepared by spray pyrolysis for solar cell applications", Journal of Vacuum Science and Technology, 16:994, (1979)

[111] S. Bose and A. K. Barua, "The role of ZnO:Al films in the performance of amorphous silicon based tandem solar cells", Journal of Physics-London-D Applied Physics, 32:213, (1999)

[112] R. Das and S. Ray, "Zinc oxide-a transparent, conducting IR-reactor prepared by rf-magnetron sputtering", Journal of Physics D: Applied Physics, 36:152, (2003)

[113] B. Szyszka, "Transparent and conductive aluminum doped zinc oxide films prepared by mid-frequency reactive magnetron sputtering", Thin Solid Films, 351:164, (1999)

[114] J. Hupkes, B. Rech, S. Calnan, O. Kluth, U. Zastrow, H. Siekmann, and M.Wuttig, "Material study on reactively sputtered zinc oxide for thin film silicon solar cells", Thin Solid Films, 502:286, (2006)

[115] C. Agashe, O. Kluth, J. Hupkes, U. Zastrow, B. Rech, and M. Wuttig, "Efforts to improve carrier mobility in radio frequency sputtered aluminum doped zinc oxide films, "Journal of Applied Physics, 95:1911, (2004)

[116] M. Berginski, J. Hupkes, M. Schulte, G. Schope, H. Stiebig, B. Rech, and M. Wuttig, "The effect of front ZnO: Al surface texture and optical transparency on efficient light trapping in silicon thin-film solar cells", Journal of Applied Physics, 101:074903, (2007)

[117] L.A. Feitknecht, "Microcrystalline silicon solar cells in the NIP configuration: optimisations on light scattering back-reectors", Universite de Neuchatel, (2000)

[118] O. Kluth, G. Schope, J. Hupkes, C. Agashe, J. Muller, and B. Rech, "Modified Thornton model for magnetron sputtered zinc oxide: film structure and etching behavior", Thin Solid Films, 442:80, (2003)

[119] A. N. Mariano and R. E. Hanneman, "Crystallographic polarity of ZnO Crystals", Journal of Applied Physics, 34:384, (1969)

[120] G. Heiland and P. Kunstmann, "Polar surfaces of zinc oxide crystals", Surface Science, 13:72, (1969)

[121] K. Ellmer, A. Klein, and B. Rech, "Transparent conductive zinc oxide: basics and applications in thin film solar cells", Springer Verilag, (2008)

[122] J.A. Thornton, "Influence of apparatus geometry and deposition conditions on the structure and topography of thick sputtered coatings", Journal of Vacuum Science and Technology, 11:666, (1974)

[123] O. Kluth, B. Rech, and H. Wagner, "Sputtered zinc oxide films for silicon thin film solar cells: material properties and surface texture", Thin Solid Films, (2002)

[123] W.W. Wenas, A. Yamada, K. Takahashi, M. Yoshino, and M. Konagai, "Electrical and optical properties of boron-doped ZnO thin films for solar cells grown by metalorganic chemical vapor deposition", Journal of Applied Physics, 70:7119, (1991)

[124] S. Fay, L. Feitknecht, R. Schluchter, U. Kroll, E. Vallat-Sauvain, and A. Shah, "Rough ZnO layers by LP-CVD process and their effect in improving performances of amorphous and microcrystalline silicon solar cells", Solar Energy Materials and Solar Cells, 90:2960, (2006)

[125] C. Ballif, J. Bailat, D. Domine, J. Steinhauser, S. Fay, M. Python, and L. Feitknecht, "Fabrication of high efficiency microcrystalline and micromorph thin film solar cells on LPCVD ZnO coated glass substrates", In Proceedings of the 21st European Photovoltaic Solar Energy Conference, page 1552, (2003)

[126] J. Springer, B. Rech, W. Reetz, J. Muller, and M. Vanecek, "Light trapping and optical losses in microcrystalline silicon pin solar cells deposited on surface-textured glass/ZnO substrates", Solar Energy Materials and Solar Cells, 85:1, (2005)

[127] F. Leblanc, J. Perrin, and J. Schmitt, "Numerical modeling of the optical properties of hydrogenated amorphous-silicon-based p-i-n solar cells deposited on rough transparent conducting oxide substrates", Journal of Applied Physics, 75:1074, (1994)

[128] M. Zeman, R. van Swaaij, J.W. Metselaar, and R.E.I. Schropp, "Optical modeling of a-Si:H solar cells with rough interfaces: Effect of back contact and interface roughness", Journal of Applied Physics, 88:6436, (2000)

[129] J. Krc, M. Zeman, O. Kluth, F. Smole, and M. Topic, "Effect of surface roughness of ZnO:Al films on light scattering in hydrogenated amorphous silicon solar cells", Thin Solid Films, 426:296, (2003)

[130] Schade H. Rech B. Kluth O. Lechner, Geyer R. and Stiebig H, "Optical TCO properties and quantum efficiencies in thin-film silicon solar cells", In Proceedings of the 19th European Photovoltaic Solar Energy Conference, Paris, volume E02, (2004)

[131] O. Kluth, B. Rech, L. Houben, S. Wieder, G. Schope, C. Beneking, H. Wagner, A. Lo, and H. W. Schock, "Texture etched ZnO: Al coated glass substrates for silicon based thin film solar cells", Thin Solid Films, 351:247, (1999)

[132] J. Bhattacharya, N. Chakravarty, S. Pattnaik, W. Slaffer, R. Biswas and V. Dalal, "A photonic-plasmonic structure for enhancing light absorption in thin film solar cells", Applied Physics Letter, 99:131114, (2011)

[133] M. Kambe, M. Fukawa, N. Taneda, Y. Yoshikawa, K. Sato, K. Ohki, S. Hiza, A. Yamada, M. Konagai, R. Center, "Improvement of light-trapping effect on microcrystalline silicon solar cells by using high haze transparent conductive oxide films", In Photovoltaic Energy Conversion, volume 2, (2003)

[134] R.H. Franken, R.L. Stolk, H. Li, C.H.M. van der Werf, J.K. Rath, and R.E.I. Schropp, "Understanding light trapping by light scattering textured back electrodes in thin film n-i-p-type silicon solar cells", Journal of Applied Physics, 102:014503, (2007)

[135] Stiebig H. Rech B. Kluth O., Zahren C. and Schade H, "Surface morphologies of rough transparent conductive oxide films applied in silicon thin-film solar cells", In Proceedings of the 19th European Photovoltaic Solar Energy Conference, Paris, volume E02, (2004)

[136] R.H.J. Franken, "Transparent conducting oxide contacts and textured metal back reflectors for thin film silicon solar cells", PhD thesis, Utrecht University, (2000)

[137] E. Yablonovitch, "Statistical ray optics", J. Opt. Soc. Am, 72:899, (1982)

[138] T. Tiedje, E. Yablonovitch, G.D. Cody, and B.G. Brooks, "Limiting efficiency of silicon solar cells. IEEE Transactions on Electron Devices, 31:711, (1984)

[139] P. Sheng, "Optical absorption of thin film on a Lambertian reflector substrate", Electron Devices, IEEE Transactions, 31:634, (1984)

[140] V.L. Dalal, J. Graves, and J. Leib, "Influence of pressure and ion bombardment on the growth and properties of nanocrystalline silicon materials", Applied Physics Letters, 85:1413, (2004)

[141] G. Lihui and L. Rongming, "Studies on the formation of microcrystalline silicon with PECVD under low and high working pressure", Thin Solid Films, 376:249, (2000)

[142] P. Torres, J. Meier, R. Fluckiger, U. Kroll, J.A.A. Selvan, H. Keppner, A. Shah, S.D. Littelwood, I.E. Kelly, and P. Giannoulfes, "Device grade microcrystalline silicon owing to reduced oxygen contamination", Applied Physics Letters, 69:1373, (1996)

[143] Y. Nasuno, M. Kondo, and A. Matsuda, "Passivation of oxygen-related donors in microcrystalline silicon by low temperature deposition", Applied Physics Letters, 78:2330, (2001)